RESONANCE RAMAN SPECTROSCOPIC STUDIES

OF TYPE 1 COPPER PROTEINS

Jane Han
B.S., Wuhan University (China), 1982
M.S., Hubei Chemistry Research Institute (China), 1985

A dissertation submitted to the faculty of the
Oregon Graduate Institute of Science & Technology
in partial fulfillment of the requirements for the degree of
Doctor of Philosophy
in
Chemistry

October, 1993

The thesis "Resonance Raman Spectroscopic Studies of Type 1 Copper Proteins" by Jane Han has been examined and approved by the following Examination Committee:

Professor Thomas M. Loehr, Thesis Advisor
Department of Chemistry, Biochemistry, and Molecular Biology

Professor Joann Sanders-Loehr, Co-Advisor
Department of Chemistry, Biochemistry, and Molecular Biology

Professor Ninian J. Blackburn
Department of Chemistry, Biochemistry, and Molecular Biology

Professor William Fish
Department of Environmental Science and Engineering

ACKNOWLEDGMENTS

I am deeply indebted to my advisors, Drs. Thomas M. Loehr and Joann Sanders-Loehr, for directing me throughout the course of my Ph.D. work. Without their patient guidance, strong support, and many inspiring suggestions and discussions, this work could not have been successful. I am also grateful to Dr. Ninian J. Blackburn for his instructions and stimulating discussions in the early part of my Ph.D. study at OGI, and to him and Dr. William Fish for their time spent reviewing this document and for their helpful comments.

I would like to thank Dr. Gabriele Backes for her friendship and help, and the faculty, staff and students in the Department of Chemistry, Biochemistry, and Molecular Biology for the supportive environment they provided. Special thanks go to Nancy Christie and Terrie Hadfield for their help in preparing this dissertation.

Finally, I would like to thank my husband, Dr. Youfeng Wu, for his understanding and support.

TABLE OF CONTENTS

LIST OF FIGURES

LIST OF TABLES

ABSTRACT

RESONANCE RAMAN SPECTROSCOPIC STUDIES OF TYPE 1 COPPER PROTEINS

Jane Han, Ph.D.

Supervising Professor, Thomas M. Loehr

This thesis presents a resonance Raman (RR) spectroscopic study of natural and protein-engineered cupredoxins that function as biological oxidation-reduction catalysts. The "type 1" copper proteins studied include the wild-type proteins plastocyanin, pseudoazurin, azurin, and nitrite reductase (NiR), and the mutant proteins His117Gly azurin and His80Cys (Cu/Cu-H80C) from bovine Cu/Zn superoxide dismutase. The RR spectra of these proteins are characterized by 7 to 11 vibrational modes between 250-500 cm^{-1}. The fact that these vibrational modes occur at a relatively constant set of frequencies is testimony to the highly conserved ground state structures of the common Cu-S(Cys) moiety in which the five atoms Cu-S_γ-C_β-C_α-$N_{peptide}$ are essentially coplanar among all structurally characterized type 1 Cu proteins.

These proteins have similar RR spectra when excited within either the ~460 or the ~600 nm absorption band. The ~600-nm band has been shown to arise from (Cys)S → Cu charge transfer (CT). The RR results indicate that the ~460-nm band should also have predominantly (Cys)S → Cu CT character. The occurrence of the two CT transitions helps to explain the observation that the sum of ϵ_{460} and ϵ_{600} is remarkably constant. The assignment of RR spectral modes to Cu-ligand stretches and internal ligand vibrations has been achieved by isotope studies employing $^{63/65}Cu$, $^{14/15}N$, and H_2O/D_2O substitutions for native and mutant azurins. The most intense Raman band has the greatest Cu-S(Cys) stretching character. The frequency differences of this band

among various type 1 Cu proteins reflect small variations in Cu-S(Cys) bond strengths. The multiple intense peaks near 400 cm^{-1} are due to coupling of the Cu-S(Cys) stretching with Cys deformation modes which is favored by the coplanarity of Cu-S_γ-C_β-C_α-N. The contribution of His ligands to the RR spectrum is minimal, with only the weak band near 280 cm^{-1} being due to Cu-N(His) vibrations. Thus, RR spectra of type 1 Cu proteins predominantly monitor the Cu-S(Cys) chromophore, i.e., the Cu-S(Cys) bond lengths and the conformation of the cysteinate ligand.

Chapter 1

TYPE 1 AND TYPE 2 COPPER SITES IN PROTEINS

Copper (Cu) is an essential trace element in biological systems. Single Cu sites in proteins have been classified as type 1 or 2 based on their spectroscopic properties and biological function (Fee, 1975; Adman, 1985; Adman, 1991). Type 1 Cu proteins function as electron transfer proteins. Examples include plastocyanin (plants), azurin (bacterial), and nitrite reductase (bacterial). The Cu site in a type 1 Cu protein contains a short Cu-S(Cys) bond of $\sim$2.15 Å and the Cu is within a trigonal or a distorted tetrahedral coordination environment. Type 1 Cu proteins have abnormally high redox potentials (E^0: 200-800 mV) and an exceptional affinity for both Cu(I) and Cu(II) forms, indicating a low activation energy (barrier) between the two oxidation states. Spectroscopically, the type 1 Cu protein is characterized by *(i)* an extraordinarily intense (Cys)S $\rightarrow$ Cu(II) charge transfer absorption near 600 nm together with a second absorption band at about 460 nm, *(ii)* an unusually small parallel hyperfine coupling constant in the EPR spectrum of the oxidized protein, and *(iii)* a rich and intense resonance Raman (RR) spectrum of fundamental vibrations in the 200-500 cm^{-1} region.

Type 2 Cu proteins function as enzymatic reaction centers. Examples include Cu,Zn-superoxide dismutase (bovine and yeast), dopamine-β-monooxygenase (mammalian), and galactose oxidase (fungal). The Cu is normally square planar and coordinated by amino acid side chains containing nitrogen (N) and/or oxygen (O) as donor atoms. The redox potential of the metal in a type 2 Cu protein has a normal E^0 value of $\sim$200 mV. In addition, the Cu is usually coordinated by another labile molecule, such as water, the site where substrates may bind. Spectroscopically, the properties of type 2 Cu proteins are similar to those of normal aqueous cupric complexes, with *(i)* only weak ligand-field absorptions, *(ii)* large parallel hyperfine coupling constant in the EPR spectrum, and *(iii)* a weak or absent resonance Raman spectrum.

Study of the structural and spectroscopic properties of type 1 and type 2 Cu proteins is important in understanding their biological function, and many of these proteins have been structurally and spectrally well characterized. It is becoming clear that, instead of relying on a single approach, classification of a Cu protein as a type 1 or a type 2 Cu protein requires a variety of analytical methods. Here, we will discuss the structural and spectral properties of type 1 and type 2 Cu proteins, and emphasize their similarities and differences.

1.1 Protein and Cu Site Structures

1.1.1 Type 1 Cu Proteins

Bacterial (*Pseudomonas aeruginosa*) azurin and plant (poplar) plastocyanin are two type 1 Cu proteins that were structurally characterized in the late 1970s (Adman et al., 1978; Colman et al., 1978). The structure of another bacterial azurin from *Alcaligenes denitrificans* has been refined to 1.8-Å resolution (Baker, 1988). Figure 1.1A is the schematic of the protein-folding topology. The folding can be described as a β-sheet sandwich composed of eight strands, four in a primarily C-terminal layer and four in an N-terminal layer. The loop between two of the C-terminal strands of the β-sheet contains three of the ligands to the Cu: Cys112, His117, and Met121 (Fig. 1.2A). Another Cu ligand is His46, which is located on an adjacent strand, but is considerably closer toward the N-terminus. The H-bonding residues next to His46 and Cys112 further strengthen the interaction between these adjacent strands of the β-sheet.

The Cu in azurin is located only about 8 Å inside of the protein with an edge of His117 protruding through a hydrophobic surface. The three equatorial ligands Cys112, His117, and His46 form a trigonal SNN plane around the Cu ion that is also weakly bound by the sulfur of Met121 and the carbonyl oxygen of Gly45 in the axial positions (Fig. 1.2A). In the azurins, the Cu site geometry is best described as a trigonal bipyramid (Fig. 1.3A). The three equatorial ligands are further fixed in position by H-bonds shown in Figure 1.2A. Upon reduction, the protein as well as the Cu site structures remain the same, but the distances from Cu to the axial S(Met) and the carbonyl oxygen each increase by about 0.1 Å (Shepard et al., 1990). In plastocyanin (Guss et al., 1992), the Cu is also coordinated to three equatorial ligands (His37, Cys84,

His87) similar to azurin, but there is only one axial ligand (Met92). This results in the Cu being positioned 0.36 Å out of the NNS plane, compared to a value of 0.12 Å for azurin (Chapter 4). Structural studies on apoplastocyanin demonstrate that the Cu site is preformed by the protein including the general orientation of the ligating amino acids (Garrett et al., 1984).

Another conserved structural feature among type 1 Cu sites is the conformation of the cysteine ligand. Typically the dihedral angles for Cu-S-C_β-C_α and S-C_β-C_α-N are close to 180°, indicating that the five atoms (Cu, S, C_β, C_α, and N) are nearly coplanar (Chapter 3). For example, the respective cysteine dihedral angles are 169°, 173° in azurin and 168°, 169° in plastocyanin. This coplanar conformation of the cysteinate ligand is important to the interpretation of RR spectra (Chapter 3). It may be a highly conserved feature because it provides an electron transfer pathway through the protein.

The remarkable structural similarities of type 1 Cu proteins are further documented in Chapter 3. There are also some significant differences. Although all type 1 Cu sites have the same SNN ligand set, the Cu site geometry varies between trigonal planar and distorted tetrahedral, regulated by the fourth axial ligand. In plastocyanin, the Cu-S(Met) distance of 2.82 Å is shorter than the 3.13 Å distance in azurin. Nitrite reductase and cucumber basic protein have even shorter Cu-S(Met) distances of 2.62 Å, resulting in a distortion toward tetrahedral geometry (Fig. 1.3B). This structural variability and its spectroscopic consequences are detailed in Chapter 4. The contents of Chapters 3 and 4 have been published by Han et al. (1991 and 1993, respectively).

1.1.2 Type 2 Cu Proteins

Cu_2,Zn_2-superoxide dismutase (SOD) is a well-known type 2 Cu protein (Valentine and Pantoliano, 1981; Getzoff et al., 1983). The 2-Å structure refinement of bovine SOD was reported in 1982 (Tainer et al.). The protein functions as a dimer, but has independent active sites 33.8 Å apart. The protein has an eight-stranded β-barrel plus three external loops. As shown in Figure 1.1B, this folding topology is very similar to that of azurin, with some insertions and deletions in the non-repetitive structure. However, the Cu site is located at the middle of the β sheet rather than in the C-terminal loop of the type 1 Cu sites. The placement of Cu site in SOD is actually similar to the type 2 site of NiR (Fig. 1.1C).

The Cu is coordinated by four His side chains in a distorted square plane with the more open side facing the solvent. The square planar geometry is the one most often encountered for inorganic Cu(II) complexes. The Cu lies on the outside of its β-barrel about 4 Å from a smoothed surface of the protein. The amino acids near the surface provide a pocket into which a superoxide ion can both fit and be actively guided by an electrostatic field gradient (Tainer et al., 1983). The Cu site is capable of binding other anions such as cyanide (Han et al., 1992). The Zn is tetrahedrally coordinated to three His and an aspartic acid ligand. This Zn, as a structural metal center, is completely buried inside the protein. The Cu and Zn are 6.3 Å apart and the two metal ions are bridged by a common His ligand (Fig. 1.2B).

Nitrite reductase (NiR) represents a class of copper proteins containing both type 1 and type 2 Cu sites. Structural data for *Achromobacter cycloclastes* NiR show that the location of the type 2 Cu site is more flexible since the Cu is held at a domain interface (Godden et al., 1991). The protein is a trimer, in which each monomer folds into two domains. Each domain possesses the Greek-key β-sheet folding topology as in azurin, and is shown in Figure 1.1C. The N-terminal domain binds a type 1 Cu. The type 2 Cu site is found between domain 1 of one molecule in the trimer and domain 2 of a second molecule, so that in all, six Cu atoms are bound by the trimer (Fig. 1.1D).

The presence of a Cu-S(Cys) bond alone does not necessarily give a type 1 Cu site. For example, site-directed ligand mutations in SOD, in which one of the type 2 Cu ligands was replaced by Cys (e.g., His120Cys and H46Cys) show type 2 Cu spectroscopic properties. However, the Zn site mutant His80Cys, now with Cu substituted for Zn, shows type 1 Cu properties (Lu, 1992; Lu et al., 1993). The main difference between the Cu and Zn sites is their geometry: Cu is in a distorted square plane, while Zn is in a distorted tetrahedral environment. These results demonstrate that the geometry is a critical structural element for a type 1 Cu site.

In summary, type 1 and type 2 Cu proteins are different with respect to Cu ligands, Cu site geometry, Cu location, and biological function. A type 1 Cu site must have the important Cu-S(Cys) bond, and the three strong SNN ligands are located in a trigonal or tetrahedral coordination environment around the Cu. A type 2 Cu site consists of four strong equatorial ligands in a nearly square planar coordination

environment. However, type 1 and type 2 Cu proteins can have similar β-sheet folding topology, indicating a distant evolutionary relationship. Even within the type 1 Cu family, the sequence homology is less than 10%, the only fully conserved residues being the Cu ligands (Ouzounis and Sander, 1991; Ryden and Hunt, 1993). Nonetheless, their active site structures and, to a large degree, their overall structures, are superimposable.

1.2 Electronic Absorption Spectra

1.2.1 Type 1 Cu Proteins

The intense absorption band near 600 nm (ϵ = 2,000-8,000 M^{-1} cm^{-1}) is one of the unique features used to characterize oxidized type 1 Cu sites (Adman, 1985). This band has been assigned as sulfur to Cu(II) charge transfer (CT) since the early studies of Solomon et al. (1976). A complete review of the electronic structures of the Cu-ligand bonding in type 1 and type 2 Cu proteins was published recently by Solomon and coworkers (1992). Their combined studies using polarized single crystal electronic absorption and low temperature magnetic circular dichroism (LTMCD) spectroscopy, together with SCF-Xα-SW calculations on plastocyanin reveal a detailed picture of the unusual Cu-S(Cys) interaction.

The ligand-field orbital energies of Cu-S(Cys) binding in plastocyanin are shown in Figure 1.4. The highest occupied orbitals in free thiolate are a doubly degenerate π set which are mostly S3*p* orbitals. Upon binding to the Cu, the Cu-S-C bond angle is 107°. As the result of bending, the two π orbitals split into non-degenerate levels. The higher-energy orbital is oriented perpendicular to the Cu-S-C plane and is thus π bonding to the Cu. The lower-energy orbital is now a σ bonding orbital having mostly S-C character. The remaining π level of the free ligand, the S3*p* orbital which is in the C-S-Cu plane, has electron density lying mostly along the S-Cu bond and has become σ bonding to the Cu. This has been defined as a pseudo-σ bond by Solomon et al. (1992). Therefore, in plastocyanin, the Cu-thiolate bond contains a strong π, a pseudo-σ, and a weak σ interaction (rather than a strong σ and two weak π interactions for a normal metal-sulfur bond). This unusual bonding occurs because of the Cu-S-C orientation, which changes the orbitals of the (Cys)S with respect to Cu, as shown in Figure 1.5.

A spectral analysis of plastocyanin is summarized in Figure 1.6A and Table 1.1 (Gewirth and Solomon, 1988). The low-energy bands 5 through 8, which are relatively weak in the absorption spectrum, are intense in the LTMCD spectrum and were identified as *d-d* transitions with the ordering $d_{x^2-y^2} \ll d_{z^2} \ll d_{xy} \ll d_{xy+yz} \ll d_{xz-yz}$ in the elongated C_{3v}-symmetry Cu site. The high-energy bands 1 and 2 were assigned to Met → Cu and His → Cu CT, respectively. The most intense band 4 at ~600 nm was identified as (Cys)S(π) → Cu CT, with the strong intensity being due to the good overlap between the ground and the excited state wave functions (Fig. 1.5B). Band 3 at ~535 nm was identified as (Cys)S(pseudo-σ) → Cu CT by these authors. Its intensity would also be expected to depend on the extent of overlap of the ground and the excited state wave functions.

Our studies of the Raman enhancement profiles of several type 1 Cu proteins (Chapter 4) have led us to question the assignment of bands 2 and 3. In the case of azurin, pseudoazurin, nitrite reductase, and Cu_2Cu_2H80C mutant SOD we found that the ~460-nm electronic transition can have large (Cys)S → Cu(II) CT character. Hence, we have proposed that both 460- and 600-nm absorptions are likely due to CT transitions of the Cu-S(Cys) chromophore. The occurrence of two different (Cys)S → Cu(II) CT transitions at ~460 and ~600 nm helps to explain the fact that although their relative absorptivities vary, the sum of ϵ_{460} and ϵ_{600} appears to be fairly constant (Chapter 4). The ~460-nm absorption band may well be due to (Cys)S(pseudo-σ) → Cu CT rather than, or in addition to, the His(p_1) → Cu CT suggested in Table 1.1.

A correlation between the intensity of the ~460-nm absorption band and Cu site geometry was discovered by Lu and coworkers (1993) and is more fully discussed in Chapter 4. A trigonal Cu site with a long Cu-S(Met) bond has a weak 460-nm absorption as in plastocyanin (Fig. 1.6A). A distorted tetrahedral Cu site with a shorter Cu-S(Met) bond and Cu out of the SNN plane has a stronger 460-nm absorption. NiR has a particularly tetrahedral site with Cu out of the SNN plane by 0.5 Å. The intensity of its ~460-nm absorption has greatly increased and, in fact, has become the most intense band in the spectrum (Fig. 1.5C). A similar spectrum is observed for Cu in the Zn-site of SOD-His80Cys (Fig. 1.5B), which is also believed to be tetrahedral. Therefore, the relative intensities of two absorption bands at ~460 and ~600 nm appear to be good indicators of Cu site geometry.

1.2.2 Type 2 Cu Proteins

Type 2 Cu proteins have absorption spectral properties resembling normal cupric inorganic complexes. The ligand-field transitions are weak ($\epsilon < 50\ M^{-1}\ cm^{-1}$) and occur between 550 and 800 nm. The ligand-to-metal charge-transfer transitions (LMCT) are generally at energies higher than 400 nm. Both σ and π transitions are expected with the σ transition at higher energy and with greater intensity due to its greater overlap with the $d_{x^2-y^2}$ orbital (Fig. 1.4a). With the same coordinated ligand set, the ligand-field transitions and LMCT transitions are expected to shift to lower energy when the Cu center geometry changes from tetragonal to tetrahedral (Fawcett et al., 1980; Lu, 1992). Cu_2Cu_2-SOD has both type 1 and type 2 Cu absorption spectra (Fig. 1.6D). The His → Cu CT bands at high energy are very weak and are overwhelmed by the strong protein absorption band at 280 nm. In the low energy region, the ligand field transitions are also very weak. The band at 664 nm (inset, curve 1) is due to the *d-d* transition of the square planar Cu (Cu in the Cu site), and the band at 810 nm (inset, curve 2) is due to the *d-d* transition of the tetrahedral Cu (Cu in the Zn site). The red shift is consistent with the geometry change from tetragonal to tetrahedral.

A type 2 Cu site containing a Cu-S(Cys) bond is expected to have an intense (Cys)S → Cu CT transition. In the SOD Cu-site mutant His46Cys, the Cu is coordinated by Cys in a distorted square planar site (Lu, 1992). As shown in Figure 1.6E, the absorption spectrum has a high energy band at 397 nm. The 397-nm band is likely due to (Cys)S(σ) → Cu CT, as illustrated in Figure 1.5A. In addition to the mutant His46Cys example, there are many other synthetic complexes containing a Cu-SR linkage (Kitajima, 1993; Chapter 4). These complexes usually have long Cu-SR bonds of about 2.25-2.35 Å and have more regular Cu centers such as square planar or square pyramidal. Absorption spectra of Cu complexes with aliphatic thiolates show an intense band between 380-520 nm (Chapter 4). The extinction coefficient is in the range of 1,000-4,000 $M^{-1}\ cm^{-1}$, similar to the value of type 1 Cu. These bands are assigned to the RS → Cu CT transitions, more specifically to the RS(σ) → Cu CT based on the theoretical interpretation of Solomon et al. (1992).

In conclusion, absorption spectral studies have exposed the differences between type 1 and type 2 Cu proteins, with or without the Cu-SR bond. Square planar

(tetragonal) versus tetrahedral geometries are readily distinguished by the *energies* of their *d-d* and LMCT bands. Trigonal planar versus tetrahedral geometries are distinguished by the *intensities* of their different S → Cu CT bands. The unusual absorption spectral properties of type 1 Cu proteins are a consequence of the Cu-S(Cys) being in a trigonal plane or tetrahedral coordination environment. How the absorption spectrum relates to the Cu-S(Cys) bond length is not yet clear. In addition, since most Cu-SR containing complexes have large ϵ values, we cannot use the ϵ value to distinguish type 1 and type 2 Cu sites. We also cannot distinguish between the two types when the absorption maximum is between 440 and 550 nm, but EPR and RR can address this topic.

1.3 Electron Paramagnetic Resonance Spectra

1.3.1 Type 2 Cu Proteins

Type 2 Cu proteins have EPR spectra similar to those of normal cupric complexes which exhibit a signal with $g_{\parallel} > g_{\perp} > 2.0023$ and a large parallel hyperfine splitting ($A_{\parallel} > 140 \times 10^{-4}$ cm^{-1}). The Cu site of SOD (His80Cys mutant) has $g_{\parallel} = 2.26$ and $g_{\perp} = 2.05$ (Fig. 1.7A). The fact that these observed g values deviate from 2.0023 and are anisotropic is due to the orbital angular momentum of the d orbitals and the orientations of the d orbitals in the applied magnetic field (Wertz and Bolton, 1986). The small rhombic splitting of $g_{\perp}$ indicates a lower symmetry of the Cu site, which is best described as a distorted square-planar Cu site in which the four His ligands are inequivalent.

A and g values are the two important features in the EPR spectrum (Addison, 1983). The g value is a measure of spin and orbital angular momentum. The magnitude of $g_{\parallel}$ in four-coordinate cupric complexes is determined by the following factors: the identity of the ligands, the coordination geometry, and the overall charge of the complex. With respect to the ligands, $g_{\parallel}$ values follow the series $O_4 < N_2O_2 < N_3O < N_4 < N_2S_2 < S_4$ (Fig. 1.8). This trend reflects an increasing covalency and decreasing ligand electronegativity. For a given set of ligands, $g_{\parallel}$ increases as the coordination geometry changes from square planar to tetrahedral. Although the overall charge on a cupric

complex has a relatively small effect on $g_{\parallel}$, in general increasing the positive charge increases $g_{\parallel}$.

The A value is a measure of electron-nuclear interaction, and is called the electron-nuclear hyperfine coupling constant (Addison, 1983). Generally, an increase of the positive charge on a cupric complex decreases the $A_{\parallel}$. For a given set of ligands, increasing distortion from square planar to tetrahedral invariably results in a decrease in the value of $A_{\parallel}$. Substitution of an N or O donor ligand for an S donor generally decreases $A_{\parallel}$ value, reflecting the increased bond covalency. However, formation of a Cu-SR bond does not in itself guarantee a small value of $A_{\parallel}$. As an example, the SOD Cu site mutant His46Cys has a type 2 EPR spectrum with a large $A_{\parallel}$ of 151 $\times$ 10^{-4} cm^{-1} (Chapter 4). There are other Cu-SR-containing complexes having large $A_{\parallel}$ as well (Chapter 4). Thus, both the ligand and the Cu site geometry are important in determining $A_{\parallel}$. For a given set of similar ligands, there is usually a linear relationship between increasing $g_{\parallel}$ and decreasing $A_{\parallel}$ as shown in Figure 1.8.

1.3.2 Type 1 Cu Proteins

$A_{\parallel}$ is the most important parameter used to distinguish type 1 and type 2 Cu proteins. As shown in Figures 1.7C and 1.8, all type 1 Cu proteins have small $A_{\parallel}$ values (10-90 $\times$ 10^{-4} cm^{-1}). The origin of this small $A_{\parallel}$ has been an interesting issue. The distorted tetrahedral (D_{2d}) $CuCl_4^{2-}$ complex also exhibits small EPR parallel hyperfine splittings similar to that of type 1 Cu proteins. This small $A_{\parallel}$ has been explained as arising from $4p_z$ mixing into the $3d_{x^2-y^2}$ ground state wave function in this distorted tetrahedral Cu complex (Bates et al., 1962; Yokoi and Addison, 1977; Roberts et al., 1980). The $4p_z$ orbital has a spin dipolar contribution which opposes that of the $3d_{x^2-y^2}$ orbital; thus this mixing reduces the coupling between the unpaired electron spin and the Cu nuclear spin. A 12% p_z mixing into $d_{x^2-y^2}$ would lower the value of $A_{\parallel}$ to the experimentally observed value (Sharnoff, 1965). Since most type 1 Cu proteins have their active sites described as distorted tetrahedral, the small value of $A_{\parallel}$ has also been explained by a $4p_z$ mixing mechanism. Thus, the small hyperfine values of type 1 Cu sites would depend on the geometry rather than on the presence of the Cu-S(Cys) bond.

Results from recent EPR and X-ray absorption spectroscopic (XAS) studies on a single crystal of plastocyanin, however, have eliminated the $4p_z$ mixing as the explanation for the small $A_\parallel$ in this protein (Solomon et al., 1992; Shadle et al., 1993). The Cu site in plastocyanin is best described as having elongated C_{3v} symmetry (Penfield et al., 1981). However, in C_{3v} symmetry, group theory allows the $3d_{x^2-y^2}$ orbital to mix with $4p_x p_y$ which would increase, not decrease, the $A_\parallel$ hyperfine splitting. Xα calculations indicate that the Cu site ground state wave function contains only $\sim$1% $4p$ mixing involving the $p_x p_y$ orbitals (Penfield et al., 1985; Gewirth and Solomon, 1988). This 1% $4p_x p_y$ mixing would not lead to a large $A_\parallel$, in agreement with the small $A_\parallel$ in plastocyanin. Similar calculations on the distorted tetrahedral (D_{2d}) $CuCl_4^{2-}$ complex indicate only $\sim$4% $4p_z$ mixing into the $d_{x^2-y^2}$ orbital (Gewirth et al., 1987), compared to the expected 12% mixing of the earlier model. Therefore, the $4p_z$ mixing explains partially the small $A_\parallel$ in the $CuCl_4^{2-}$ complex, but cannot be the reason for the small $A_\parallel$ in the type 1 Cu proteins.

According to Solomon and coworkers, the unusually high covalency of the Cu-thiolate bond becomes the effective origin of the reduction in the $A_\parallel$ constant of the type 1 Cu site (Shadle et al., 1993). Xα calculations indicate that the ground state wave function is highly covalent, consisting of 42% Cu $3d_{x^2-y^2}$ and 36% S(Cys) $3p$. A high degree of covalency delocalizes the unpaired electron spin from the Cu onto the Cys ligand, thereby reducing its coupling to the Cu nuclear spin. This explanation focuses on the unique Cu-S(Cys) bond as the most important feature of a type 1 Cu site. Interestingly, the Xα calculations on the (D_{2d}) $CuCl_4^{2-}$ complex do not indicate that its ground state wave function is unusually covalent (Gewirth et al., 1987). Furthermore, RR studies of the SOD mutants which provide a measure of Cu-S(Cys) bond lengths have indicated that this quantity does not correlate with the $A_\parallel$ value (Andrew et al., 1993). Therefore, the explanations for a small $A_\parallel$ may not be unique: both the nature of the Cu ligand and the Cu site geometry are important in establishing the $A_\parallel$ value.

In addition to the small $A_\parallel$, type 1 Cu proteins can be divided into two groups based on whether the X-band EPR spectrum is axial ($g_x = g_y$), or rhombic ($g_x \neq g_y$). For axial EPR spectra, the Cu site has an n-fold axis of symmetry (n = 3 for the type

1 Cu site). When the spectral character converts from axial to rhombic, the Cu site symmetry decreases, losing the n-fold symmetry. Examples of axial and rhombic EPR spectra can be seen in Figures 1.7A and 1.7C, respectively. Rhombic splitting of $g_\perp$ ($g_x \neq g_y$) could be initiated by pulling Cu away from the SNN plane by the fourth axial ligand, or by distortion in the SNN plane. In other words, an axial or a rhombic EPR spectrum does not necessarily correspond to a planar or non-planar Cu site, but indicates the symmetry of the Cu site. For these symmetry arguments, S is like N; i.e., the SNN plane has three-fold symmetry. One expects that all type 1 Cu proteins will show rhombicity to some extent because the two Cu-N(His) bonds are different from the Cu-S(Cys) bond, and this is, in fact, so in their Q-band EPR spectra (Penfield et al., 1985). However, there does appear to be a strong correlation between the axial ligand bond strength and EPR spectral properties. Type 1 Cu sites with rhombic EPR spectra tend to have structures closer to tetrahedral (Fig. 1.3B), whereas type 1 Cu sites with axial EPR spectra tend to have structures closer to trigonal planar (Fig. 1.3A). This is discussed in greater detail in Chapter 4.

1.4 Resonance Raman Spectra

1.4.1 Type 1 Cu Proteins

The extraordinary charge-transfer absorption bands of type 1 Cu proteins make RR spectroscopy a powerful tool for structural studies. Resonance Raman spectra of type 1 Cu proteins show the following common features: *(i)* excitation within the (Cys)S → Cu absorption band produces strong enhancement of as many as nine fundamental vibrational peaks in the 330-500 cm^{-1} region, in addition to one or two weak bands in the 250-300 cm^{-1} region; *(ii)* the RR spectra exhibit a multiplicity of intense bands (Fig. 1.8). The understanding of the spectra in terms of protein structure has come a long way since the first report in 1974; its evolution can be arranged into three periods: an early period (1974-1978); a transition period (1979-1988); and recent developments (1989-1993). A brief view of the history is given here to illustrate, in general, how a scientific problem is approached, how a technique has utility as well as pitfalls in the interpretation of results, and how the combination of results from several techniques makes maximal impact on the elucidation of the problem.

1.4.1.1 Early Period, 1974-1978

During this early phase, RR spectra were collected and categorized. Since no X-ray crystal structure was yet available, attempts were made to predict type 1 Cu center structure, geometry, and ligands. The first RR study was reported by Siiman and coworkers in 1974, and included the proteins stellacyanin, laccase, and ceruloplasmin (Siiman et al., 1974). Soon after, RR spectra of azurin, plastocyanin, and ascorbate oxidase were reported (Tosi et al., 1975; Miskowski et al., 1975; Siiman et al., 1975), and together make up the four noteworthy studies in this period. Common features of the spectra are a cluster of peaks around 400 cm^{-1}, and a weak peak near 260 cm^{-1}. The observed bands are all polarized, with depolarization ratios of about 0.3-0.6, indicative of totally symmetric vibrations. Peaks near 400 cm^{-1} were assigned to Cu-N or Cu-O bond stretching, where the N or O are not from aromatic ring ligands, and the weak band near 260 cm^{-1} was assigned to Cu-S(Cys) or Cu-N(His) stretching, with a preference for Cu-S stretching mode (Miskowski et al., 1975). These assignments were based on the knowledge of the inorganic cupric complexes, Cu(II) peptide complexes, and analogous protein systems. For the Cu-S(Cys) stretching frequency, only a limited number of systems were available for comparison and all these frequencies appear at <300 cm^{-1} (Ferris et al., 1978).

Core structures of type CuN_3S, or CuN_2OS, and CuN_3OS with N(amide), S(Cys), and O(carbonyl) as ligands were suggested. The Cu site geometry was predicted to be rather low, lower than the three-fold axial symmetry suggested by EPR spectra. The Cu was proposed to have either an approximately trigonal bipyramidal coordination, with a sulfur and two nitrogen ligands in the equatorial plane and less strongly bound nitrogen or oxygen ligands at axial positions, or a distorted tetrahedral coordination with one ligand at an axial position. It turns out that the predicted geometries are very close to what we know from X-ray structure analysis.

These early studies successfully predicted the Cu site geometry, pioneered the field, and defined some of the issues. However, several important problems were present. The first is that the intensity of the Cu-S(Cys) stretching mode assigned at ~ 280 cm^{-1} was too low. At that time, it was clear that the intense ~ 600-nm absorption was a LMCT involving Cys sulfur to Cu (Solomon et al., 1976). Therefore, the Cu-

S(Cys) stretching frequency is expected to be the most strongly enhanced mode based on Franck-Condon overlap arguments. The second is the multiplicity of peaks near 400 cm^{-1}. It was believed that the *number* of ligands could be determined simply by counting the *number* of peaks in the belief that only metal-ligand stretching bands were active and that internal ligand modes could not contribute to the RR spectrum in this region (Miskowski et al., 1975).

1.4.1.2 Transition Period, 1979-1988

The first X-ray crystal structure of a type 1 Cu protein (plastocyanin) was reported in 1978 (Colman et al., 1978). This milestone launched RR studies into a transitional period wherein the emphasis became the understanding of the spectra in terms of the known structures. The structural data of plastocyanin and, soon to follow, two azurins (Adman et al., 1978; Norris et al., 1983), established the identity of the ligands as N_2SS^*, where the two nitrogens are imidazoles from His residues, S is Cys, and S* is the thioether of Met. A surprisingly short Cu-S(Cys) bond of 2.13 Å was discovered, and the Cu is indeed in a trigonal bipyramidal (azurins) or a distorted tetrahedral (plastocyanin) coordination environment.

Crystallographic evidence of the unusually short Cu-S(Cys) bond now suggested that the Cu-S stretching frequency may be as high as 400 cm^{-1}, where a cluster of intense peaks is observed. The high intensity of the 400-cm^{-1} bands supports their assignment as Cu-S(Cys) related modes, which would be strongly enhanced during (Cys)S → Cu CT. The Cu-N(His) stretches were reassigned to the 260-cm^{-1} band. The Cu-S*(Met) stretching mode could not be at $\sim$400 cm^{-1} because of the long Cu-S*(Met) bond (2.92 Å in plastocyanin; 3.13 Å in *A. denitrificans* azurin). Based on studies of thioether model complexes, the Cu-S(Met) stretch was then proposed to be near 260 cm^{-1} (Ferris et al., 1978). However, resonance Raman studies of Se-methionine-substituted azurin offered convincing evidence that an assignment of the 260-cm^{-1} band to the Cu-S*(Met) stretching mode was also unlikely (Thamann et al., 1982). Normal coordinate analysis on a five-atom model ML_4 (L = S,N,N,S*; Thamann et al., 1982) suggested for the first time that trigonal rather than tetrahedral was the appropriate description of the Cu site in azurin, in agreement with the structural data. This work also emphasized the likelihood of coupled vibrational motions. However, the persistent belief that the RR

peaks represented M-ligand stretches exclusively failed to explain the spectral multiplicity.

Attempts to explain the spectral multiplicity and improve spectral quality were further aspects of RR studies in this period. Since 1983, most of the spectra were recorded under cryogenic conditions (Woodruff et al., 1983), in which dramatic improvements in spectral resolution and signal-to-noise ratio allowed the observation of features that had previously gone unnoticed. The most obvious discovery was that there are at least nine peaks between 330-500 cm^{-1}, far too many to be accounted for entirely by M-ligand stretches. Clearly, ligand internal motions must also be resonance enhanced. With the recognition of the contribution of ligand internal modes, the large number of RR bands became tenable but needed to be proved experimentally. A large number of studies, including Ainscough et al. (1987), Blair et al. (1985), Maret et al. (1983; 1986) and Nestor et al. (1984), with efforts in H/D and $^{63/65}Cu$ isotope labeling, ligand substitutions, excitation profiles, and additional vibrational analyses on improved models, were performed. Much of this and earlier work was reviewed by Woodruff et al. (1988).

The most important conclusions of the work from this period are summarized below: *(i)* The only Cu-ligand stretching mode near 400 cm^{-1} is the Cu-S(Cys) stretch, and the remainder of the fundamental motions near this frequency are Cys and His internal deformations. *(ii)* All the observed modes near 400 cm^{-1} are highly mixed, and most derive their intensity by coupling with the Cu-S(Cys) stretching mode. *(iii)* The Cu-N(His) stretching motion(s) is(are) best identified with the peak(s) near 260 cm^{-1}.

The realization that ligand internal motions participate to give rise to the complex RR spectra of type 1 Cu protein is the most important development during this time, even though no direct evidence was yet available. Only selective mutations and further, careful isotope labeling studies on Cu ligands have made it possible to address this issue.

1.4.1.3 Recent Developments, 1989-1993

Advances in other fields are now brought to bear on the reinterpretation of the RR data. The most significant achievements are as follows: *(i)* Seven type 1 Cu proteins have refined or high-resolution X-ray crystal structures including the new members of *Alcaligenes faecalis* pseudoazurin (Petratos et al., 1988; Adman et al., 1989) and

Achromobacter cycloclastes nitrite reductase (2.5-Å resolution) (Godden et al., 1991). *(ii)* The near-coplanarity of the Cu-Cys side chain, as revealed by crystallography for several azurins and plastocyanins makes Cys the most likely candidate involved in the coupling (Han et al., 1991). *(iii)* Protein engineering techniques are successfully used in making site-directed mutants (den Blaauwen and Canters, 1993; Lu, 1992). *(iv)* The first good low MW model for a type 1 Cu site is reported (Kitajima et al., 1990). *(v)* Many new copper proteins as well as the mutants are spectroscopically characterized. With this enormous amount of new information, RR studies can now focus not only on better assignments for the RR spectra of type 1 Cu proteins, but also on finding relationships between spectroscopic properties and protein structure.

The major RR studies in this period are presented and discussed in Chapters 3-5. Of particular importance are the studies on isotope-labeled azurin ($^{15/14}$N and $^{34/32}$S) and several azurin ligand mutants. The principal conclusions from this work are the following: *(i)* The most intense Raman band has the greatest Cu-S(Cys) bond character and is predominantly the Cu-S(Cys) stretch. The frequency differences of this band among various type 1 Cu proteins reflect small variations in their Cu-S(Cys) bond strengths, caused by changes in Cu site geometry and/or the ligand field. These small variations in Cu-S(Cys) bond strength are beyond the precision of the X-ray structure determinations. From this point of view, RR is a more sensitive method for probing the Cu-S(Cys) bond. *(ii)* The multiple intense peaks near 400 cm^{-1} are due to the coupling of Cu-S(Cys) stretching with Cys deformation modes, but, most likely, do not include His ligand internal modes. Both kinematic and vibronic coupling are likely to be involved. The conformation of the Cu-S(Cys) moiety, in which the five atoms Cu-S_γ-C_β-C_x-$N_{peptide}$ are essentially coplanar, is a conserved feature common to all structurally characterized type 1 Cu proteins, and can account for the extensive kinematic coupling. *(iii)* One or two weak bands in the 250-300 cm^{-1} region are due to Cu-N(His) interaction. Observation of this mode may depend on the imidazole-ring orientation relative to the primary Cu-SNN coordination plane. *(iv)* Resonance Raman excitation profiles indicate multiple Cys → Cu CT transitions in type 1 Cu proteins. Absorptions near 460 and 600 nm are both characteristic of type 1 Cu sites. *(v)* The relatively constant set of Raman

frequencies of all type 1 Cu proteins is the consequence of the highly conserved ground state structure of the Cu-S(Cys) moiety, especially the conformation of the Cys side chain. The conserved Cu-S_γ-C_β-C_α-N conformation may indicate a favored pathway for electron transfer. *(vi)* The RR spectrum appears to detect predominantly the Cu-S(Cys) moiety: the Cu-S bond strength and the conformation of the cysteinate ligand. Thus, RR spectroscopy is sensitive to different factors than those detected by EPR spectroscopy.

1.4.2 Type 2 Cu Proteins

Generally, type 2 Cu proteins do not have resonance-enhanced Raman spectra because of the absence of a suitable chromophore, and, consequently, it is hard to obtain Cu-ligand vibrational information. However, type 2 Cu complexes of proteins containing a Cu-SR linkage can show resonance-enhanced Raman spectra through the RS → Cu CT transition at ~400 nm. Their RR spectra are discussed in Chapter 4 and other publications from this laboratory (den Blaauwen et al., 1993; Andrew et al., 1993). Their spectral properties differ from those of type 1 Cu proteins in the following aspects: *(i)* The frequency of the most intense RR band is within the 320- to 360-cm^{-1} region, about 20-100 cm^{-1} lower than those in type 1 Cu proteins. *(ii)* Raman band intensities are much lower than those in type 1 Cu proteins. *(iii)* The RR spectra generally show fewer peaks than those of type 1 Cu proteins, giving the two classes different spectral patterns. These differences can be explained based on the structural properties of the type 2 Cu site: the longer Cu-SR bond may account for the low Cu-SR stretching frequency; the weaker interaction between Cu and the SR ligand may account for the low RR intensity. Finally, the square planar geometry of the type 2 site, which could disrupt the coplanarity of the Cu-S(Cys) moiety, may account for the low Raman intensity and fewer enhanced bands due to impaired coupling.

In conclusion, RR spectroscopy is an effective technique for the characterization of the Cu-SR bond. From the frequency of the most intense band, the RR spectrum can provide information on the Cu-SR bond strength, which is under the influence of the other Cu ligands and the site geometry. The RR spectra assist in the identification of type 1 and type 2 Cu sites. The short Cu-S(Cys) bond in a trigonal or a distorted tetrahedral site with conserved Cys side chain conformation are the essential properties

of the type 1 Cu site that makes it such an excellent RR chromophore. Nonetheless, significant advances in the elucidation of the copper active-site properties have come about from a variety of approaches and techniques. The principal physical properties discussed here and in later chapters involve electronic and vibrational spectroscopy, EPR spectroscopy, and X-ray crystallography, as well as the powerful new techniques afforded via molecular biology.

References

Addison, A. W. (1983) in Copper Coordination Chemistry: Biochemical and Inorganic Perspectives (Karlin, K. D., and Zubieta, J., eds) pp 109-128, Adenine Press, New York.

Adman, E. T. (1985) in Metalloproteins (Harrison, P., ed.), Part I, pp 1-42, Verlag Chemie, Weinheim, Germany

Adman, E. T. (1991) Adv. Protein Chem. 42, 145-197.

Adman, E. T., Stenkamp, R. E., Sieker, L. C., and Jensen, L. H. (1978) J. Mol. Biol. 123, 35-40.

Adman, E. T., Turley, S., Bramson, R., Petratos, K., Banner, D., Tsernoglou, D., Beppu, T., and Watanabe, H. (1989) J. Biol. Chem. 264, 87-99.

Ainscough, E. W., Bingham, A. G., Brodie, A. M., Ellis, W. R., Gray, H. B., Loehr, T. M., Plowman, J. E., Norris, G. E., and Baker, E. N. (1987) Biochemistry 26, 71-82.

Andrew, C. R., Yeom, H., Han, J., Loehr, T. M., Sanders-Loehr, J., and Valentine, J. S. (1993), in preparation.

Baker, N. E. (1988) J. Mol. Biol. 203, 1071-1095.

Bates, C. A., Moore, W. S., Standley, K. J., and Stevens, K. W. H. (1962) Proc. Phys. Soc. 79, 73-83.

Blair, D. F., Campbell, G. W., Schoonover, J. R., Chan, S. I., Gray, H. B., Malmström, B. G., Pecht, I., Swanson, B. I., Woodruff, W. H., Cho, W. K., English, A. M., Fry, H. A., Lum, V., and Norton, K. A. (1985) J. Am. Chem. Soc. 107, 5755-5766.

Colman, P. M., Freeman, H. C., Guss, J. M., Morata, M., Norris, V. A., Ramshaw, J. A. M., and Venkatappa, M. P. (1978) Nature 272, 319-324.

den Blaauwen, T., Hoitink, C. W. G., Canters, G. W., Han, J., Loehr, T. M., and Sanders-Loehr, J. (1993), submitted.

den Blaauwen, T., and Canters, G. W. (1993) J. Am. Chem. Soc. 115, 1121-1129.

Fawcett, T. G., Bernarducci, E. E., Krogh-Jespersen, K. K., and Schugar, H. J. (1980) J. Am. Chem. Soc. 102, 2598-2604.

Fee, J. A. (1975) Struct. Bonding (Berlin) 23, 1-60.

Ferris, N. S., Woodruff, W. H., Rorabacher, D. B., Jones, T. E., and Ochrymowycz, L. A. (1978) J. Am. Chem. Soc. 100, 5939-5942.

Forster, D., and Weiss, V. W. (1968) J. Phys. Chem. 72, 2669-2671.

Garrett, T. P. J., Clingeleffer, D. J., Guss, J. M., Rogers, S. J., and Freeman, H. C. (1984) J. Biol. Chem. 259, 2822-2825.

Getzoff, E. D., Tainer, J. A., Weiner, P. K., Kollman, P. A., Richardson, J. S., and Richardson, D. C. (1983) Nature (London) 306, 287-290.

Gewirth, A. A., Cohen, S. L., Schugar, H. J., and Solomon, E. I. (1987) Inorg. Chem. 26, 1133-1146.

Gewirth, A. A., and Solomon, E. I. (1988) J. Am. Chem. Soc. 110, 3811-3819.

Godden, J. W., Turley, S., Teller, D. C., Adman, E. T., Liu, M. Y., Payne, W. J., and LeGall, J. (1991) Science 253, 438-442.

Gould, D. C., and Ehrenberg, A. (1968) Eur. J. Biochem. 5, 451-455.

Guss, J. M., Bartunik, H. D., and Freeman, H. C. (1992) Acta Cryst. B 48, 790-811.

Han, J., Adman, E. T., Beppu, T., Codd, R., Freeman, H. C., Hug, L., Loehr, T. M., and Sanders-Loehr, J. (1991) Biochemistry 30, 10904-10913. [Chapter 3]

Han, J., Blackburn, N. J., and Loehr, T. M. (1992) Inorg. Chem. 31, 3223-3229.

Han, J., Loehr, T. M., Lu, Y., Valentine, J. S., Averill, B. A., and Sanders-Loehr, J. (1993) J. Am. Chem. Soc. 115, 4256-4263. [Chapter 4]

Kitajima, N. (1993) Adv. Inorg. Chem., in press.

Kitajima, N., Fujisawa, K., and Moro-oka, Y. (1990) J. Am. Chem. Soc. 112, 3210-3212.

Lu, Y. (1992) Ph.D. dissertation, University of California-Los Angeles.

Lu, Y., Lacroix, L. B., Lowery, M. D., Solomon, E. I., Bender, C. J., Peisach, J., Row, J. A., Gralla, E. G., and Valentine, J. S. (1993) J. Am. Chem. Soc. 115, in press.

Maret, W., Shiemke, A. K., Wheeler, W. D., Loehr, T. M., and Sanders-Loehr, J. (1986) J. Am. Chem. Soc. 108, 6351-6359.

Maret, W., Zeppezauer, M., Loehr, T. M., and Sanders-Loehr, J. (1983) Biochemistry 22, 3202-3206.

Miskowski, V., Tang, S.-P. W., Spiro, T. G., Shapiro, E., and Moss, T. H. (1975) Biochemistry 14, 1244-1250.

Nestor, L., Larrabee, J. A., Woolery, G., Reinhammar, B., and Spiro, T. G. (1984) Biochemistry 23, 1084-1093.

Norris, G. E., Anderson, B. F., and Baker, E. N. (1983) J. Mol. Biol. 165, 501-521.

Ouzounis, C., and Sander, C. (1991) FEBS Lett. 279, 73-78.

Peisach, J., and Blumberg, W. E. (1974) Arch. Biochem. Biophys. 165, 691-708.

Penfield, K. W., Gay, R. R., Himmelwright, R. S., Eickman, N. C., Norris, V. A., Freeman, H. C., and Solomon, E. I. (1981) J. Am. Chem. Soc. 103, 4382-4388.

Penfield, K. W., Gewirth, A. A., and Solomon, E. I. (1985) J. Am. Chem. Soc. 107, 4519-4529.

Petratos, K., Dauter, Z., and Wilson, K. S. (1988) Acta Crystallogr. B44, 628-636.

Roberts, J. E., Brown, T. G., Hoffman, B. M., and Peisach, J. (1980) J. Am. Chem. Soc. 102, 825-829.

Ryden, L. G., and Hunt, L. T. (1993) J. Mol. Evol. 36, 41-66.

Shadle, S. E., Penner-Hahn, J. E., Schugar, J. J., Hedman, B., Hodgson, K. O., and Solomon, E. I. (1993) J. Am. Chem. Soc. 115, 767-776.

Sharnoff, M. (1965) J. Chem. Phys. 42, 3383-3395.

Shepard, W., Anderson, B. F., Baker, E. N., and Norris, G. E. (1990) Abstr. Congr. Int. Union Crystallogr. 16, C-85.

Siiman, O., Young, N. M., and Carey, P. R. (1974) J. Am. Chem. Soc. 97, 4483-5585.

Siiman, O., Young, N. M., and Carey, P. R. (1975) J. Am. Chem. Soc. 98, 744-748.

Solomon, E. I., Baldwin, M. J., and Lowery, M. D. (1992) Chem. Rev. 92, 521-542.

Solomon, E. I., Hare, J. W., and Gray, H. B. (1976) Proc. Natl. Acad. Sci. USA 73, 1389-1393.

Tainer, J. A., Getzoff, E. D., Beem, K. M., Richardson, J. S., and Richardson, D. C. (1982) J. Mol. Biol. 160, 181-217.

Tainer, J. A., Getzoff, E. D., Richardson, J. S., and Richardson, D. C. (1983) Nature 306, 284-287.

Thamann, T. J., Frank, P., Willis, L. J., and Loehr, T. M. (1982) Proc. Natl. Acad. Sci. USA 79, 6396-6400.

Tosi, L., Garnier, A., Herve, M., and Steinbuch, M. (1975) Biochem. Biophys. Res. Commun. 65, 100-106.

Valentine, J. S., and Pantoliano, M. W. (1981) in Copper Proteins (Spiro, T. G., ed.) pp 293-357, Wiley, New York.

Wertz, J. E., and Bolton, J. R. (1986) Electron Spin Resonance, pp 17-20, 131-161, Chapman Hall, New York.

Woodruff, W. H., Norton, K. A., Swanson, B. I., and Fry, H. A. (1983) J. Am. Chem. Soc. 105, 657-658.

Woodruff, W. H., Dyer, R. B., and Schoonover, J. R. (1988) Applications of Raman Spectroscopy (Spiro, T. G., ed.) Vol. 3, pp 413-438, Wiley, New York.

Yokoi, H., and Addison, A. W. (1977) Inorg. Chem. 16, 1341-1349.

Table 1.1. Assignments of the Electronic Absorption Spectra of Plastocyanin and Cu_2Cu_2-SOD-His80Cys[a]

Band	Assignment	Plastocyanin		SOD-His80Cys	
		cm^{-1}	nm	cm^{-1}	nm
8	dz2	~5,500	~1,820	4,000	~2,500
7	dxy	10,800	925	8,425	1,190
6	dxz+yz	12,800	780	10,950	915
5	dxz-yz	13,950	715	12,400	800
4	Cys-π	16,700	600	17,000	590
3	pseudo-σ	18,700	535	19,000	525
2	His-p_1	21,390	470	21,850	460
1	Met-a_1	23,440	430	25,500	390
0	---	32,500	310	~33,750	300

[a]Data for plastocyanin are adapted from Gewirth et al. (1988); data for SOD Zn site mutant His80Cys are adapted from Lu et al. (1993).

FIGURE LEGENDS

Figure 1.1. Schematic folding topology of copper proteins. The striped sphere is the copper atom. The ligand residues are marked by small open spheres. H, His; C, Cys; M, Met. Dark arrows indicate strands of β-sheet in the C-terminal layer of the β-sandwich. (A) Azurin. (B) Superoxide dismutase. The large open sphere is the zinc atom. (C) Nitrite reductase domain 1. The type 1 Cu is in the upper loop and the type 2 Cu is in the central β-sheet region. (D) Trimeric arrangement of NiR. Figures are adapted from Adman (1991).

Figure 1.2. Active sites of copper proteins. (A) Type 1 Cu site in azurin from *A. denitrificans* (drawing obtained from E. N. Baker). Dashed lines indicate H-bonds between residues. (B) Type 2 Cu site in yeast Cu_2Zn_2-SOD (from Han et al., 1993).

Figure 1.3. Geometries of Cu(II)-S(Cys) complexes. The large filled sphere is the Cu atom, and the small open spheres are the ligands. (A) A trigonal planar site formed by the strong SNN ligands in type 1 Cu protein. (B) Type 1 Cu site could distort toward tetrahedral due to Cu moving away from the trigonal plane toward the 4th ligand. In an ideal tetrahedral site the Cu is 0.7 Å away from the trigonal plane. (C) An ideal square planar site for type 2 Cu. Arrows indicate that there is generally some tetragonal distortion. Figure from Lu et al. (1993).

Figure 1.4. Energy level diagram showing Cu-S(Cys) bonding of the type 1 Cu site of plastocyanin. The levels are not in accurate scale. Diagram based on Solomon et al. (1988, 1992).

Figure 1.5. Proposed Cu(II)-SR bonding mechanisms. (A) "normal" bonding in a type 2 Cu site with a strong σ and two weak π interactions. (B) Cu(II)-S(Cys) bonding in plastocyanin with a strong π, a pseudo-σ (orbital not shown), and a weak σ interaction. The orientations of (Cys)S and Cu orbitals are changed due to the Cu-S-C angle. This results in a reduction of the σ overlap and an increase of the π overlap. Diagram from Lu et al. (1993).

Figure 1.6. Electronic absorption spectra of Cu proteins. (A) Plastocyanin (Gewirth and Solomon, 1988). (B) Cu in Zn site of His80Cys-SOD. (C) *A. cycloclastes* nitrite reductase (Chapter 4). (D) Wild-type SOD. Curve 1: apoprotein plus 2 eq Cu^{2+} (Cu in Cu site); curve 2: apoprotein plus 4 eq Cu^{2+} (Cu in Cu and Zn sites). (E) SOD Cu site mutant His46Cys. Spectra B, D, and E are adapted from Lu (1992).

Figure 1.7. EPR spectra of SOD Zn-site mutant H80C. (A) Apoprotein plus 2 equivalents of Cu (in type 2 Cu site). (B) Apoprotein plus 4 equivalents of Cu (in Cu and Zn sites). (C) Spectrum B - A = spectrum of Cu in type 1 (Zn) site. From Lu et al. (1993).

Figure 1.8. The relationship between $g_{\parallel}$ and $A_{\parallel}$ for Cu proteins (●) and model compounds (- - -). From Peisach and Blumberg (1974).

Figure 1.9. RR spectrum of azurin from *A. denitrificans* obtained with 647.1-nm excitation. The inset shows high frequency overtones and combination bands derived from the low frequency fundamentals, particularly the most intense peak at 411 cm^{-1}. From Ainscough et al., 1987.

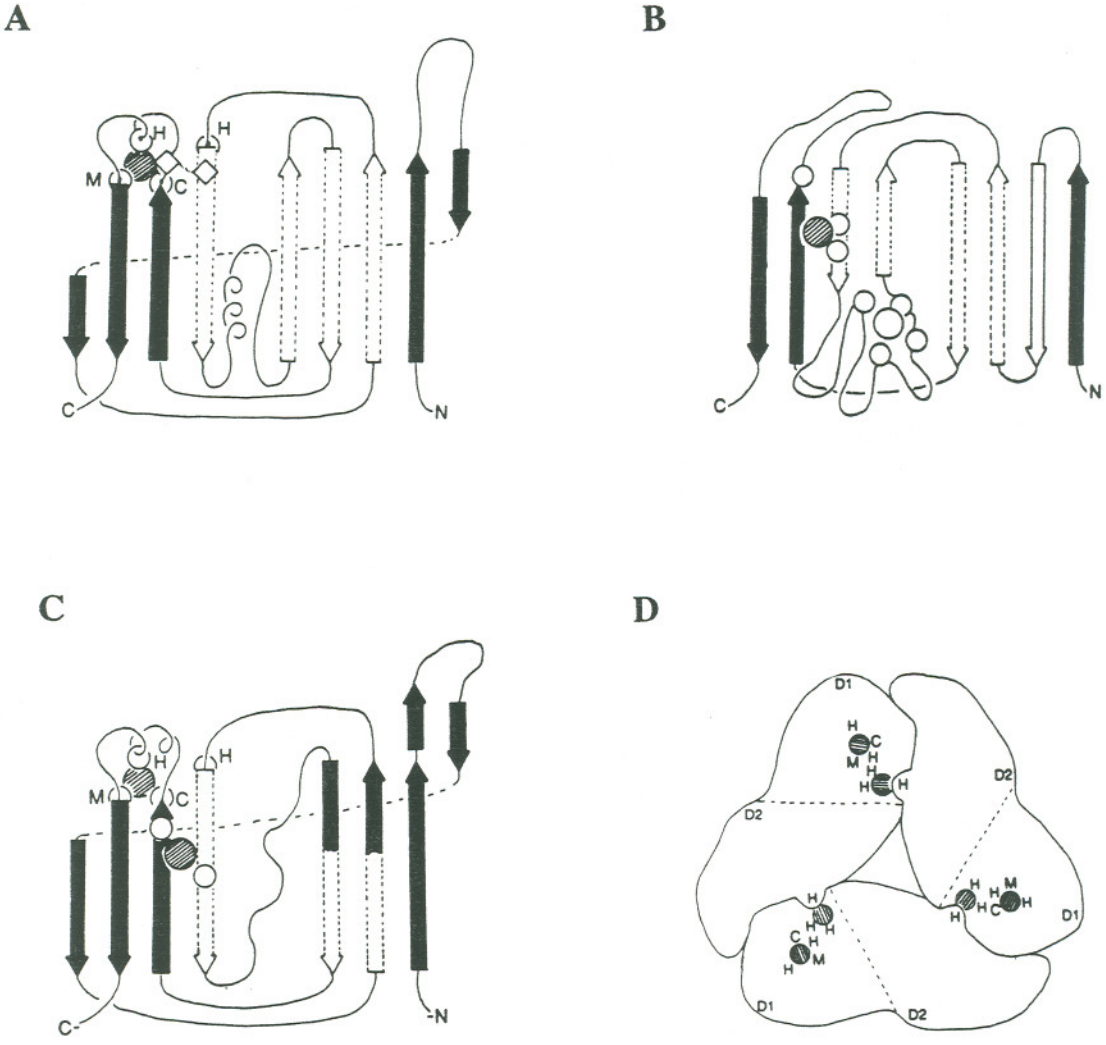

Figure 1.1

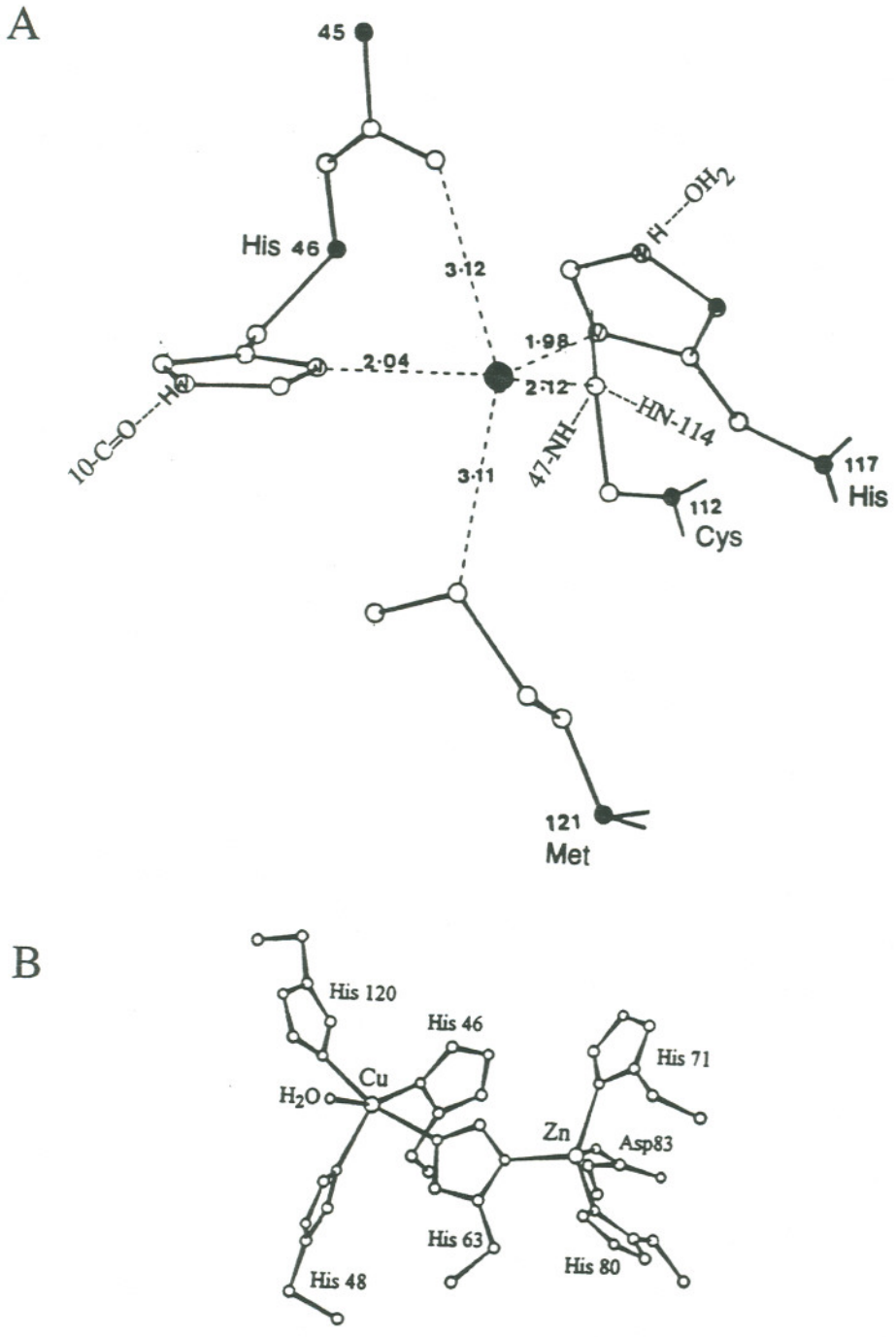
A
45
His 46
3·12
2·04
1·98
2·12
3·11
10-C=O---H
47-NH
HN-114
117
His
112
Cys
121
Met
B
His 120
His 46
Cu
H_2O
His 71
Zn
Asp83
His 63
His 48
His 80

Figure 1.2

A. Trigonal

B. Tetrahedral

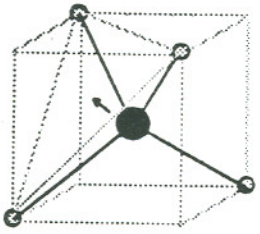

C. Tetragonal

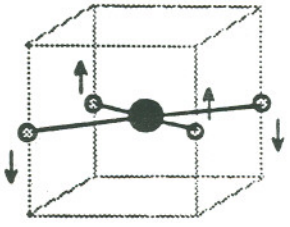

Figure 1.3

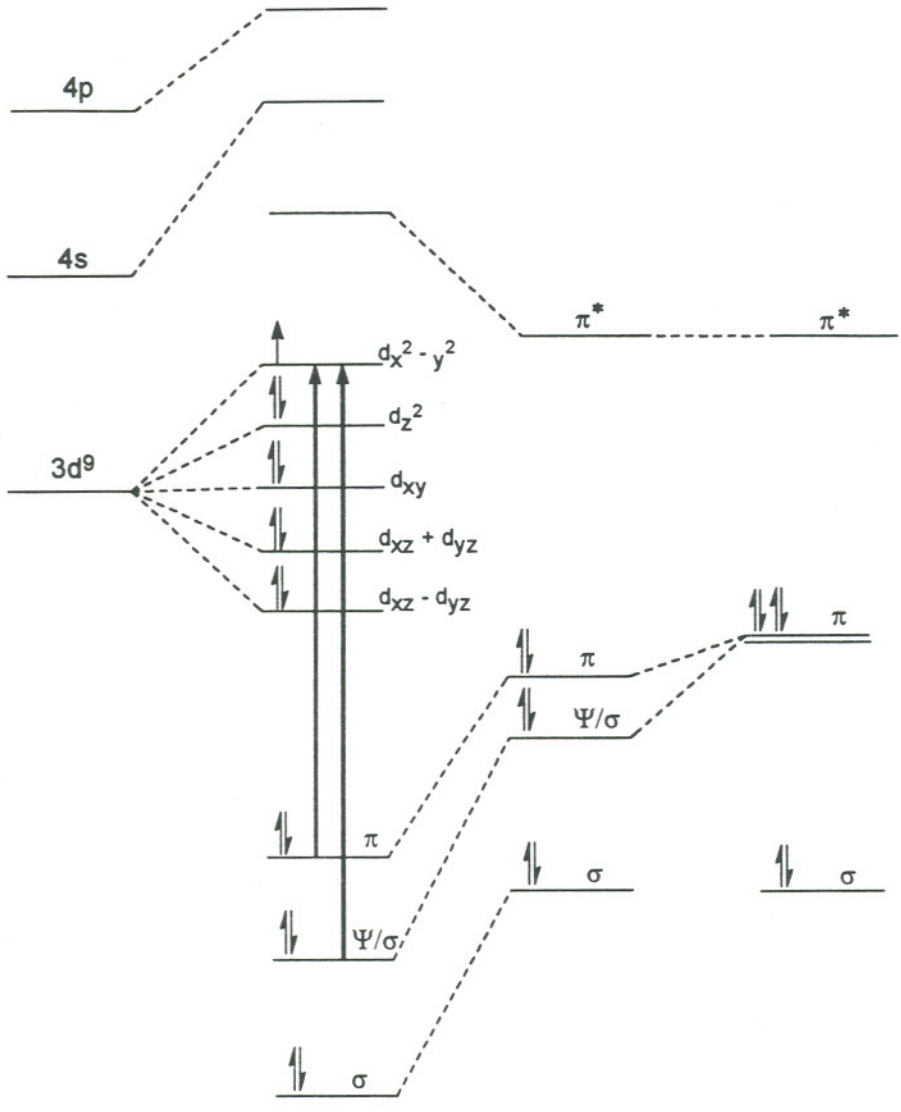
4p
4s
π*
π*
$d_{x^2-y^2}$
d_{z^2}
$3d^9$
d_{xy}
$d_{xz} + d_{yz}$
$d_{xz} - d_{yz}$
π
π
Ψ/σ
π
σ
σ
Ψ/σ
σ
Cu(II)
Cu - S(Cys) in *Pc*
$(Cys)S^-$ in *Pc*
$(Cys)S^-$

Figure 1.4

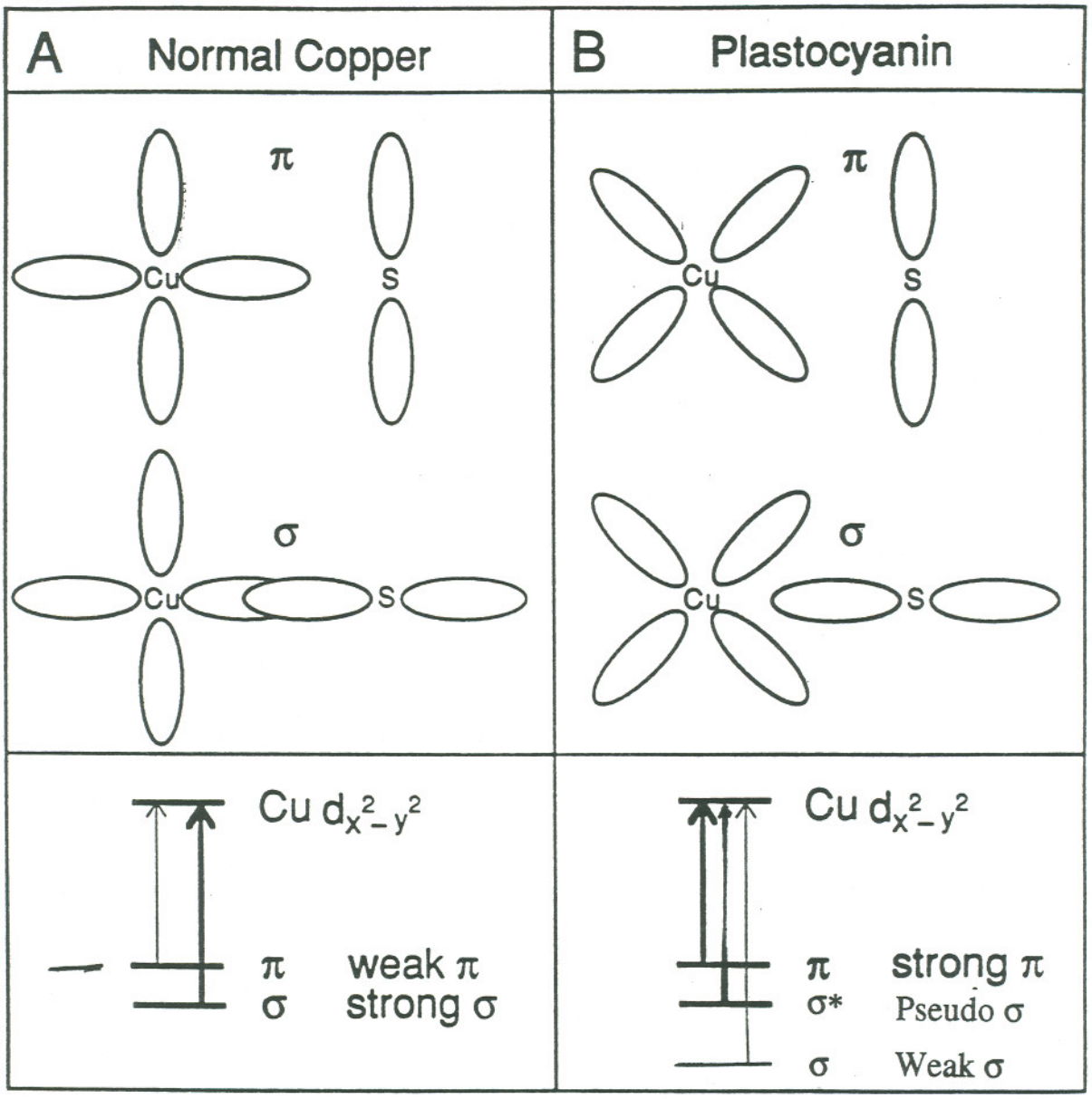
A
Normal Copper
B
Plastocyanin
π
σ
Cu
S
Cu $d_{x^2-y^2}$
π
σ
weak π
strong σ
Cu $d_{x^2-y^2}$
π
σ*
σ
strong π
Pseudo σ
Weak σ

Figure 1.5

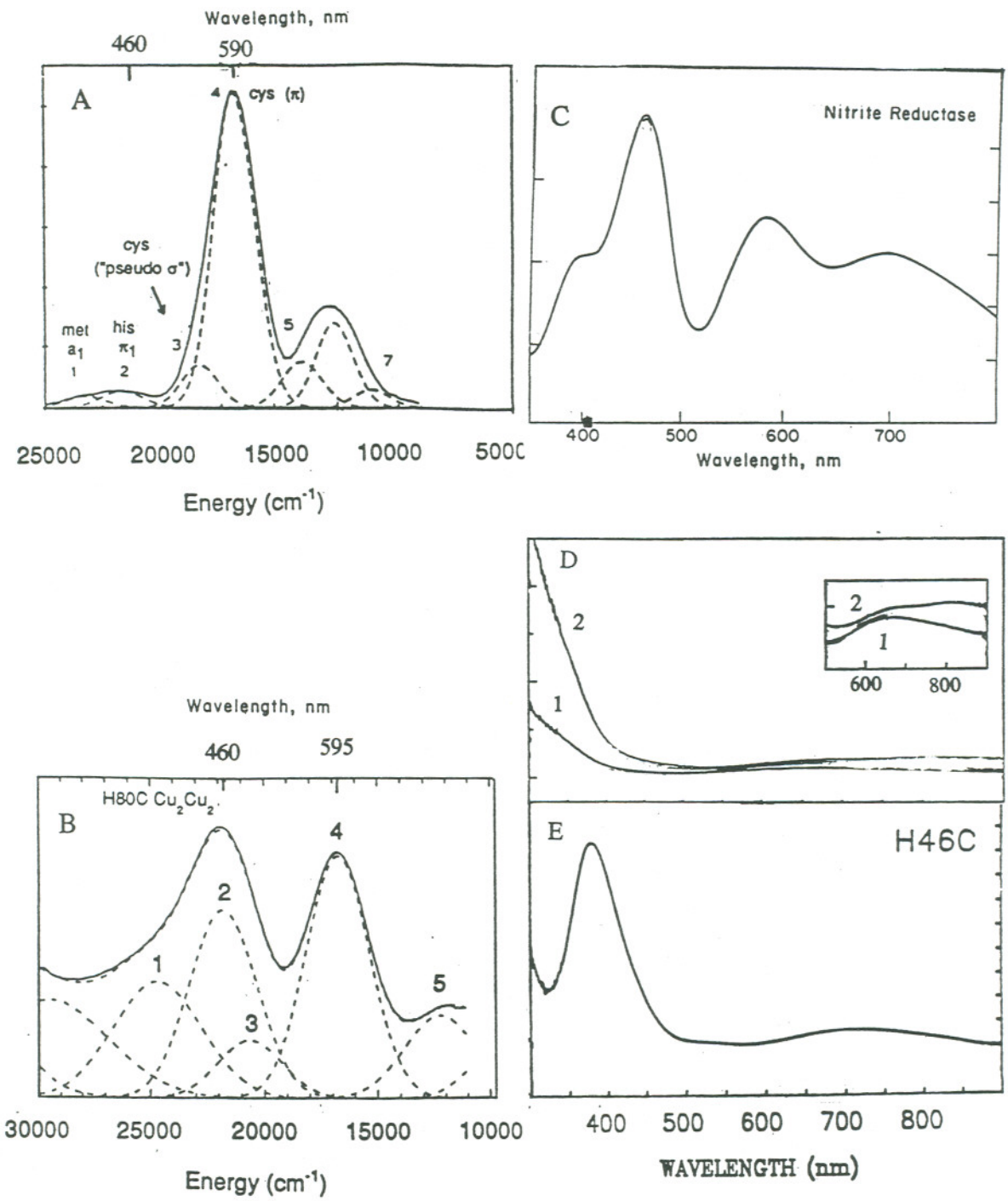
Wavelength, nm
460
590
A
cys (π)
cys
("pseudo σ")
met
a1
1
his
π1
2
3
4
5
7
25000
20000
15000
10000
5000
Energy (cm-1)
C
Nitrite Reductase
400
500
600
700
Wavelength, nm
D
2
1
600
800
Wavelength, nm
460
595
B
H80C Cu2Cu2
1
2
3
4
5
30000
25000
20000
15000
10000
Energy (cm-1)
E
H46C
400
500
600
700
800
WAVELENGTH (nm)

Figure 1.6

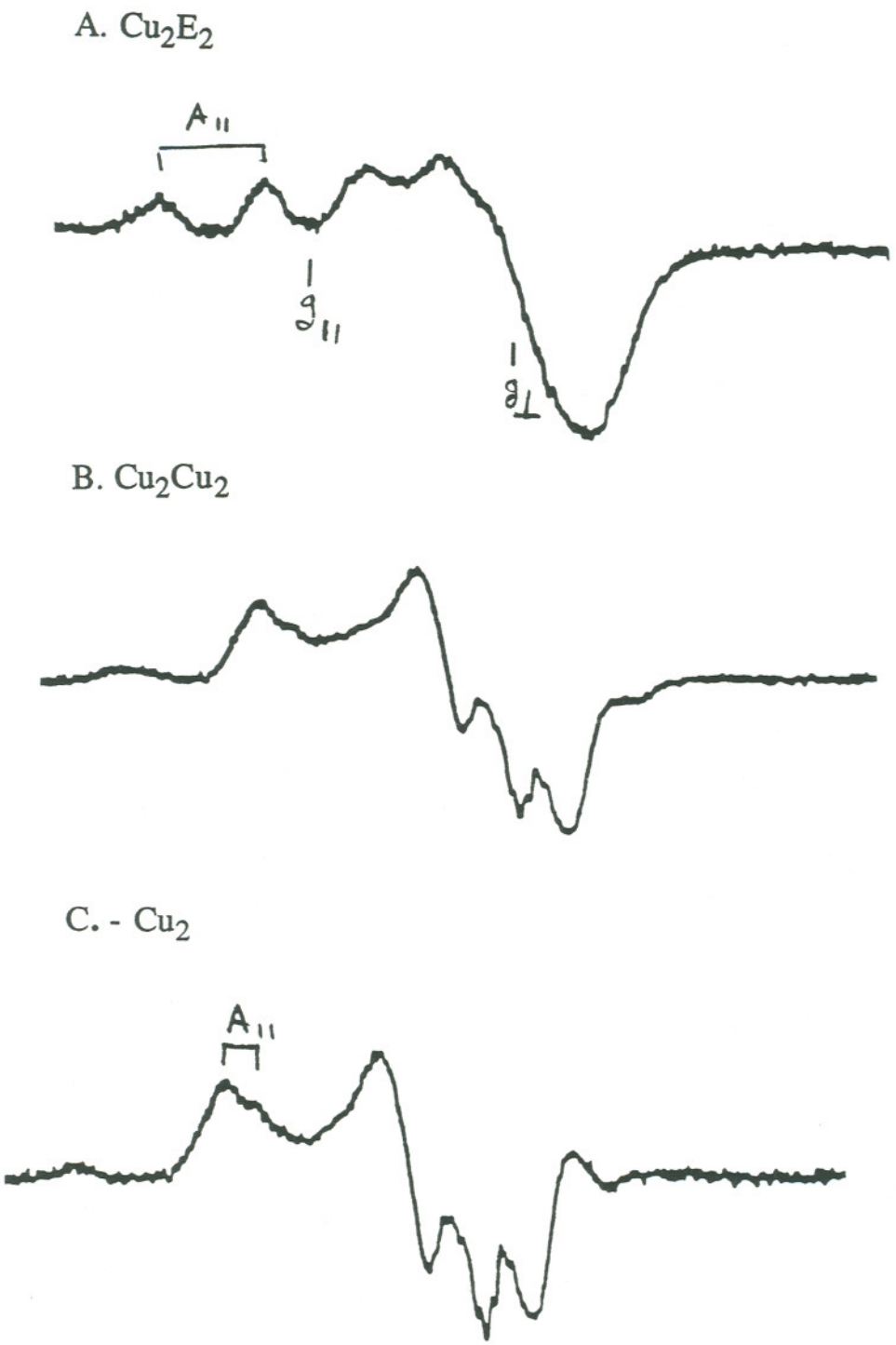

Figure 1.7

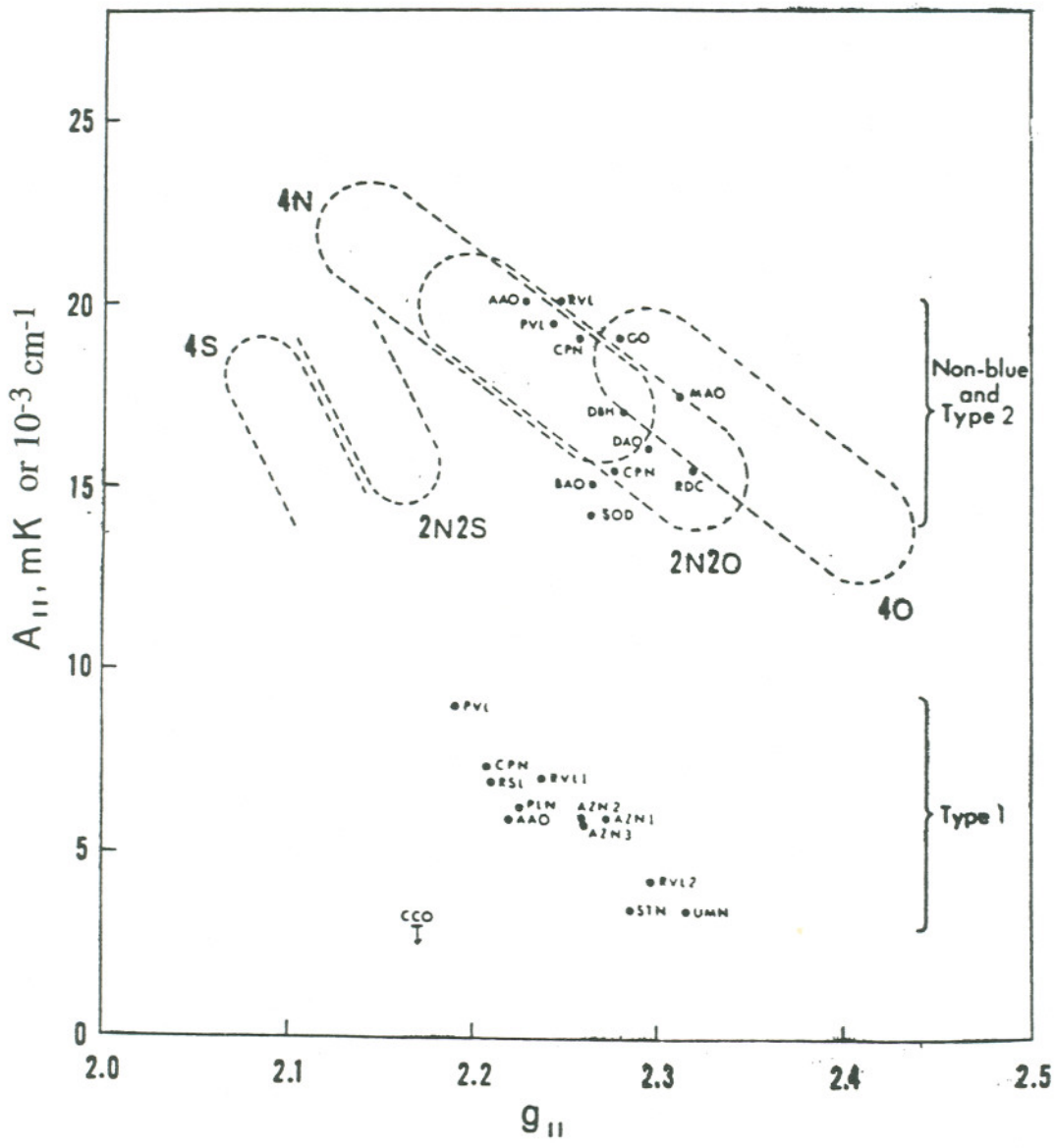
4N
4S
2N2S
2N2O
4O
Non-blue and Type 2
Type 1
AAO
RVL
PVL
CPN
CO
MAO
DBH
DAO
BAO
RDC
SOD
RSL
RVL1
PLN
AZN2
AZN1
AZN3
RVL2
STN
UMN
CCO
A_{II}, mK or 10^{-3} cm^{-1}
g_{II}
0
5
10
15
20
25
2.0
2.1
2.2
2.3
2.4
2.5

Figure 1.8

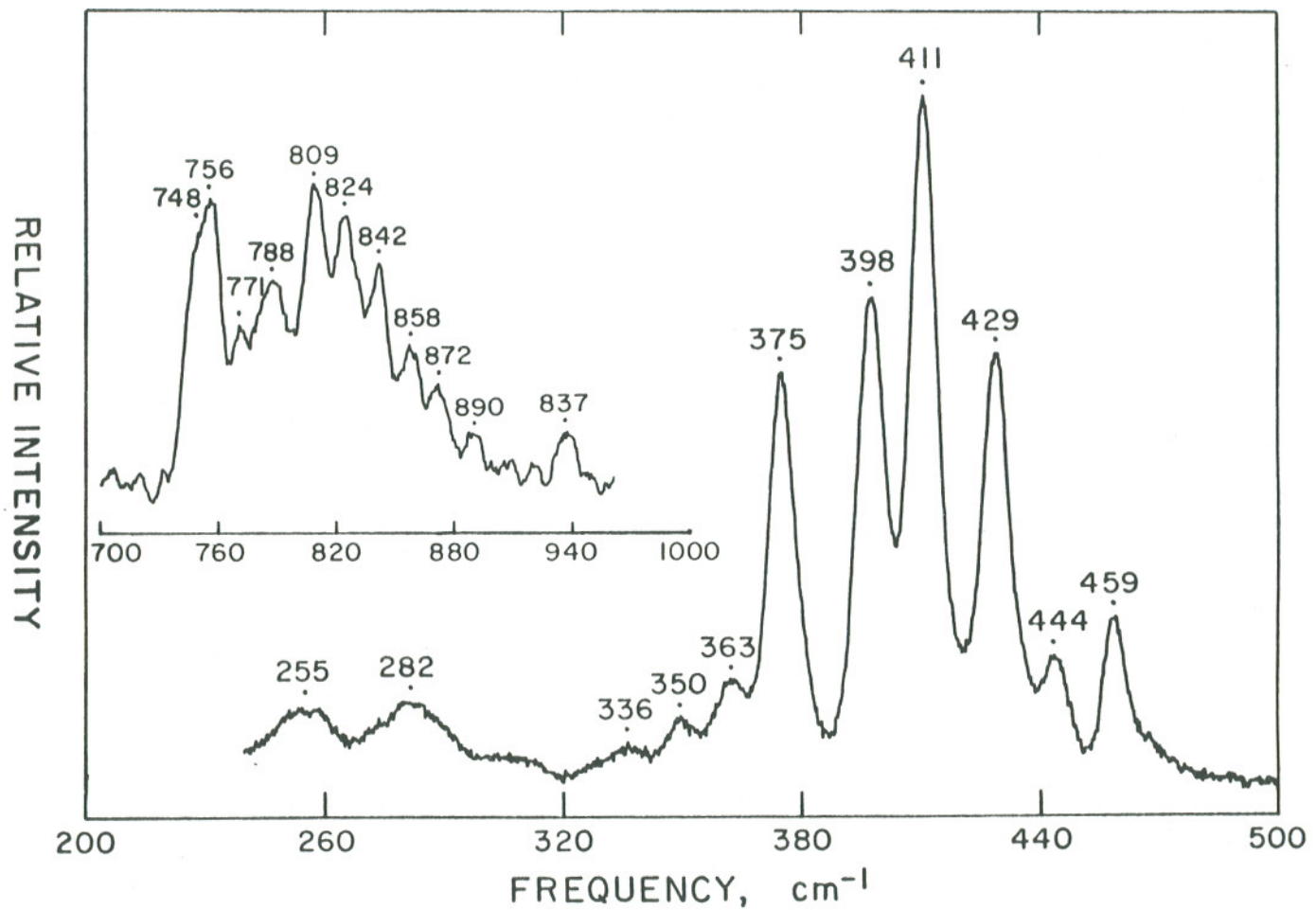
RELATIVE INTENSITY
411
398
429
375
809
824
756
748
842
788
771
858
872
890
837
700
760
820
880
940
1000
459
444
363
350
336
255
282
200
260
320
380
440
500
FREQUENCY, cm⁻¹

Figure 1.9

Chapter 2

METHODS

Infrared (IR) and Raman spectroscopy is the determination of the frequencies of the interatomic vibrations of a molecule and is widely used for structural studies of molecules. Both IR and Raman spectra give similar information, but the spectral mechanisms are completely different. IR spectroscopy is an absorption process, whereas Raman is a scattering phenomenon. For the study of biomolecules in an aqueous milieu, Raman is more useful because water is a weak scatterer but a strong absorber of infrared radiation. However, Raman scattering is a relatively weak phenomenon and, in general, requires sample concentrations ≥ 0.1 M. Biological specimen are normally not available at such a high concentration.

Resonance effects make Raman spectroscopy a more practical and powerful tool for the study of biological systems. When the energy of the incident radiation falls within an electronic absorption band of the sample, vibrations which are coupled to an electronic transition may gain intensity by up to several orders of magnitude compared to normal Raman scattering. Thus, it becomes possible to study chromophoric biological samples at a concentration < 1 mM. Type 1 Cu proteins have strong electronic absorptions at ~ 600 and ~ 460 nm, and, consequently, resonance Raman (RR) spectra of the chromophore may be obtained by using laser excitation wavelengths within these absorption bands.

The techniques used in our laboratory for obtaining resonance Raman spectra of metalloproteins have been fully reviewed by Loehr and Sanders-Loehr (Meth. Enzymol. 226, 431-470, 1993). Furthermore, experimental methods used in this research are given in individual chapters, and will not be further discussed in this chapter. Rather, the focus of this chapter is on the RR spectral data analysis, with particular emphasis on the

problem of overlapping and unresolved bands. The conclusions will be applicable to spectral data in general.

2.1 Use of the LabCalc Program for Raman Spectral Analysis

The frequency, band width (at half-height), and band intensity (area) are the three most important features that define a spectral band. For separated bands, these parameters can be determined straightforwardly from crosshair readings. However, for overlapping bands, other arithmetic tools are needed. Precise frequency determinations are particularly important for identifying band shifts due to isotope substitution.

Our goal is to characterize overlapping Raman bands, especially the band frequencies, using the LabCalc program (Galactic Industries, Salem, NH). In this experiment, we first applied the program to test spectra which were created with known band frequencies, widths, and intensities. Then, a set of protein Raman data were analyzed by the program.

Our results have shown that the curve fitting program is useful for determining frequencies and intensities of overlapping Raman bands. Using either the auto-fitting or the fixed-width fitting routines, it is possible to locate a band frequency to within ± 0.5 cm^{-1}, and a band intensity to within $\pm 5\%$. The ± 0.5 cm^{-1} variability in band frequency is similar to that obtained using a cursor on an isolated peak and approaches the maximum precision possible with typical protein samples at a slit width of ~ 5 cm^{-1}. Thus, only shifts > 0.5 cm^{-1} can be considered significant. Other arithmetic tools such as derivatives (1st or 2nd) can enhance the definition of overlapping bands, but they do not necessarily lead to correct frequency readings.

2.2 Experimental Section

2.2.1 Creating Two-Band Raman Spectra

The Raman spectrum used to initiate this process was that of an indene standard, which had no peaks between 600 and 700 cm^{-1}. This provided an essentially straight baseline to which other peaks were added. To add a Raman peak, the following sequence was used. (1) Press F2 key to get the menu. (2) Select Arithmetic and Zap from the menu. (3) Chose "Add gaussian". (4) Use the F9 and F10 keys to define the

width of the gaussian. (5) Move the cursor cross hair to define the height and the center position of the band. (6) Press the ENTER key to add the band to the trace. In the same way, a second band was also created. By adjusting the locations of the two bands, we generated two spectra: IndLC1 where the two bands were completely separated (Fig. 2.1) and IndLC2 where the two bands were largely overlapped and not resolved (Fig. 2.2). File retrieve was used to display the spectrum file in LabCalc. Band widths and relative intensities were typical of those in actual Raman spectra.

2.2.2 Applying LabCalc to Created Spectra

For 1st and 2nd derivatives: (1) Press F2 key to get the menu. (2) Select Arithmetic, Do program, and then Derivative from the menu. The number of convolution points was set to 9.

For Curve fitting: (1) Press F2 to get the menu. (2) Select Arithmetic, Other, then Curve fitting from the menu. The curve fitting program was tested under two conditions. One was "Auto fitting" in which initial parameters were given but no parameters were fixed. The other was "fixed-width fitting" in which the band width at half height was kept at a fixed value throughout the fitting procedure. For simplicity, it was assumed that the peaks were 100% Gaussian. (The laser line shape is Gaussian while the shape of vibrational peaks is in Lorentzian. Thus, Raman peaks are probably 60-90% Lorentzian and 10-40% Gaussian.)

2.3 Results and Discussion

2.3.1 Applying LabCalc to Created Spectra

2.3.1.1 Derivatives

Figs. 2.1 and 2.2 show the created spectra IndLC1 and IndLC2. True peak parameters are listed in Table 2.1. The 1st and 2nd derivative curves for IndLC1 are shown in Fig. 2.1. The $(dy/dx)=0$ point of the 1st derivative and the minimum intensity point of the 2nd derivative correspond to the peak maxima in the original spectrum and give the same frequency readings of 622.0 and 676.1 cm^{-1} as in Table 2.1. This indicates that the differentiation programs function correctly, and we can use either of them to determine the band frequency for an isolated peak.

For overlapping bands, the frequency readings from the 1st and the 2nd derivatives have larger errors (Fig. 2.2). Due to band overlapping, the 1st derivative curve is no longer symmetric and it is hard to define the (dy/dx)=0 line. Furthermore, the peak minimum in the 2nd derivative no longer corresponds to the correct frequency reading. In summary, for overlapping bands, the 1st and 2nd derivatives help in resolution (finding out the number of bands), but often do not lead to the correct frequency reading.

2.3.1.2 Auto Fitting

Results are listed in Tables 2.1 and 2.2. For separated peaks (IndLC1), auto fitting with rough initial guesses in band width, center position, and intensity gives only a ± 0.1 cm^{-1} error in the frequency reading (Table 2.1). Even when band width initial guesses differ from the true values by -2.8 to $+3.4$ cm^{-1}, the fitted band widths all come out close to the true widths within ± 0.4 cm^{-1} (Table 2.2). For overlapped peaks (IndLC2), similar results are obtained with a slightly increased error of 0.5 cm^{-1} in frequency determination (Table 2.1). In both cases, the fitted peak heights are also close to the true values ($\pm 4\%$). Furthermore, results are highly reproducible when the fitting routine is repeated several times. In auto fitting, the initial guesses are not important to the final results and the fitted widths are close to the true values no matter how far off the initial guesses are. The chi-square value reached its lowest point within 100 passes, and additional passes gave very little further improvement.

2.3.1.3 Fixed-width fitting

Results are listed in Table 2.3. In each fitting test, the input fixed band width differ from true value by -2.8 to $+4$ cm^{-1}. For the separated bands in IndLC1, the fitted band frequencies are within 0.1 cm^{-1} of the true values. For the overlapped bands in LndLC2, the errors are ± 0.5 cm^{-1} which are slightly larger than those in auto fitting. In addition, the band heights and areas are surprisingly variable. Compared to auto fitting, the Chi values are about 2 fold bigger (the larger the deviations in fixed width, the poorer the fitting). With a fixed band width, the program simply cannot arrive at as good a fit to the true spectrum as when the band width is allowed to vary.

Our testing results show that the curve fitting program works properly. Auto fitting and fixed-width fitting give similar results for band frequency with an error of

± 0.5 cm^{-1}. However, if we also consider band areas and Chi values, we find that auto fitting works better than fixed-width fitting, especially in the case of overlapping bands. We, therefore, decided to use auto fitting to determine isotope shifts in the RR spectra of azurin.

2.3.2 Raman Band Frequency of Azurin from Curve Fitting

2.3.2.1 RR Spectra of $^{65/63}$Cu Labeled Azurin

$^{65/63}$Cu-labeled azurin samples were obtained by reconstitution of apo-H117G mutant with ^{65}Cu or ^{63}Cu and imidazole. Fig. 2.3A shows the spectra of Cu-isotope labeled azurin between 350-450 cm^{-1}. In addition to bands at 372, 408, 429, and 441 cm^{-1}, there is clearly another unresolved strong band near 400 cm^{-1}. In ^{65}Cu, two bands have shifted slightly to lower frequencies. The intensities of the 372- and 400-cm^{-1} bands increase, but the 429-cm^{-1} band stays the same in both frequency and intensity. We used curve fitting to determine band parameters, particularly for the near 400-cm^{-1} shoulder.

The auto fitting procedure gives a good match between the fitted and observed spectra (Fig. 2.4A). The $\Delta\nu_{calc}$ values from auto fitting (Table 2.4) agree well with $\Delta\nu_{obs}$ from visual inspection of the spectra and $\Delta\nu_{lit}$ reported previously. The fact that the fitted band widths for the ^{63}Cu and ^{65}Cu data sets are constant within ± 0.4 cm^{-1} lends credibility to the auto fitting results. The shifts of the 372- and 408-cm^{-1} bands are detected consistently and, thus, are likely to be real shifts. The shifts of 429- and 441-cm^{-1} bands are within the experimental error of ± 0.5 cm^{-1} and, thus, are not significant.

It is surprising that the 399-cm^{-1} shoulder is not shifted according to curve fitting. This band looks like it has shifted in the overplotted spectra (Fig. 2.3A). However, curve fitting makes it apparent that the gap between solid and dotted lines is caused by an intensity increase of the 399-cm^{-1} band in the ^{65}Cu sample, rather than a frequency change. Curve fitting shows a 16% increase in intensity of the 399-cm^{-1} band with ^{65}Cu (Table 2.4). We conclude that the frequency of the 399-cm^{-1} band is not significantly different in ^{65}Cu and ^{63}Cu azurin. The increased intensity of this band is most likely due to intensity borrowing as the major band at 408 cm^{-1} shifts 0.6 cm^{-1} to lower energy.

2.3.2.2 RR spectra of $^{15/14}$N-labeled WT Azurin

$^{15/14}$N labeled azurin samples were obtained by growing protein in ^{15}N- or ^{14}N-ammonia. Thus, all nitrogen atoms in the protein are labeled. Fig. 2.3B shows the expanded spectra of $^{15/14}$N-labeled azurins in 350-450-cm^{-1} region. Compared to Fig. 2.3A, the ~400-cm^{-1} shoulder is better resolved in the wild-type protein (Fig. 2.3B). In ^{15}N-NH_3, all bands are shifted to lower energy and 428-cm^{-1} band has the largest changes in intensity and frequency.

Curve fitting results are shown in Fig. 2.4B and Table 2.5. Bands at 400, 408, 428, 435, and 441 cm^{-1} are shifted to low frequencies by 2.7, 1.4, 3.8, 3.4, and 3 cm^{-1}, respectively. The larger shift of the 400-cm^{-1} band than the 408 cm^{-1} band is obvious from Fig. 2.3B and explains why the 400-cm^{-1} band is better resolved in ^{15}N-NH_3 sample. Comparison of $\Delta\mu_{calc}$ and $\Delta\nu_{obs}$ (Table 2.5) shows very good agreement. Given the large isotope shifts in this data set, the estimation of $\Delta\nu_{obs}$ from expanded overplots is fairly accurate. The good agreement with $\Delta\nu_{calc}$ verifies that the auto fitting procedure is an excellent method for determining isotope shifts. Auto fitting has the further advantage that the frequency determinations are not biased by user perceptions.

2.3.3 Raman Intensities in SOD-H80C mutant from Curve Fitting

Auto fitting is the best choice for finding the frequency changes between a pair of spectra (e.g., isotope effects), provided that band widths remain constant. However, in a study of peak intensities in a series of spectra for a RR excitation profile, we found that auto fitting gave incorrect results. Fig. 2.5 shows the RR spectra of the blue copper site of SOD-H80C mutant at 3 different excitation wavelengths. Each spectrum has two major peaks at 341 and 352 cm^{-1}. Table 2.6 lists the band width and intensity values from auto fitting. At 458-nm excitation, the 341-cm^{-1} band intensity is only 42%, which appears too low by looking at the actual spectrum in Fig. 2.5. It is clear that the underestimated intensities of 341-cm^{-1} band with 457-514-nm excitation are due to the anomalously small band widths from the auto fitting procedure.

Band width is an essential property of a vibrational mode. Based on $\Delta t\Delta E \geq h/4\pi$ (constant), the band width should not change with excitation wavelengths provided that temperature, solvent, and slit width remain the same. Therefore, the changes in band width obtained by auto fitting are incorrect. The reason for the change is not

known. From the range of auto fitting band widths, it appeared that the actual band width was between 13 and 14 cm^{-1} (typical values for protein Raman bands). Thus, a value of 13.5 cm^{-1} was utilized for the fixed-width fitting procedure. The results are shown in Table 2.6. Using fixed-width fitting, the intensities of the 341 cm^{-1} band are higher with blue excitation and closer to the observed data shown in Fig. 2.5.

Excitation profiles resulting from the two methods are shown in Fig. 2.6. As we can see, auto fitting and fixed-width fitting give similar excitation maxima, but the relative intensities are different. In Fig. 2.6B, the two Raman bands appear to have similar relative intensities with 460- and 650-nm excitation, which is clearly not correct as seen in the data shown in Fig. 2.5. Therefore, for quantitating Raman intensities, the fixed-width fit appears to be the safe and right choice.

2.3.4 Other Factors Affecting Curve Fitting

(i) When curve fitting is performed over a different spectral range, e.g., 350-450 cm^{-1} instead of 385-450 cm^{-1}, the results can be slightly different due to the tails of the Gaussian bands. (ii) A band near the end of the spectral range will sense the fitting range change most and will be more difficult to fit accurately. (iii) The larger the range and the greater the number of peaks to be fitted, the bigger the Chi value. (iv) Curve fitting seems to give the biggest errors and strangest results when two bands are separated by less than 5 cm^{-1}. The key points are to analyze each set of data the same way and always to check the curve fitting results against the original spectra.

2.4 CONCLUSIONS

(1) To determine frequency shifts from a pair of isotope spectra, use the auto fitting procedure. However, check that the band width for a given mode remains constant in the spectra for the two isotopes.

(2) To obtain Raman intensities for an excitation profile, first use auto fitting. If the band widths vary excessively, determine a median or average band width and use this value for a fixed-width fitting.

(3) The frequency error in curve fitting was found to be ± 0.5 cm^{-1}. In comparing isotope data, if the frequency shift is ≥ 0.5 cm^{-1} and the shift is consistently detected in several independent experiments, then it is likely to be a real shift. Shifts ≤ 0.4 cm^{-1} are not significant.

(4) Curve fitting is particularly useful in the case of overlapped bands, when there are intensity as well as frequency changes and for small shifts (≤ 1 cm^{-1}). Even for large shifts (≥ 1 cm^{-1}), curve fitting gives more accurate results than cursor reading because it is less subjective and more likely to locate the true peak positions.

Table 2.1. Auto Fitting Results on Created Spectra

File Peak	Parameter[a]	True[b]	F-1[c]	F-2[c]	$\lvert\Delta_{F-T}\rvert$[d]
IndLC1					
(I)	ν	622.0	622.1	622.1	0.1
	W	10.1	10.5	9.98	0.4
	H(%)	64	64	62	2%
	A(%)		61	57	
(II)	ν	676.1	676.1	676.1	0
	W	11.2	10.9	10.7	0.5
	Chi-sq		1.71×10^5	4.88×10^5	
IndLC2					
(I)	ν	649.3	649.5	649.5	0.2
	W	9.8	9.4	9.4	0.4
	H(%)	54	58	58	4%
	A(%)		49	49	
(II)	ν	659.6	660.1	660.1	0.5
	W	11.6	11.3	11.3	0.3
	Chi-sq		1.34×10^5	1.34×10^5	

[a] ν, W, H and A stand for frequency, width at half width, height, and area, respectively. H of peak I is normalized to 100% for peak II. [b] Parameters of created spectra. The parameters for peaks I and II in spectra IndLC1 and IndLC2 are similar, but not identical, due to the fact that a cursor was used to generate peak height and position. [c] F-1 and F-2 are two fitting tests performed with slightly different initial parameters. [d] Absolute value of maximum difference of fitted results from the true value.

Table 2.2. Guessed Band Width and Fitted Band Width in Auto Fitting on IndLC2

Fitting	Peak	Guessed W (cm^{-1})	Fitted W (cm^{-1})	True W (cm^{-1})	$\lvert\Delta_{F-T}\rvert$ (cm^{-1})
1	I	11	9.4	9.8	0.4
	II	14	11.3	11.6	0.3
2	I	7	9.4	9.8	0.4
	II	15	11.3	11.6	0.3

Table 2.3. Fixed-Width Fitting Results on Created Spectra*

File (Peak)	Parameter	True	F-1	F-2	F-3	$\lvert\Delta_{F\text{-}T}\rvert$
IndLC1						
(I)	ν	622.0	622.1	622.1	622.1	0.1
	W	10.1	11.1	12.5	8.3	2.4
	H(%)	64	65	64	64	1%
	A(%)		63	68	61	
(II)	ν	676.1	676.1	676.1	676.1	0
	W	11.2	11.5	11.7	8.7	2.5
	Chi-sq		2.50×10^5	3.82×10^5	6.74×10^5	
IndLC2						
(I)	ν	649.3	649.5	649.8	649.2	0.5
	W	9.8	10.5	13.86	7.0	4
	H(%)	54	58	51	59	5%
	A(%)		49	51	46	
(II)	ν	659.6	660.1	660.1	660.0	0.5
	W	11.6	12.1	14.1	9	3.2
	Chi-sq		2.11×10^5	4.49×10^5	1.09×10^6	

* See notes for Table 2.1. W values in F-1, F-2, and F-3 are fixed widths.

Table 2.4. Auto Fitting Parameters for $^{65/63}$Cu Spectra of Azurin

^{63}Cu			^{65}Cu			$\Delta\nu_{calc}$	$\Delta\nu_{obs}$	$\Delta\nu_{lit}$
ν	W	H%	ν	W	H%			
371.8	10.7	53	371.3	10.8	67	-0.5	-0.5	-0.6
399.1	10.7	56	399.07	10.9	72	0.0	~-1	-0.6
407.9	10.3	100	407.3	10.3	100	-0.6	~-1	-0.6
428.9	10.0	53	428.6	9.7	56	-0.3	0	-0.2
441.2	7.1	7	440.8	7.4	7	-0.4	0	N.d.

* $\Delta\nu_{calc}$ are shifts from auto fitting. $\Delta\nu_{obs}$ are shifts estimated from cursor positions in expanded overplots. $\Delta\nu_{lit}$ are shifts reported by Blair et al., *J. Am. Chem. Soc. 107*, 5755 (1985). H refers to band height relative to the most intense 408-cm^{-1} band.

Table 2.5. Auto Fitting Parameters for $^{15/14}$N-NH_3 Spectra of Azurin*

^{14}N-NH_3			^{15}N-NH_3			$\Delta\nu_{calc}$	$\Delta\nu_{obs}$
ν	W	H(%)	ν	W	(H%)		
371.8	8.2	45	371.3	9.3	41	-0.9	-1
399.6	8.7	46	396.9	7.9	42	-2.7	~-2.5
407.9	7.5	100	406.5	8.3	100	-1.4	-1
427.9	7.3	46	424.1	8.2	56	-3.8	-3.7
434.6	4.6	8	431.2	4.3	11	-3.4	N.d.
440.6	5.1	5	437.6	6.9	10	-3	-3.7

* See notes for Table 2.4.

Table 2.6. Curve Fitting Parameters for RR Spectra of SOD-H80C

Excitation Wavelength (nm)	Auto-Fitting Procedure[a]			Fixed-width[b]
	341 cm^{-1} W	352 cm^{-1} W	$A_{341/352}$ (%)	$A_{341/352}$ (%)
458	11.6	14	42	87
488	11.8	16	39	78
514	11	16	41	79
568	13	14	56	72
599	15	13	64	65
610	15	14	69	57
624	14	12	64	54
647	14	12	51	43
676	13	13.6	38	28

[a] W is the derived band width. A is the area of the 341-cm^{-1} band relative to that of the 352-cm^{-1} band. [b] Areas calculated by fixing both band widths at 13.5 cm^{-1}.

FIGURE LEGENDS

Figure 2.1. Created Raman spectrum IndLC1 and its 1st and 2nd derivatives.

Figure 2.2. Created Raman spectrum IndLC2 and its 1st and 2nd derivatives.

Figure 2.3. RR spectra of isotope-labeled azurin from *P. aeruginosa* obtained with 647-nm excitation. Dotted lines are the heavy isotope samples. A: $^{65/63}$Cu substituted into H117G mutant plus imidazole. B: $^{15/14}$N-NH_3 in wild-type azurin.

Figure 2.4. Examples of curve fitting results for RR spectra of azurin. Spectra have been baseline corrected, but not smoothed.

Figure 2.5. RR spectra of the H80C mutant of superoxide dismutase obtained at three different excitation wavelengths.

Figure 2.6. RR excitation profiles for SOD-H80C. Raman intensities were measured as the area of the protein peak relative to the area of the ice peak at 230 cm^{-1}.
A: Results from fixed-width fitting. B: Results from auto fitting.

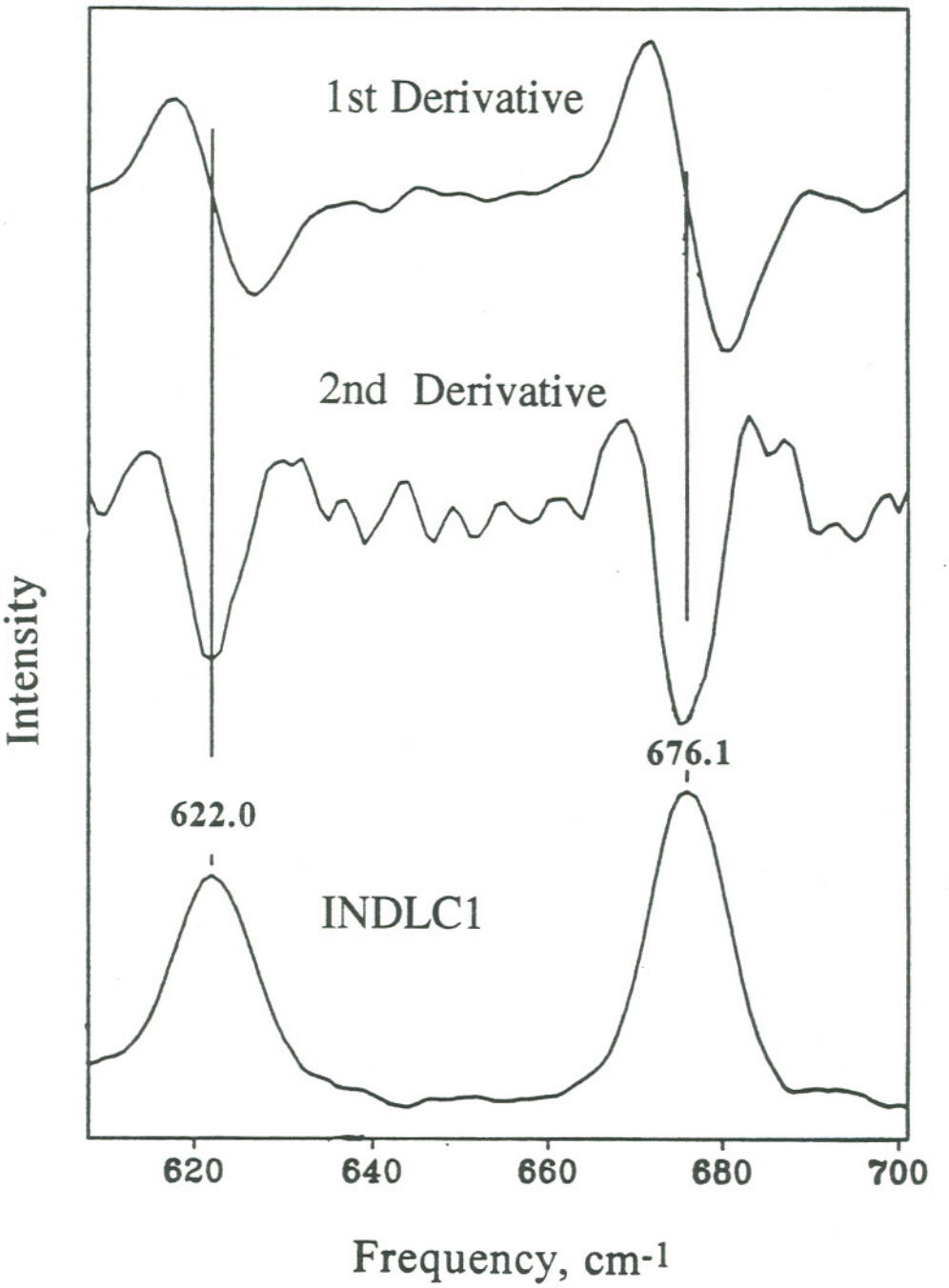
1st Derivative
2nd Derivative
Intensity
676.1
622.0
INDLC1
620
640
660
680
700
Frequency, cm-1

Figure 2.1

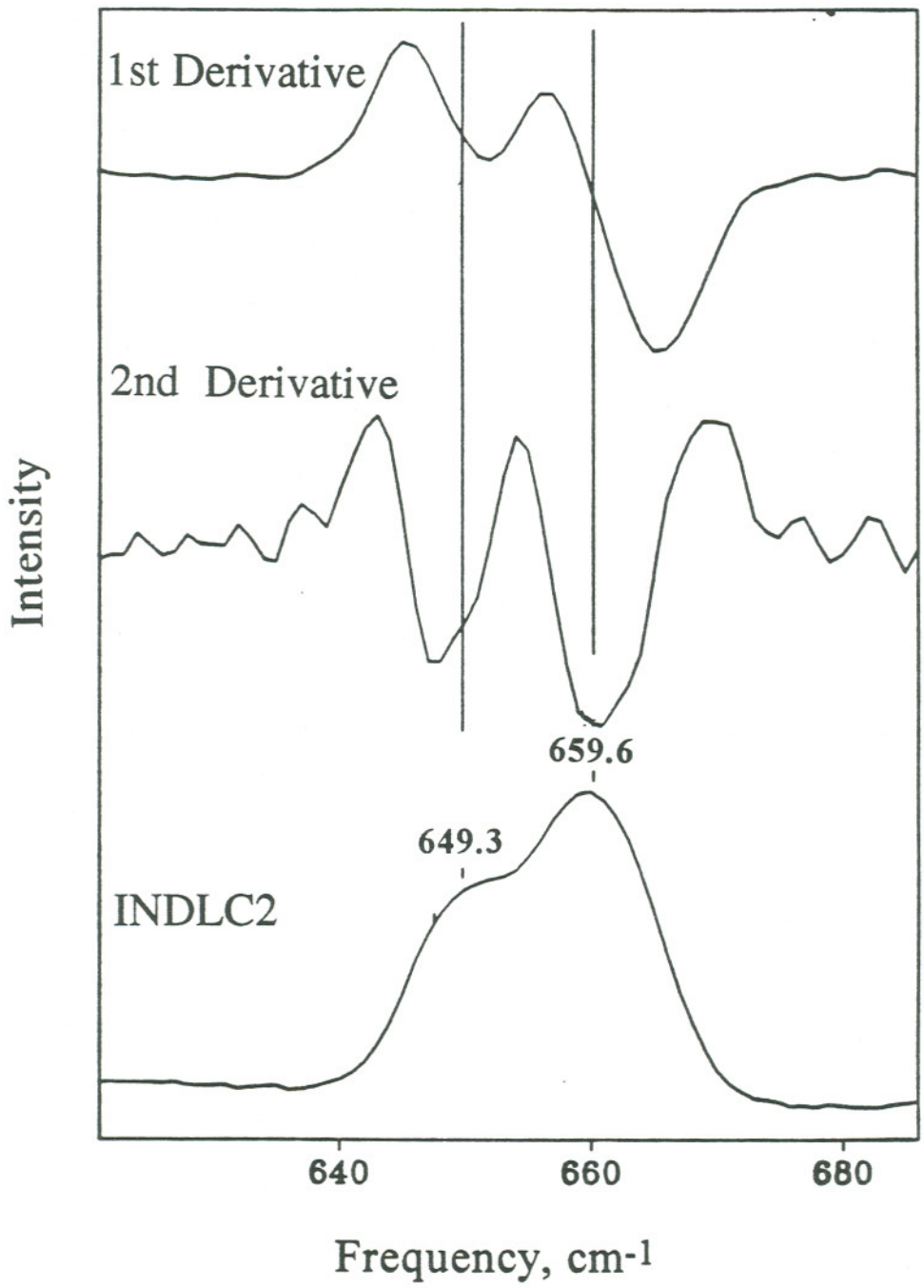
1st Derivative
2nd Derivative
Intensity
659.6
649.3
INDLC2
640
660
680
Frequency, cm-1

Figure 2.2

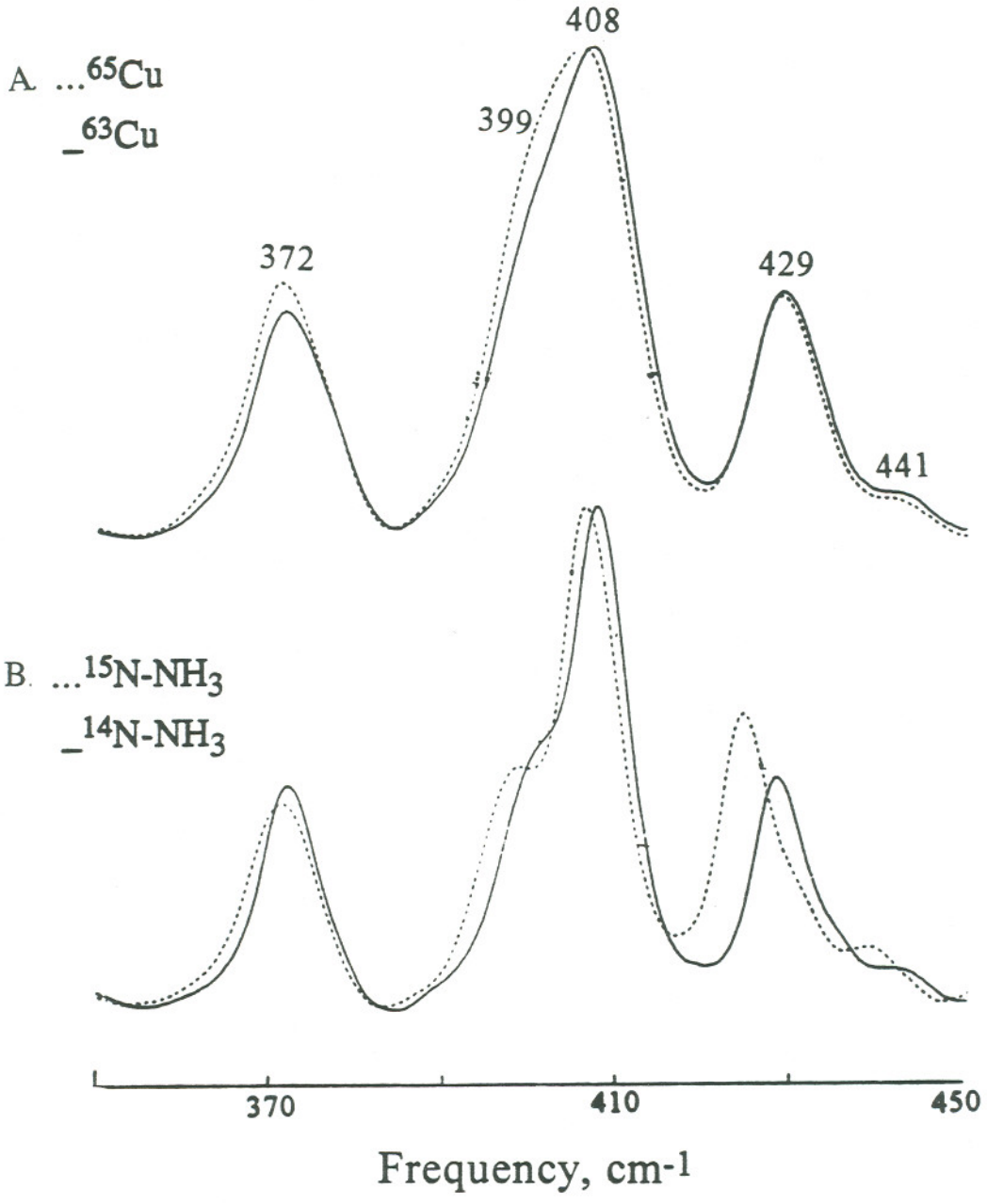
408
A. ...65Cu
_63Cu
399
372
429
441
B. ...15N-NH3
_14N-NH3
370
410
450
Frequency, cm-1

Figure 2.3

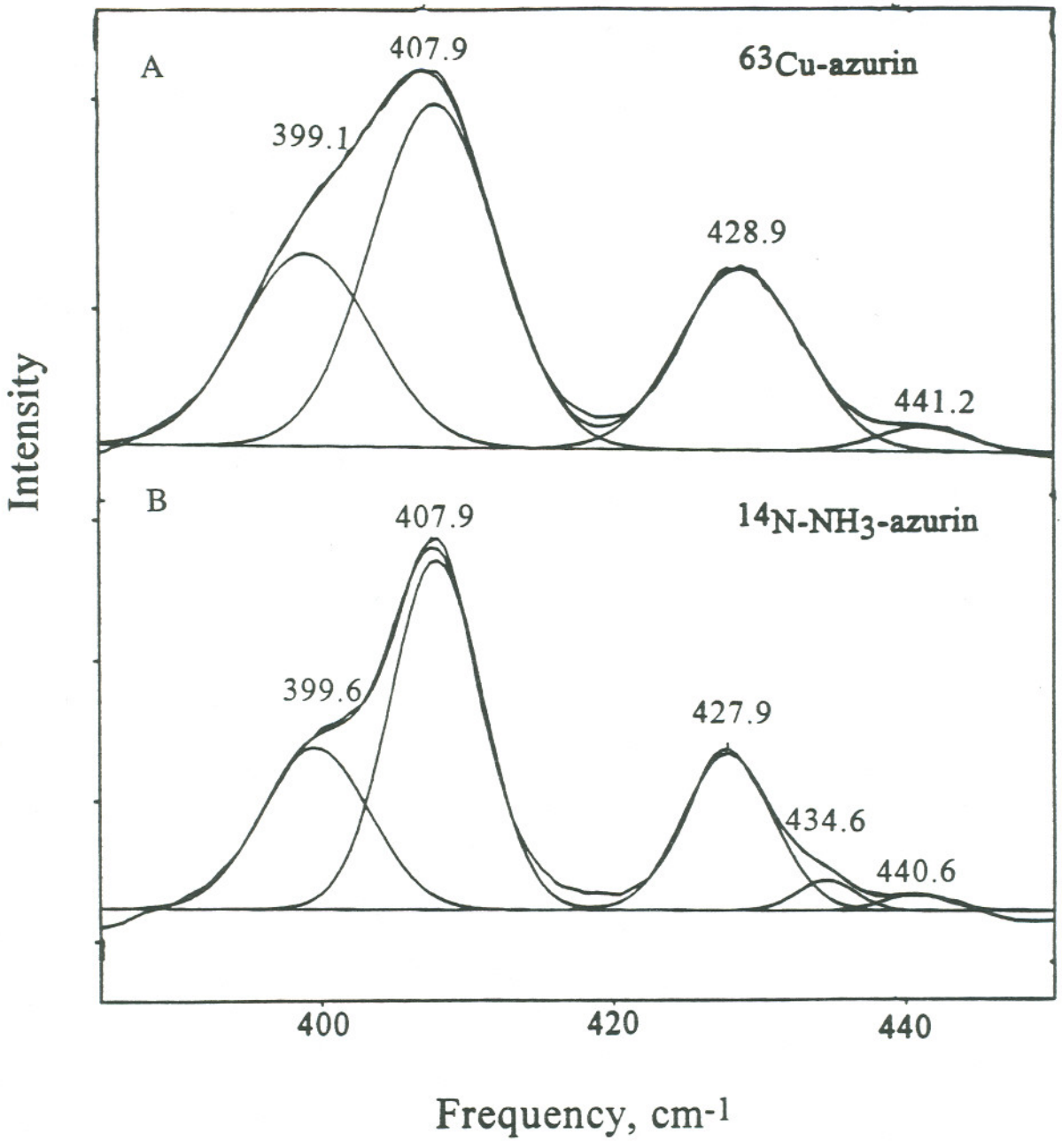
A
407.9
399.1
428.9
441.2
63Cu-azurin
B
407.9
399.6
427.9
434.6
440.6
14N-NH3-azurin
Intensity
400
420
440
Frequency, cm-1

Figure 2.4

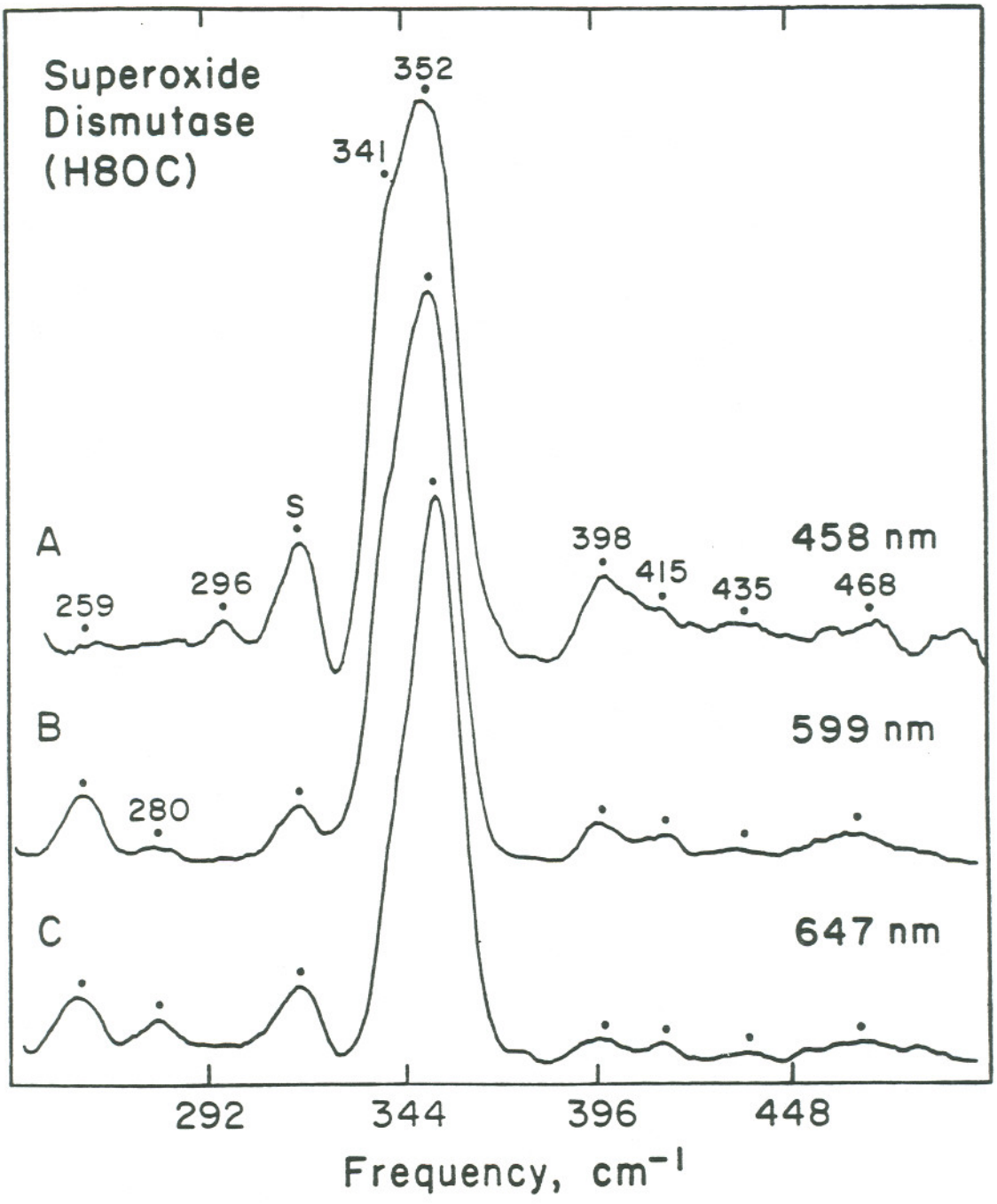
Superoxide
Dismutase
(H80C)
352
341
S
A
259
296
398
415
435
468
458 nm
B
280
599 nm
C
647 nm
292
344
396
448
Frequency, cm⁻¹

Figure 2.5

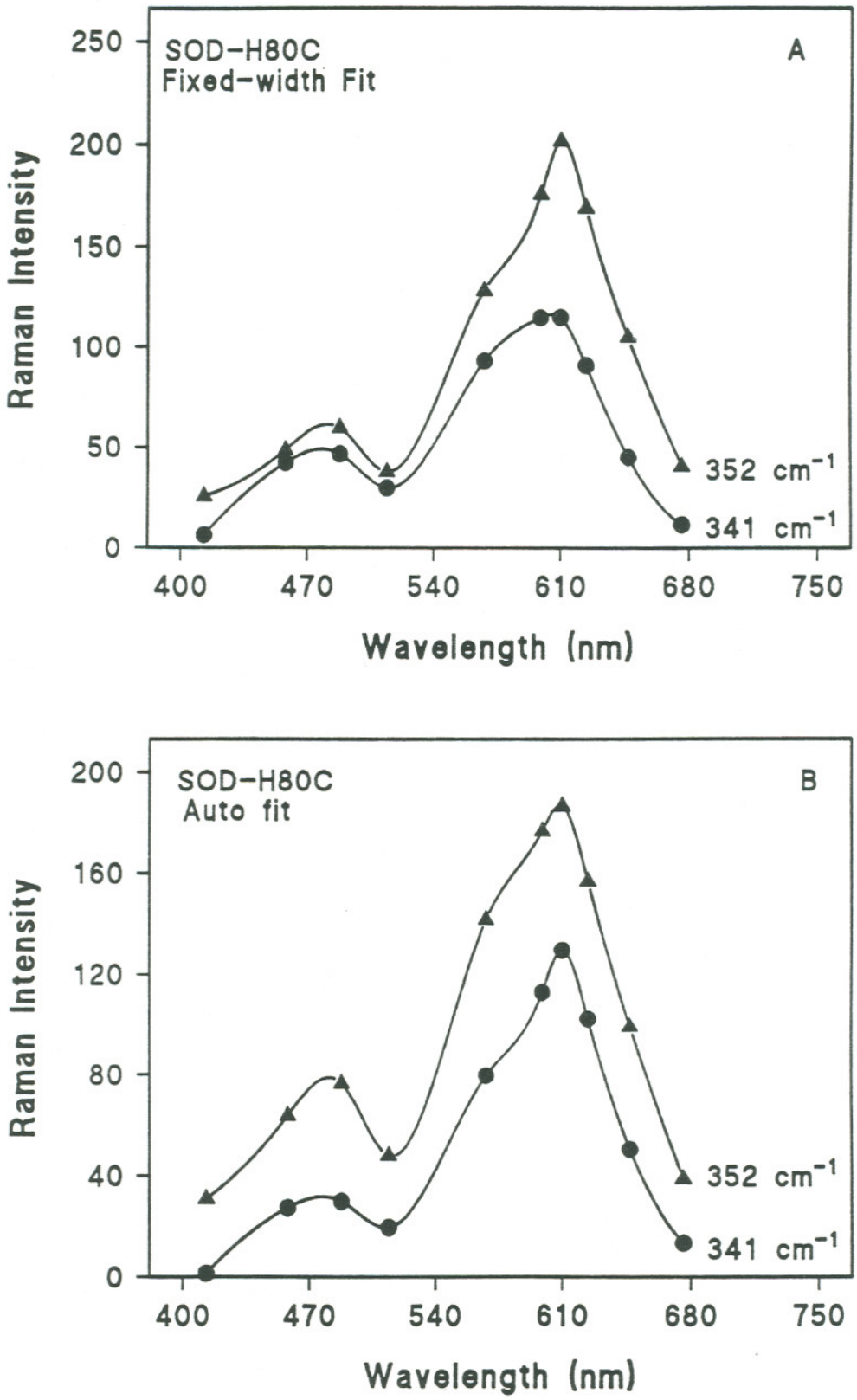
SOD-H80C
Fixed-width Fit
A
Raman Intensity
250
200
150
100
50
0
352 cm-1
341 cm-1
400
470
540
610
680
750
Wavelength (nm)
SOD-H80C
Auto fit
B
Raman Intensity
200
160
120
80
40
0
352 cm-1
341 cm-1
400
470
540
610
680
750
Wavelength (nm)

Figure 2.6

Chapter 3

RESONANCE RAMAN SPECTRA OF PLASTOCYANIN AND PSEUDOAZURIN. EVIDENCE FOR CONSERVED CYSTEIN LIGAND CONFORMATIONS IN CUPREDOXINS (BLUE COPPER PROTEINS)[1]

3.1 Introduction

The blue copper proteins have been the subject of intensive spectroscopic and structural studies (Adman, 1985, 1991; Solomon et al., 1986). Particularly noteworthy are their very intense (ϵ = 3000 to 5000 M^{-1} cm^{-1}) absorption bands in the visible spectrum (590 to 625 nm) arising from cysteinate S → Cu(II) charge transfer. In addition, they exhibit distinctive resonance Raman (RR) spectra, axial or rhombic EPR spectra with abnormally low copper hyperfine splitting constants, and relatively high redox potentials of 200 to 700 mV (compared to the standard potential of 160 mV for the Cu^{2+}/Cu^{1+} pair). Blue copper centers are found in both mononuclear and multinuclear copper proteins. Where the biological function has been established, it is invariably electron transfer [see, e.g. Farver and Pecht (1984) and Rydén (1984)]. For this reason, Adman (1985) has proposed that the mononuclear copper proteins be described collectively as cupredoxins.

The cupredoxins for which high resolution X-ray crystal structures are available comprise poplar (*Populus nigra*) plastocyanin algal (Guss and Freeman, 1983), (*Enteromorpha prolifera*) plastocyanins (Collyer et al., 1990), *Alcaligenes denitrificans* azurin (Norris et al., 1986), cucumber basic blue protein (Guss et al., 1988), and *Alcaligenes faecalis* pseudoazurin (Petratos et al., 1988; Adman et al., 1989). There is also a cupredoxin-type domain in the multinuclear copper protein, zucchini ascorbate

[1] As published in *Biochemistry* **1991,** *30,* 10904-10913.

oxidase (Messerschmidt et al., 1989), and the existence of similar domains in two other multinuclear copper proteins, laccase and ceruloplasmin, has been inferred from the primary structures (Messerschmidt and Huber, 1990). Despite their different plant and bacterial origins, all five proteins have similar β-sandwich structures and blue copper sites (Adman, 1991). In all cases, the copper is coordinated to one cysteine and two histidines in a distorted trigonal geometry with a weakly ligated axial methionine at a longer distance. In the azurins from *A. denitrificans* (Norris et al., 1986) and *Pseudomonas aeruginosa* (Adman, 1985), there is also a weakly coordinated peptide carbonyl group serving as a fifth ligand. Both the intensity of the ~600-nm absorption band ($\epsilon > 3{,}000\ M^{-1}\ cm^{-1}$) and the narrowness of the EPR copper hyperfine splitting ($A_{\parallel} < 65 \times 10^{-4}\ cm^{-1}$) have been attributed to a strong trigonal ligand set having a symmetry lower than C_{3v} (Gewirth et al., 1987; Ainscough et al., 1987).

Despite the close similarities in the structures of the blue copper sites, there are some surprising differences. For some of the proteins, the X-band EPR spectrum is axial, whereas for others it is rhombic. Resonance Raman (RR) spectra show even greater variability. In all cases, excitation within the S(Cys) → Cu(II) CT band produces strong enhancement of four to five fundamental vibrational modes in the 330- to 460-cm^{-1} region. The multiplicity of these modes has been attributed to coupling between the Cu-S stretch and internal modes of the cysteine ligand (Nestor et al., 1984; Woodruff et al., 1988). However, the most intense RR mode can be located anywhere between 360 and 445 cm^{-1}.

In order to gain a better understanding of the structural factors responsible for the complexity and variability of the RR spectra, we have chosen to investigate poplar plastocyanin and *A. faecalis* pseudoazurin and to compare their spectroscopic behaviors with those of other blue copper proteins of known structure. We find that the vibrational frequencies among the blue copper proteins are actually fairly constant, which is consistent with the strong conservation of structure observed crystallographically. This would argue against the previous suggestion (Blair et al., 1985) that the frequency of the most intense vibrational mode can be used as an indicator of Cu-S(Cys) bond length. Rather, the uniqueness of the spectral pattern for each protein appears to be due mainly to variations in the vibrational intensities. Thus, the differences in the blue copper sites

which are detected by RR spectroscopy are reflecting differences in the electronic excited-state structure of the Cu-cysteinate chromophore.

3.2 Experimental Procedures

3.2.1 Protein Samples

Pseudoazurin from *Alcaligenes faecalis* S-6 was purified as described previously (Kakutani et al., 1981). Samples for Raman spectroscopy were prepared from the same material which had been used for X-ray crystallography and had an A_{280}/A_{593} of 2.14. Concentrated samples ~1.5 mM in pseudoazurin were diluted 20-fold in 0.02 M KH_2PO_4, 0.04 M KCl (pH meter reading 6.3) in either H_2O or D_2O. The samples were then concentrated by centrifugation in a Centricon 10 (Amicon) ultrafiltration device. Two more dilution and reconcentration steps were performed. Before the last reconcentration step, the dilute solutions were incubated overnight at 5°C. The final protein concentrations were ~1.5 mM.

Poplar (*Populus nigra* var. *italica*) and oleander (*Oleander nerium*) plastocyanins were purified as described previously (Chapman et al., 1977). During the purification of poplar plastocyanin, the second ion-exchange chromatographic separation step yielded two blue components to which we shall refer as Pc I and Pc II. These components were treated separately in subsequent steps of the procedure. For RR spectroscopy, lyophilized samples were dissolved in 0.1 M sodium phosphate in H_2O or D_2O (pH meter reading 6.0) yielding a concentration ~0.5 mM in Cu(II) and were incubated overnight at 5°C.

3.2.2 Resonance Raman Spectroscopy

RR spectra were obtained with a computer-interfaced Jarrell-Ash spectrophotometer using a Spectra Physics 2025-11 (Kr) laser for 647.1-nm excitation and a Coherent Innova 90-6 (Ar)/599-01 (dye) laser system for 570-nm excitation. The detector was an RCA C31034 photomultiplier tube with an ORTEC model 9302 amplifier/discriminator. The Raman spectra were collected in an ~150° backscattering geometry with samples at a temperature of ~15 K by using a closed-cycle helium refrigerator (Air Products Displex). For isotopic comparisons, samples were run consecutively under identical instrumental conditions. Peak positions were determined

by abscissa expansion and curve fitting (typical values: 40% Gaussian, 60% Lorentzian, full width at half-height of 7 to 9 cm^{-1}). Although absolute frequencies are accurate to only ± 1 cm^{-1}, isotope shifts are reproducible to within ± 0.3 cm^{-1}.

3.3 Results and Discussion

3.3.1 Copper Site Structures in Pseudoazurin and Plastocyanin

Pseudoazurin from *A. faecalis* is a protein with a molecular weight of 14,000 that serves as an electron donor to nitrite reductase under anaerobic conditions (Kakutani et al., 1981). Its crystal structure has been determined at high resolution (Petratos et al., 1988; Adman et al., 1989). The cupric ion in pseudoazurin has three strongly coordinated ligands (His-40, Cys-78, His-81) forming an approximately trigonal planar array with a fourth ligand (Met-86) at a longer distance, resulting in a distorted tetrahedral structure (Figure 3.1A). Despite its name, pseudoazurin has a structure, as well as EPR and RR properties (see below), which are distinctly different from those of the bacterial azurins.

Bacterial pseudoazurin is structurally more closely related to plant plastocyanin, an electron carrier in chloroplasts. Much of the polypeptide backbone of pseudoazurin (70 of the 123 residues) can be superposed upon the structure of plastocyanin (Guss and Freeman, 1983) with an r.m.s. deviation of only 0.7 Å (petratos et al., 1987). The copper sites of the two proteins, including the four ligating amino-acids (His-37, Cys-84, His-87, and Met-92 in plastocyanin) and the connecting polypeptide backbone segments, are identical within the limits of precision of the determinations (Figure 3.1A). Similar ligand arrangements are observed at the blue copper sites of the cucumber basic protein (Guss et al., 1988) and ascorbate oxidase (Messerschmidt et al., 1989) despite insertions and deletions in the loop regions of the polypeptide backbones. The azurins also maintain a similar orientation of these four ligating amino acids (Figure 3.1B) despite their having a weakly coordinated carbonyl as a fifth ligand (Adman, 1985; Norris et al., 1986).

3.3.1.1 Bond Distances

One of the most unusual and apparently persistent characteristics of the blue copper site is the shortness of the Cu-S(Cys) bond. The average value in the five high-

resolution structures (Table 3.1) is 2.13 Å. Although the values appear to range from 2.07 to 2.16 Å, they are subject to estimated uncertainties of at least 0.05 Å (Table 3.1) so that they are effectively indistinguishable from one another. The estimated uncertainty of $\pm$0.05 Å is in keeping with the structure analysis of poplar platocyanin at 1.6 Å resolution where two independent refinements were made with two independently recorded data sets (Guss and Freeman, 1983). It is supported by the recent finding that the Cu-S(Cys) bond length in poplar plastocyanin changed from 2.16 Å to 2.07 Å when the structure was further refined using new data at 1.3 Å resolution (Guss, J.M., Bartunik, H.D. and Freeman, H.C., unpublished results). Similarly, the Cu-S(Cys) bond length in *A. faecalis* pseudoazurin changed from 2.07 Å at 2.0-Å resolution (Adman et al., 1989) to 2.16 Å at 1.55-Å resolution (Table 3.1). It is likely that the 2.13 $\pm$0.05 Å distance and estimate of precision for Cu-S(Cys) is applicable to the other cupredoxin structures. In contrast with the cupredoxins, low molecular weight cupric thiolate complexes more typically exhibit Cu-S bond distances of 2.2 to 2.4 Å (Guss et al., 1986; Anderson et al., 1986; Bharadwaj et al., 1986).

The bonds to axial ligands such as Met in blue copper proteins are much weaker than the bonds to the trigonal Cys, His_2 ligand set. The Cu-S(Met) values range from 2.6 to 3.1 Å (Table 3.1), the difference of 0.5 Å being well beyond experimental error. The unusually long value of 3.13 Å in azurin may be a reflection of the presence of a second axial ligand. Plastocyanin and pseudoazurin have intermediate Cu-S(Met) distances near 2.80 Å, whereas the cucumber basic protein has a significantly shorter distance of 2.62 Å.

The irregular geometry of the blue copper site appears to be imposed by the protein and the framework in which the ligands are located. Thus, the ligand positions in plastocyanin are essentially unaffected by replacement of Cu(II) with Hg(II) or by removal of Cu(II) to form the apoprotein (Church et al., 1986; Garrett et al., 1984). In plastocyanin, pseudoazurin, and azurin, a high degree of ordering is also evident from the lower thermal parameters in the vicinity of the copper site (Guss et al., 1986; Adman et al., 1989; Ainscough et al., 1987).

An important factor in maintaining the structural integrity of the blue copper site is the hydrogen-bond network involving the ligands and adjacent residues (Guss and

Freeman, 1983; Adman et al., 1989). In both pseudoazurin and plastocyanin (Figure 3.1A), the sulfur atom of the ligating Cys (residue 78/84) is the acceptor of an NH···S hydrogen bond from the peptide-backbone N (residue 41/38). The orientation of the imidazole ring of the more buried His ligand (residue 40/37) is stabilized by a hydrogen bond to a backbone carbonyl (residue 9/13). The geometry of the Cu stite is further stabilized by two interactions involving the residues immediately following the ligand His and the ligand Cys. The residue adjacent to the ligand His is a conserved Asn (residue 41/38) whose side-chain amide group forms hydrogen bonds with the N(peptide) atom and side-chain O_γ atom of a Thr/Ser (residue 79/85) adjacent to the ligand Cys. All these interactions occur with minor variations in all the known cupredoxin structures.

3.3.1.2 Dihedral Angles

Copper-ligand dihedral angles are a sensitive indicator of the extent to which ligand conformation is conserved in blue copper proteins. In keeping with the near superposability of copper-site structures, these dihedral angles have approximately constant values (Table 3.1). Thus, the S_δ(Met)-Cu-S_γ-C_β(Cys) angle, the Cu-S_γ-C_β-C_α(Cys) angle, and the S_γ-C_β-C_α-N(Cys) angle have values near 0°, -170°, and +170°, respectively. A dihedral angle of 180° or 0° means that the four contributing atoms must be coplanar. In the case of the blue copper proteins, this near coplanarity extends over six atoms from the S_δ of methionine to the N(amide) of cysteine, as can be seen in Figure 3.1. The apparent conservation of atomic positions at the blue copper site is all the more remarkable in view of the extensive differences among the primary and tertiary structures of other parts of the protein molecules. For example, the sequence identities between pseudoazurin and plastocyanin and between azurin and plastocyanin are only 22 and 7%, respectively (Rydén, 1984).

The conservation of cysteine ligand dihedral angles is also observed in other classes of protein that contain metal thiolate bonds. The crystal structures for the $Fe(Cys)_4$ sites in rubredoxins (Adman et al., 1977; Frey et al., 1987) and the $FeS_4(Cys)_4$ sites in ferredoxins (Backes et al., 1991) reveal that the geometry of a particular cysteine ligand is maintained in homologous proteins. The distribution of Fe-S_γ-C_β-C_α angles in rubredoxins is two at ~180° and two at ~270°, whereas in ferredoxins it is two at ~70° and two at ~270° (Chakrabarti, 1989). A similar range of values is observed for

the equally conserved S_γ-C_β-C_α-N dihedral angles in rubredoxins and ferredoxins. Chakrabarti (1989) has observed that the S_γ-C_β-C_α-N angle tends to be near 180° when the M-S_γ-C_β-C_α angle is also close to 180°, as in the blue copper sites (Table 3.1).

In the crystal structure of liver alcohol dehydrogenase, the catalytic Zn(II) is coordinated to two cysteines, one histidine, and a water (Eklund and Brändén, 1983). One of the cysteine ligands appears to have a short metal-sulfur bond and Zn-S_γ-C_β-C_α-N coplanarity (Table 3.1). This is the probable reason why Cu(II)-substituted alcohol dehydrogenase exhibits the optical, EPR, and RR spectroscopic properties of a blue copper site (Maret et al., 1986). Although the structure of the Cu(II) derivative has not been determined crystallographically, it is likely to be close to that of the native zinc enzyme as the ligand geometry is known to be preserved in the Co(II) and Cd(II) analogs as well as in the apoprotein (Schneider et al., 1983, 1985).

3.3.2 Resonance Raman Spectra of Plastocyanin and Pseudoazurin

Raman spectra of blue copper proteins are maximally enhanced by excitation within the intense S(Cys) → Cu(II) CT band near 600 nm (Woodruff et al., 1988). All exhibit a large set of cupric-cysteinate-related vibrational modes between 350 and 450 cm^{-1}. The pattern of relative intensities of these modes appears to be characteristic of the particular type of blue copper protein. For the plastocyanins, the strongest peak is near 425 cm^{-1} and the next strongest is near 375 cm^{-1}, with an additional 4 to 5 smaller peaks in this region (Figure 3.2). There is also an isolated ν(Cu-His) mode near 265 cm^{-1}. This pattern is observed for plastocyanins from oleander and poplar (Figure 3.2), as well as from spinach and bean (Blair et al., 1985).

Plastocyanin is the form of poplar Pc used in the crystallographic studies (Guss and Freeman, 1983). A sequence for poplar Pc II determined in 1980 (R.P. Ambler, personal communication to H.C. Freeman) is in agreement with that recently published by Dimitrov et al. (1987), with the exception of residues 39-40 where no difference from Pc I was noted. All of the amino acid changes are conservative, and none of the eleven sequence differences between Pc I and Pc II involves a residue close to the copper site in Pc I. Yet the RR spectra (Figure 3.2B,C) indicate small differences in peak frequencies and relative intensities, suggesting that these remote amino acid changes have

some small effect on the blue copper site. The difficulty of crystallizing PcII has prevented a direct structural comparison.

Pseudoazurin from *A. faecalis* has its own unique pattern of RR intensites in the Cu-Cys region with three equally strong peaks at 386, 397, and 444 cm^{-1} (Figure 3.3A). In addition, a moderately strong peak at 415 cm^{-1} and five peaks of lower intensity between 339 and 461 cm^{-1} are observed. Yet another intensity pattern is seen for azurin where proteins from seven bacterial species all have their strongest RR peak at $\sim$410 cm^{-1} (Blair et al., 1985; Ainscough et al., 1987).

3.3.3 Deuterium Isotope Shifts in RR Spectra

Another common attribute of the RR spectra of blue copper proteins is that many of the vibrational modes show small shifts to lower energy when the proteins are equilibrated in D_2O (Ainscough et al., 1987; Sharma et al., 1988). The RR spectra of pseudoazurin and plastocyanin show the expected deuterium sensitivity as documented in Figure 3.3 and Table 3.2. Both proteins exhibit a -1 cm^{-1} shift in the $\sim$265-cm^{-1} peak as well as shifts of -1 to -3 cm^{-1} for most of the peaks in the 330- to 460-cm^{-1} region.

There is general agreement that the deuterium dependence of the ν(Cu-His) mode at $\sim$265 cm^{-1} is due to exchange of one or two protons on the imidazole ring (Nestor et al., 1984; Blair et al., 1985). The deuterium effects in the 330- to 460-cm^{-1} region have also been ascribed to histidine contributions (Woodruff et al., 1988), but that interpretation no longer seems correct. We have observed similar deuterium-dependent shifts in the RR spectra of dinuclear and tetranuclear iron-sulfur proteins which lack histidine ligands (Mino et al., 1987; Backes et al., 1991). These observations indicate that deuterium isotope effects on metal-sulfur vibrational modes are due to the hydrogen-bonding interactions of sulfur ligands with exchangeable amide NH groups of the polypeptide backbone. Thus, the deuterium shifts in the RR spectra of plastocyanin, pseudoazurin, azurin, and Cu-substituted alcohol dehydrogenase (Table 3.2) can all be attributed to hydrogen bonding of a cysteine-thiolate ligand (Figure 3.1; Mino et al., 1987; Maret et al., 1986).

The deuterium dependences of the RR spectra of plastocyanin and pseudoazurin are similar in the number of affected peaks and in the extent of the isotope shifts (Table 3.2). A similar pattern of deuterium sensitivity is observed for azurins from *P.*

aeruginosa (Table 3.2) and *A. denitrificans* (Ainscough et al., 1987). Although the azurins have two H bonds to the cysteine-sulfur ligand compared to one in plastocyanin and pseudoazurin, the difference in overall hydrogen-bond strength is apparently insufficient to be detected by RR spectroscopy. In native Zn(II)-containing alcohol dehydrogenase, the Cys-46 ligand is also H bonded to the amide NH of residue 48 (H. Eklund, personal communication). This feature is likely to be conserved in the Cu(II)-substituted protein where the deuterium-isotope effects (Table 3.2) are even more remarkable than for native blue copper proteins. The spectral changes in Cu(II)-alcohol dehydrogenase involve large frequency shifts to both higher and lower energy as well as marked decreases in various peak intensities, all of which can be attributed to hydrogen bonding effects (Maret et al., 1986). Similarly, the 415-cm^{-1} peak of pseudoazurin undergoes a significant lowering of intensity in D_2O (Figure 3.3A).

3.3.4 Resonance Raman Frequencies

The origin of the complex set of vibrational modes between 330 and 460 cm^{-1} in the RR spectra of blue copper proteins has been the subject of much discussion (Woodruff et al., 1988). Enhancement profiles (RR intensities versus excitation wavelength) have shown that the vibrational intensities all track the ~600-nm S(Cys) → Cu(II) CT absorption band (Ainscough et al., 1987; Maret et al., 1986; Musci et al., 1985). Therefore, each of these RR frequencies is expected to have have a Cu-S stretching component contributing to its normal mode. Involvement of the axial methione ligand can be ruled out because the substitution of selenomethionine for methionine in azurin has no detectable effect on the RR spectrum (Thamann et al., 1982). Similarly, contributions from the histidine ligands are unlikely because binding of exogenous imidazole or pyrazole ligands to the copper center of Cu(II)-alcohol dehydrogenase has no significant effect on the RR spectrum of the Cu-cysteinate chromophore (Maret et al., 1986). These considerations, as well as the smaller-than-expected Cu-isotope dependence, have led to the conclusion that the vibrational modes between 330 and 460 cm^{-1} must represent admixtures of the Cu-S(Cys) stretch and cysteine ligand deformation modes (Nestor et al., 1984).

Potential candidates for cysteine ligand deformation modes in the 300- 500-cm^{-1} range include the S_γ-C_β-C_α bend involving the S_γ ligating group, the C_β-C_α-(CO) bend,

the C_β-C_α-N bend, the N-C_α-(CO) bend, and a Cu-S_γ-C_β-C_α torsional mode (Nestor et al., 1984). Coupling of ν(M-S) with δ(S-C-C) is expected to be strongly dependent on the M-S_γ-C_β-C_α dihedral angle, being maximal at 180° and minimal at 90° (Han et al., 1989). This type of coupling has been detected in the RR spectra of iron-sulfur proteins such as $Fe(Cys)_4$ rubredoxin (Czernuszewicz et al., 1986), $Fe_2S_2(Cys)_4$ ferredoxin (Han et al., 1989), and $Fe_4S_4(Cys)_4$ high-potential iron protein (Backes et al., 1991), all of which contain one or more Fe-S_γ-C_β-C_α dihedral angle near 180°. As can be seen in Table 3.1, all of the blue copper proteins which have been structurally characterized have Cu-S_γ-C_β-C_α dihedral angles close to 180°. The S_γ-C_β-C_α-N dihedral angle is also close to 180°, making the amide nitrogen a part of the coplanar grouping (Figure 3.1A). Thus, it is likely that the ν(Cu-S) mode in blue copper sites is coupled to both the δ(S-C_β-C_α) and δ(C_β-C_α-N) modes, as well as to several other cysteine-related deformations. In contrast, the vibrational spectra of Cu(II)-imidazole complexes exhibit ν(Cu-Im) modes below 300 cm^{-1} and imidazole ring motions above 800 cm^{-1} (Larrabee and Spiro, 1980).

Comparison of the RR spectra of blue copper proteins reveals that the [ν(Cu-S) + δ(Cys)] modes have a fairly constant set of frequencies, yielding the spectral alignments shown in Table 3.2. This constancy has been overlooked in the past because of the striking differences in peak intensities in the raw spectra, but it is more obvious from the graphical depiction in Figure 3.4. All of the proteins have a peak near 265 cm^{-1} attributable to ν(Cu-His). In the 330- to 460-cm^{-1} region, as many as nine additional modes are observed. Each such mode is confined to a narrow range of frequencies across all of the blue copper proteins. For example, most of the proteins have a peak at 440 $\pm$ 5 cm^{-1}, even though it varies from the least intense feature in stellacyanin to the most intense in pseudoazurin. Similarly there are eight other common features near 340, 360, 375, 385, 400, 415, 430, and 460 cm^{-1}. The vibrational mode which occurs at each of these frequencies probably arises from a different combination of the Cu-S(Cys) stretch with particular cysteine deformations. Since vibrational frequencies are a reflection of the structure of the ground state (Carey, 1982), the relative constancy of these frequencies in the RR spectra of blue copper proteins is consistent with the highly conserved structure of the Cu-cysteinate moiety (Table 3.1). The features of particular importance would be the short Cu-S(Cys) bond distance of $\sim$2.13 Å that raises the

frequencies into the 400-cm^{-1} region and the near coplanarity of the Cu-S_γ-C_β-C_α-N moiety that leads to kinematic coupling of cysteine deformation modes with ν(Cu-S).

3.3.5 Resonance Raman Intensities

There is a striking variability in the intensities of the different [ν(Cu-S) + δ(Cys)] modes in the blue copper RR spectra (Figure 3.4), and each class of protein has its own characteristic intensity pattern. In the plastocyanins, the feature at 424 cm^{-1} is the most strongly enhanced; in azurins, it is the feature at 409 cm^{-1}; and in pseudoazurin, it is a set of three peaks at 386, 397, and 444 cm^{-1} (Table 3.2). It has been previously suggested (Blair et al., 1985) that the most intense peak in the spectrum corresponds to the vibration with the largest ν(Cu-S) contribution and, thus, the frequency of this vibration should be related to Cu-S(Cys) bond length. This suggestion seems unlikely on several grounds: (i) the strong conservation of vibrational frequencies (vide supra) suggests a common set of vibrational modes for all blue copper proteins with each vibrational mode representing a particular combination of ν(Cu-S) and δ(Cys) components, and (ii) blue copper proteins such as pseudoazurin and Cu(II)-substituted alcohol dehydrogenase (Figure 3.4) have equally high intensities in two to three peaks which differ widely in energy. Rather, the relative constancy of RR frequencies can be taken as an indication of a conserved, short Cu-S(Cys) bond of ~2.13 Å in all blue copper sites. On the basis of its Raman frequencies (Figure 3.4), stellacyanin is also likely to have a short Cu-S(Cys) bond, despite the suggestion of a longer 2.2 Å Cu-S(Cys) distance from EXAFS analyses (Peisach et al., 1982; Feiters et al., 1988).

Whereas vibrational frequencies in resonance Raman spectra are solely a function of the structure of the molecule in the electronic ground state, vibrational intensities are related to the change in the geometry of the chromophore in the electronic excited state (Carey, 1982). Intensities are maximized when the excited-state displacement of atoms occurs along the normal coordinate of a vibration (Nishimura et al., 1978; Shin and Zink, 1989). Thus, the variability of RR intensities in blue copper proteins may be related to the degree of displacement which occurs in the excited state for the atoms participating in a particular [ν(Cu-S) + δ(Cys)] mode. Since these excited-state effects are specific for each class of blue copper protein, it is likely that they arise from

differences in amino acid composition and protein structure in the vicinity of the blue copper site (but beyond the highly conserved Cys, His_2, Met ligand set).

We propose that the conformation of the peptide loop connecting the Cys and His ligands (Figure 3.5) has an effect on the enhancement of particular RR modes in blue copper proteins. A common motif in the iron-sulfur proteins (rubredoxins, ferredoxins, and high-potential iron proteins) is that two cysteine ligands are separated by two amino acids, i.e., that the metal is coordinated by the S_γ atoms of Cys(n) and Cys($n+3$) (Backes et al., 1991). A similar ($n+3$) spacing is observed between the Cys and His ligands in some of the blue copper proteins, but many have an ($n+5$) or even larger spacing (Table 3.3). The three proteins which have the smallest spacing ($n+3$) show strongest enhancement of the mode near 430 cm^{-1} (plastocyanin, amicyanin, pseudoazurin). The proteins with ($n+5$) spacing have their most intense mode at either 410 cm^{-1} (azurin, rusticyanin, auracyanin) or 385 cm^{-1} (ascorbate oxidase, stellacyanin, cucumber basic protein). The copper sites of laccase and ceruloplasmin (as deduced from amino acid sequence alignments with ascorbate oxidase) also have an ($N+5$) spacing between Cys and His ligands (Messerschmidt and Huber, 1990), and these proteins exhibit maximal RR intensities at 400 and 383 cm^{-1}, respectively (Siiman et al., 1976). The two proteins with an even longer polypeptide segment between the Cys and His ligands (Cu-substituted alcohol dehydrogenase, nitrite reductase) show the strongest enhancement of the mode near 360 cm^{-1}.

Studies of aromatic amino acids have shown that their Raman intensities can vary considerably, depending on the nature of the protein environment (Hildebrandt et al., 1988). Thus, it is reasonable that the intensities of the cysteinate-related deformation modes are also sensitive to the protein environment in the vicinity of the cysteine ligand. Despite the highly conserved conformation of the cysteine ligand, the variablity in the conformation of the adjacent residues clearly results in differences in protein structure and amino acid side-chain placement (Figure 3.1). Analysis of the S(Cys) → Cu(II) electronic transitions in cupredoxins as a function of temperature suggests that they are coupled with ligand deformation modes (Cupane et al., 1990). Thus, a number of ligand atoms would be expected to undergo geometric displacement in the electonic excited state. The extent of displacement which a particular atom experiences may be influenced

by its environment (e.g., orientation and nature of amino acids in and around the Cys/His loop). This would then affect the Franck-Condon overlaps for a particular [ν(Cu-S) + δ(Cys)] vibrational mode. Based on the intensity data in Table 3.3 and Figure 3.4, we predict the following conserved Cys/His loop conformations in cupredoxins: (i) (n+3) loop in plastocyanin, pseudoazurin, and amicyanin; (ii) (n+5) loop in azurin, rusticyanin, and auracyanin; (iii) different (n+5) loop in cucumber basic protein, ascorbate oxidase, and stellacyanin; and (iv) (n+9) loop in nitrite reductase.

The characteristic Raman intensity pattern that is conserved within each class of cupredoxins (Figure 3.4) is surprisingly unaffected by metal substitution. Replacement of Cu(II) by Fe(III) or Ni(II) in alcohol dehydrogenase (Maret et al., 1986), Ni(II) in azurin (Ferris et al., 1979), or Ni(II) in stellacyanin (Musci et al., 1985) results in some differences in vibrational frequencies but the RR intensity pattern is preserved. This suggests that the coupling of the ν(M-S) vibration with cysteine deformations is the same in all cases. Thus, the conformation of the cysteine ligand and the Cys/His loop appears to be more important than the nature of the metal in determining the unique set of excited-state displacements which occurs in each type of blue copper protein.

3.3.6 Comparison of EPR and RR Properties

A characteristic and common feature of the blue-copper site is the narrow copper-hyperfine splitting observed in the EPR spectrum (Gewirth et al., 1987). However, the degree of rhombicity in the X-band EPR spectrum is highly variable, ranging from strongly axial, as in plastocyanin, to strongly rhombic, as in stellacyanin (Table 3.3). Q-band EPR spectra, on the other hand, exhibit marked rhombic character for all of these proteins (Penfield, 1985), even for those classed as axial from X-band EPR analysis. The extent of the axial or rhombic nature of the EPR spectra has been proposed by Gewirth et al. (1987) to be related to the relative orientations of copper-ligand bond directions with respect to the copper orbitals. Given the nearly superposable $Cu(His)_2(Cys)(Met)$ sites of poplar plastocyanin and pseudoazurin (Figure 3.1A) and the indistinguishable bond distances (within 0.05 Å) for all ligands, including the long Cu-Met bond, it is difficult to discern the structural origin of the different EPR character (axial and rhombic, respectively, in Table 3.3) of these two proteins. Further, we have noted no simple correlation between the X-band EPR spectra and RR frequencies or

intensities. This may be due to the fact that RR spectra reflect the geometry of the cysteine ligand and its connectivity to the protein, whereas EPR spectra are more influenced by the environment of the entire metal-ligand site.

3.3.7 Role of Conserved Structures in Electron Transfer

The Cys and His side chains in the Cys/His ligand binding loop are essentially superposable in all cupredoxins crystal structures (Table 3.1, Figure 3.1). This strong conservation of side-chain placement may well be of functional significance in long-range electron transfer, as both of these ligands appear to be involved in specific electron-transfer pathways (Sykes, 1985; Gray, 1986). The imidazole ring of the His ligand protrudes into a hydrophobic patch on the protein surface (Figure 3.5). This patch has been directly implicated in protein-protein interaction between electron-transfer partners: (i) azurin requires its hydrophobic patch for electron transfer from cytochrome c_{551}, as revealed by site-directed mutagenesis (van de Kamp et al., 1991), and (ii) amicyanin uses its hydrophobic patch to bind to methylamine dehydrogenase, as determined by X-ray crystallography (Chen et al., 1991).

In a number of cupredoxins, one or both of the residues adjacent to the Cys ligand have a side chain which interacts with an electron donor or acceptor at a second electron-transfer site (Figure 3.5). In plastocyanin, the conserved residue Tyr 83 adjacent to the Cu-binding residue Cys 84 has long been implicated in electron-transfer between the blue Cu site and both biological and inorganic redox partners (e.g., Colman et al., 1978; Roberts et al., 1991). In nitrite reductase, the residue preceding the blue Cu ligand, Cys^{136} is His^{135} which is a ligand of the type 2 Cu at the catalytic site (Godden et al., 1991). In ascorbate oxidase, the Cu-binding residue Cys 508 is immediately preceded and followed by residues His 507 and His 509, each of which is a ligand of a Cu atom in the catalytically active trinuclear Cu cluster (Messerschmidt et al., 1989). The existence of similar Cu-Cys-His-Cu pathways in laccase and ceruloplasmin can be inferred from sequence homology between these proteins and ascorbate oxidase (Messerschmidt and Huber, 1990).

The strong conservation of the (*n-1*)-Cys(*n*)-Cu structural motif (Figure 3.5) makes it likely that electron transfer occurs through the bonds of the Cu-ligated Cys and its neighboring residue(s). The fact that the Cu-S_γ-C_β-C_α-N bonds are approximately

coplanar in all crystallographically characterized cupredoxins (Table 3.1) suggests that coplanarity is an important feature of through-bond electon-transfer pathways. A similar degree of Cys ligand coplanarity is indicated for ascorbate oxidase, laccase, and ceruloplasmin from the appearance of characteristic cupredoxin-type RR spectra (Siiman et al., 1974). Current discussions of electron-transfer pathways have focused on distance and bonding effects (Beratan et al., 1990). In light of the present work, it appears that the dihedral angles in a through-bond electron-transfer pathway may also be important variables.

3.4 Conclusions

(1) The crystal structures of the cupredoxins plastocyanin, pseudoazurin, cucumber basic protein, and azurin show a coplanar array of five atoms in the copper cysteinate moiety that is a highly conserved feature of blue copper sites.

(2) The coplanarity of the cupric cysteinate chromophore (Cu-S_γ-C_β-C_α and S_γ-C_β-C_α-N dihedral angles close to 180°) leads to a coupling of ν(Cu-S) with δ(Cys) modes. This coupling accounts for the presence of 9 or more vibrational modes in the resonance Raman spectrum.

(3) The same set of vibrational modes in the 330- to 460-cm^{-1} region has been observed in the RR spectra of all cupredoxins thus far examined (including stellacyanin, rusticyanin, auracyanin, and amicyanin whose x-ray structures are not yet available). A coplanar copper-cysteinate configuration is likely for each of these proteins.

(4) Although the intensities of the different RR modes vary from protein to protein, the spectral patterns can be separated into four distinct categories having maximal RR intensities at 360, 385, 410, or 430 cm^{-1}, respectively. These categories correlate with the presence of $\geq$8, 4, 4, and 2 amino acids, respectively, between the Cys and His ligands.

(5) The conserved conformations of the cysteinate side chain, backbone, and flanking amino acids may be important in optimizing electron-transfer pathways which utilize the Cu-S(Cys) framework.

References

Adman, E. T. (1985) in *Metalloproteins* (Harrison, P., Ed.) Part 1, pp. 1-42, Verlag Chemie, Weinheim, FRG.

Adman, E. T. (1991) in *Adv. in Protein Chemistry*, in press.

Adman, E. T., Sieker, L. C., Jensen, L. H., Bruschi, M., and LeGall, J. (1977) *J. Mol. Biol. 112*, 113-120.

Adman, E. T., Turley, S., Bramson, R., Petratos, K., Banner, D., Tsernoglou, D., Beppu, T., and Watanabe, H. (1989) *J. Biol. Chem. 264*, 87-99.

Adman, E. T., Turley, S., Godden, J., Fenderson, F., and LeGall, J. (1991) manuscript submitted.

Ainscough, E. W., Bingham, A. G., Brodie, A. M., Ellis, W. R., Gray, H. B., Loehr, T. M., Plowman, J. E., Norris, G. E., and Baker, E. N. (1987) *Biochemistry 26*, 71-82.

Anderson, O. P., Becher, J., Frydendahn, H., Taylor, L. F., and Toftlund, H. (1986) *J. Chem. Soc. Chem. Commun.*, 699-701.

Backes, G., Mino, Y., Loehr, T. M., Meyer, T. E., Cusanovich, M. A., Sweeney, W. V., Adman, E. T., and Sanders-Loehr, J. (1991) *J. Am. Chem. Soc.*, *113*, 2055-2064.

Beratan, D. N., Onuchic, J. N., Betts, J. N., Bowler, B. E., and Gray, H. B. (1990) *J. Am. Chem. Soc. 112*, 7915-7921.

Bharadwaj, P. K., Potenza, J. A., and Schugar, H. J. (1986) *J. Am. Chem. Soc. 108*, 1352-1352.

Blair, D. F., Campbell, G. W., Schoonover, J. R., Chan, S. I., Gray, H. B., Malmstrom, B. G., Pecht, I., Swanson, B. I., Woodruff, W. H., Cho, W. K., English, A. M., Fry, H. A., Lum, V., and Norton, K. A. (1985) *J. Am. Chem. Soc. 107*, 5755-5766.

Carey, P. R. (1982) *Biochemical Applications of Raman and Resonance Raman Spectroscopies*, p. 47, Academic Press, New York.

Chakrabarti, P. (1989) *Biochemistry 28*, 6081-6085.

Chapman, G. V., Colman, P. M., Freeman, H. C., Guss, J. M., Murata, M., Norris, V. A., Ramshaw, J. A. M., and Venkatappa, M. P. (1977) *J. Mol. Biol. 110*, 187-189.

Chen, L., Mathews, F. S., and Davidson, V. L. (1991) manuscript submitted.

Church, W. B., Guss, J. M., Potter, J. J., and Freeman, H. C. (1986) *J. Biol. Chem. 261*, 234-237.

Collyer, C. A., Guss, J. M., Sugimura, Y., Yoshizaki, F., and Freeman, H. C. (1990) *J. Mol. Biol. 211*, 617-632.

Colman, P. M., Freeman, H. C., Guss, J. M., Murata, M., Norris, V. A., Ramshaw, J. A. M. and Venkatappa, M. P. (1978) *Nature 272*, 319-324.

Cupane, A., Leone, M., Vitrano, E., and Cordone, L. (1990) *Biophys. Chem. 38*, 213-224.

Czernuszewicz, R. S., LeGall, J., Moura, I., and Spiro, T. G. (1986) *Inorg. Chem. 25*, 696-700.

Dimitrov, M. I., Egorov, C. A., Donchev, A. A., and Atanasov, B. P. (1987) *FEBS Lett. 226*, 17-22.

Eklund, H. and Brändén, C.-I. (1983) in *Zinc Enzymes* (Spiro, T. G., Ed.) Chapter 4, Wiley, New York.

Farver, O., and Pecht, I. (1984) in *Copper Proteins and Copper Enzymes* (Lontie, R., Ed.) Vol. 1, pp 183-214, CRC Press, Boca Raton, Florida.

Feiters, M. C., Dahlin, S., and Reinhammar, B. (1988) *Biochim. Biophys. Acta 955*, 250-260.

Ferris, N. S., Woodruff, W. H., Tennent, D. L., and McMillin, D. R. (1979) *Biochem. Biophys. Res. Commun. 88*, 288-296.

Frey, M., Sieker, L. C., Payan, F., Haser, R., Bruschi, M., Pepe, G., and LeGall, J. (1987) *J. Mol. Biol. 197*, 525-541.

Garrett, T. P. J., Clingeleffer, D. J., Guss, J. M., Rogers, S. J., and Freeman, H. C. (1984) *J. Biol. Chem. 259*, 2822-2825.

Gewirth, A. A., Cohen, S. L., Schugar, H. J., and Solomon, E. I. (1987) *Inorg. Chem. 26*, 1133-1146.

Godden, J. W., Turky, S., Teller, D. C., Adman, E. T., Liu, M.-Y., Payne, W. J., and LeGall, J. (1991) manuscript submitted.

Gray, H. B. (1986) *Chem. Soc. Rev. 15*, 17.

Guss, J. M., and Freeman, H. C. (1983) *J. Mol. Biol. 169*, 521-563.

Guss, J. M., Harrowell, P. R., Murata, M., Norris, V. A., and Freeman, H. C. (1986) *J. Mol. Biol. 192*, 361-387.

Guss, J. M., Merritt, E. A., Phizackerley, R. P., Hedman, B., Murata, M., Hodgson, K. O., and Freeman, H. C. (1988) *Science 241*, 806-811.

Han, S., Czernuszewicz, R. S., and Spiro, T. G. (1989) *J. Am. Chem. Soc. 111*, 3496-3405.

Hildebrandt, P. G., Copeland, R. A., Spiro, T. G., Otlewski, J., Laskowski, M., Jr., and Prendergast, F. G. (1988) *Biochemistry 27*, 5426-5433.

Kakutani, T., Watanabe, H., Arima, K., and Beppu, T. (1981) *J. Biochem. 89*, 463-472.

Larrabee, J. A., and Spiro, T. G. (1980) *J. Am. Chem. Soc. 102*, 4217-4223.

Maret, W., Shiemke, A. K., Wheeler, W. D., Loehr, T. M., and Sanders-Loehr, J. (1986) *J. Am. Chem. Soc. 108*, 6351-6359.

Maret, W., and Kozlowski, H. (1987) *Biochim. Biophys. Acta 912*, 329-337.

Messerschmidt, A., Rossi, A., Ladenstein, R., Huber, R., Bolognesi, M., Gatti, G., Marchesini, A., Petruzelli, R., and Finazzi-Agro A. (1989) *J. Mol. Biol. 206*, 513-529.

Messerschmidt, A., and Huber, R. (1990) *Eur. J. Biochem. 187*, 341-352.

Mino, Y., Loehr, T. M., Wada, K., Matsubara, H., and Sanders-Loehr, J. (1987) *Biochemistry 26*, 8059-8065.

Mondovi, B., and Avigliano, L. (1984) in *Copper Proteins and Copper Enzymes* (Lontie, R., Ed.) Vol. 3, pp. 101-118, CRC Press, Boca Raton, Florida.

Musci, G., Desideri, A., Morpurgo, L., and Tosi, L. (1985) *J. Inorg. Biochem. 23*, 93-102.

Nestor, L., Larrabee, J. A., Woolery, G., Reinhammar, B., and Spiro, T. G. (1984) *Biochemistry 23*, 1084-1093.

Nishimura, Y., Hirakawa, A., Y., and Tsuboi, M. (1978) in *Advances in Infrared and Raman Spectroscopy* (Clark, R. J. H., and Hester, R. E., Eds.) Vol. 5, pp. 217-275, Heyden, London.

Norris, G. E., Anderson, B. F., and Baker, E. N. (1986) *J. Am. Chem. Soc. 108*, 2784-2785.

Peisach, J., Powers, L., Blumberg, W. E., and Chance, B. (1982) *Biochem. J. 38*, 277-285.

Penfield, K. W., Gewirth, A. A., and Solomon, E. I. (1985) *J. Am. Chem. Soc. 107*, 4519-4529.

Petratos, K., Banner, D. W., Beppu, T., Wilson, K. S., and Tsernoglou, D. (1987) *FEBS Lett. 218*, 209-214.

Petratos, K., Dauter, Z., and Wilson, K. S. (1988) *Acta Crystallogr. B44*, 628-636.

Roberts, V. A., Freeman, H. C., Getzoff, E. D., Olson, A. J., and Tainer, J. A. (1991) *J. Biol. Chem.* (in press).

Rydén, L. (1984) in *Copper Proteins and Copper Enzymes* (Lontie, R., Ed.) Vol. 1, pp. 157-182, CRC Press, Boca Raton, Florida.

Schneider, G., Eklund, H., Cedergren-Zeppezauer, E., and Zeppezauer, M. (1983) *Proc. Natl. Acad. Sci. U.S.A. 80*, 5289-5293.

Schneider, G., Cedergren-Zeppezauer, E., Eklund, H., Knight, S., and Zeppezauer, M. (1985) *Biochemistry 24*, 7503-7510.

Sharma, K. D., Loehr, T. M., Sanders-Loehr, J., Husain, M., and Davidson, V. L. (1988) *J. Biol. Chem. 263*, 3303-3306.

Shin, K.-S., and Zink, J. I. (1989) *Inorg. Chem. 28*, 4358-4366.

Siiman, O.; Young, N. M.; and Carey, P. R. (1976) *J. Am. Chem. Soc. 98*, 744-748.

Solomon, E. I., Gewirth, A. A., and Cohen, S. L. (1986) in *Excited States and Reactive Intermediates* (Lever, A. B. P., Ed.) pp. 236-266, American Chemical Society, Washington, DC.

Sykes, A. G. (1985) *Chem. Soc. Rev. 14*, 283-315.

Thamann, T. J., Frank, P., Willis, L. J., and Loehr, T. M. (1982) *Proc. Natl. Acad. Sci. USA 79*, 6396-6400.

van de Kamp, M., Silvestrini, M. C., Brunori, M., Van Beeumen, J., Hali, F. C., and Canters, G. W. (1991) *Eur. J. Biochem. 194*, 109-118.

Woodruff, W. H., Dyer, R. B., and Schoonover, J. R. (1988) in *Biological Applications of Raman Spectroscopy* (Spiro, T. G., Ed.) Vol. 3, pp. 413-438, Wiley, New York.

Table 3.1. Structural Characteristics of Blue Copper Sites

protein	M-S distance (Å)		dihedral angle (deg)		
	Cys	Met	S_δ-M-S_γ-C_β	M-S_γ-C_β-C_α	S_γ-C_β-C_αN
poplar plastocyanin[a]	2.07	2.82	-3	-168	169
algal plastocyanin[b]	2.12	2.92	-1	-166	166
oleander plastocyanin[c]	2.11	2.82	-4	-172	173
pseudoazurin[d]	2.16	2.76	-3	-178	166
cucumber basic protein[e]	2.15	2.62	-6	-171	166
azurin[f]	2.13	3.13	-1	-169	173
ascorbate oxidase[g]	2.1	2.9		-168	
alcohol dehydrogenase[h]	2.1			-174	190

[a] Bond lengths (e.s.d. = 0.04 Å) and dihedral angles for *P. nigra* var. *italica* plastocyanin at 1.33-Å resolution (J. M. Guss, H. D. Bartunik, and H. C. Freeman, unpublished results).

[b] Bond lengths (esd = 0.05 Å) and dihedral angles for *E. prolifera* plastocyanin at 1.85-Å resolution (Collyer et al., 1990).

[c] *O. nerium* plastocyanin at 1.8-Å resolution (Ton, 1991).

Table 1.1 (continued):

[d] Bond lengths for *A. faecalis* S-6 pseudoazurin at 1.55-Å resolution, R = 18% (Petratos et al., 1988); dihedryl angles from 2PAZ in The Brookhaven Protein Data Bank.

[e] Bond lengths (esd = 0.05 Å) and dihedral angles for cucumber basic protein at 1.8-Å resolution (J. M. Guss and H. C. Freeman, unpublished results.

[f] Bond lengths ± 0.05 Å for *A. denitrificans* azurin at 1.8-Å resolution, R = 16.4% (Baker, 1988); bond angles from 2AZA in The Brookhaven Protein Data Bank.

[g] Bond lengths ± 0.2 Å and bond angles for zucchini ascorbate oxidase at 1.9-Å resolution, R = 20.5% (A. Messerschmidt, personal communication).

[h] Data for catalytic *zinc* site in horse liver alcohol dehydrogenase at 2.4-Å resolution (Chakrabarti, 1989).

Table 3.2. Resonance Raman Vibrational Frequencies and Deuterium Isotope Shifts for Cupredoxins[a]

plastocyanin[b]		pseudoazurin[b]		azurin[c]		Cu(II)-ADH[d]	
H_2O	ΔD_2O	H_2O	ΔD_2O	H_2O	ΔD_2O	H_2O	ΔD_2O
266	-1	264	-1	266		264	-2
				287	-2	316	-2
339		339		333		342	
		359		348		*358	↓
375	-3	366	-1	373	-1	372	↓
383	-1	*386	-3			380	+2
403	-2	*397		401	-2	401	-3
		415	-3↓	*409	-1	*419	+2
*424				428	-2		
437	-1	*444	-2	441	-2		
459		462	-1	455	-1		

[a] Frequencies and isotope shifts in D_2O (in cm^{-1}) rounded to the nearest whole number. An asterisk (*) denotes peaks of highest itensity. An arrow (↓) denotes decrease in intensity.

[b] Poplar plastocyanin I and *A. faecalis* pseudoazurin (this work).

[c] *P. aeruginosa* azurin (T. den Blaauwen, G. W. Canters, J. Han, T. M. Loehr, and J. Sanders-Loehr, unpublished results).

[d] Cu(II)-substituted alcohol dehydrogenase containing NADH (Maret et al., 1986).

Table 3.3. Correlation of Ligand Loop Size and Maximal Raman Intensity

protein	residue number[a]			maximal Raman intensity[b]	EPR spectral type[c]
	Cys (n)	His ($n+x$)	x		
alcohol dehydrogenase	46	67	21	358 (419)	rhombic
nitrite reductase	136	145	9	362	rhombic
ascorbate oxidase	508	513	5	383	axial
stellacyanin	87	92	5	385	rhombic
cucumber basic protein	79	84	5	391	rhombic
azurin	112	117	5	409	axial
rusticyanin	138	143	5	412	rhombic
auracyanin	123	128	5	415	rhombic
plastocyanin	84	87	3	424	axial
amicyanin	86	89	3	430	axial
pseudoazurin	78	81	3	444 (386)	rhombic

[a] Residue in amino acid sequence. x = The difference between Cys(n) and His ($n+x$). Source of sequence data: ADH, AO, CBP, Az, Pc, and PAz (references in Table 3.1); NiR (Fenderson et al., 1991); Sc (Guss et al., 1988); Rc (M. Ronk, J. E. Shively, E. A. Shute, and R. C. Blake, personal communication); Arc (J. van Beeumen, J. D. McManus, and R. E. Blankenship, personal communication); Amc (Sharma et al., 1988). The protein sources and abbreviations as described in Figure 3.4.

[b] Frequency of the most intense Raman peak in cm^{-1} (additional peak of high intensity) from references in Figure 3.4.

[c] X-band EPR data sources: Cu-ADH (Maret and Kozlowski, 1987); NiR (B. A. Averill, personal communication); AO (Mondovi and Avigliano, 1984); Sc, CBP, Az, Rc, Pc, Amc (references cited by Adman, 1985); Arc (J. D. McManus and R. E. Blankenship, personal communication); PAz (Kakutani et al., 1981).

FIGURE LEGENDS

Figure 3.1. (A) Superposition of the copper sites in pseudoazurin (BPN) from *A. faecalis* (thick lines) and poplar plastocyanin (PCY) (thin lines). (B) Superposition of the copper sites in pseudoazurin (thick lines) and *A. denitrificans* azurin (AZ) (thin lines). The drawings were made from X-ray coordinates in the Brookhaven Protein Data Bank for pseudoazurin at 2.0-Å resolution (2PAZ), plastocyanin at 1.6-Å resolution (1PCY), and azurin at 1.8-Å resolution (2AZA). Also shown for pseudoazurin are the hydrogen bonds (• • •) between copper ligands and protein moieties and between the side chain of the conserved Asn-41 and the backbone NH and side chain of Thr-79. Analogous hydrogen bonds (not shown) are found in plastocyanin and azurin.

Figure 3.2. Resonance Raman spectra of plastocyanins from oleander (A), poplar component I (B), and component II (C). Spectra A and B were obtained on samples ~0.5 mM in Cu(II), pH 6.0, at 15 K with 570-nm excitation (65 mW) with a resolution of 4 cm^{-1}, a scan rate of 0.5 cm^{-1}/s, and are accumulations of 20 scans each. Spectrum C was obtained on a sample 0.35 mM in Cu(II) in 0.1 M phosphate (pH 7.0) plus 6-fold excess $K_3Fe(CN)_6$ under similar conditions except for a resolution of 5 cm^{-1}, a scan rate 1.0 cm^{-1}/s, and 10 scans. Omission of the $K_3Fe(CN)_6$ or changing the buffer to 0.1 M acetate (pH 4.2) caused no significant changes in the RR spectrum of poplar PcII. S denotes peaks from frozen solvent (translational modes of ice).

Figure 3.3. Resonance Raman spectra of pseudoazurin and plastocyanin in H_2O (—) and D_2O (• • •). (A) Pseudoazurin from *A. faecalis* (1.5 mM in H_2O, 1.2 mM in D_2O). Spectra were obtained at 15 K with 647.1-nm excitation (70 mW) with a resolution of 5 cm^{-1}, a scan rate of 0.5 cm^{-1}/s, and 20 scans each. (B) Poplar plastocyanin (0.5 mM in H_2O, 0.6 mM in D_2O). Spectral conditions as in Figure 3.2. Indicated peak frequencies are for protein in H_2O.

Figure 3.4. Relative peak intensities in the resonance Raman spectra of blue copper proteins. Data taken from the following sources: Cu(II)-alcohol dehydrogenase (ADH) (Maret et al., 1986), *Achromobacter cycloclastes* nitrite reductase (NiR) (J. Sanders-Loehr, and B. A. Averill, unpublished results), zucchini ascorbate oxidase (AO) (Siiman et al., 1976), *Rhus vernicifera* stellacyanin (Sc) (Nestor et al., 1984), cucumber basic protein (CBP) (R. B. McInnes, R. S. Armstrong, and H. C. Freeman, unpublished results), *A. denitrificans* azurin (Az) (Ainscough et al., 1987), *Thiobacillus ferroxidans* rusticyanin (Rc) (T. A. Andary, R. S. Armstrong, and H. C. Freeman, unpublished results), *Chloroflexus aurantiacus* auracyanin A (Arc) (J. D. McManus, D. C. Brune, J. Han, J. Sanders-Loehr, and R. E. Blankenship, unpublished results), *Paracoccus denitrificans* amicyanin (Amc) (Sharma et al., 1988), poplar plastocyanin (Pc) and *A. faecalis* pseudoazurin (PAZ) (this work).

Figure **3.5.** Common features of blue copper sites in cupredoxins: Electron donors or acceptors which react with cupredoxin-type domains are believed to utilize either the hydrophobic patch and/or the electron-transfer site adjacent to residue (*n-1*).

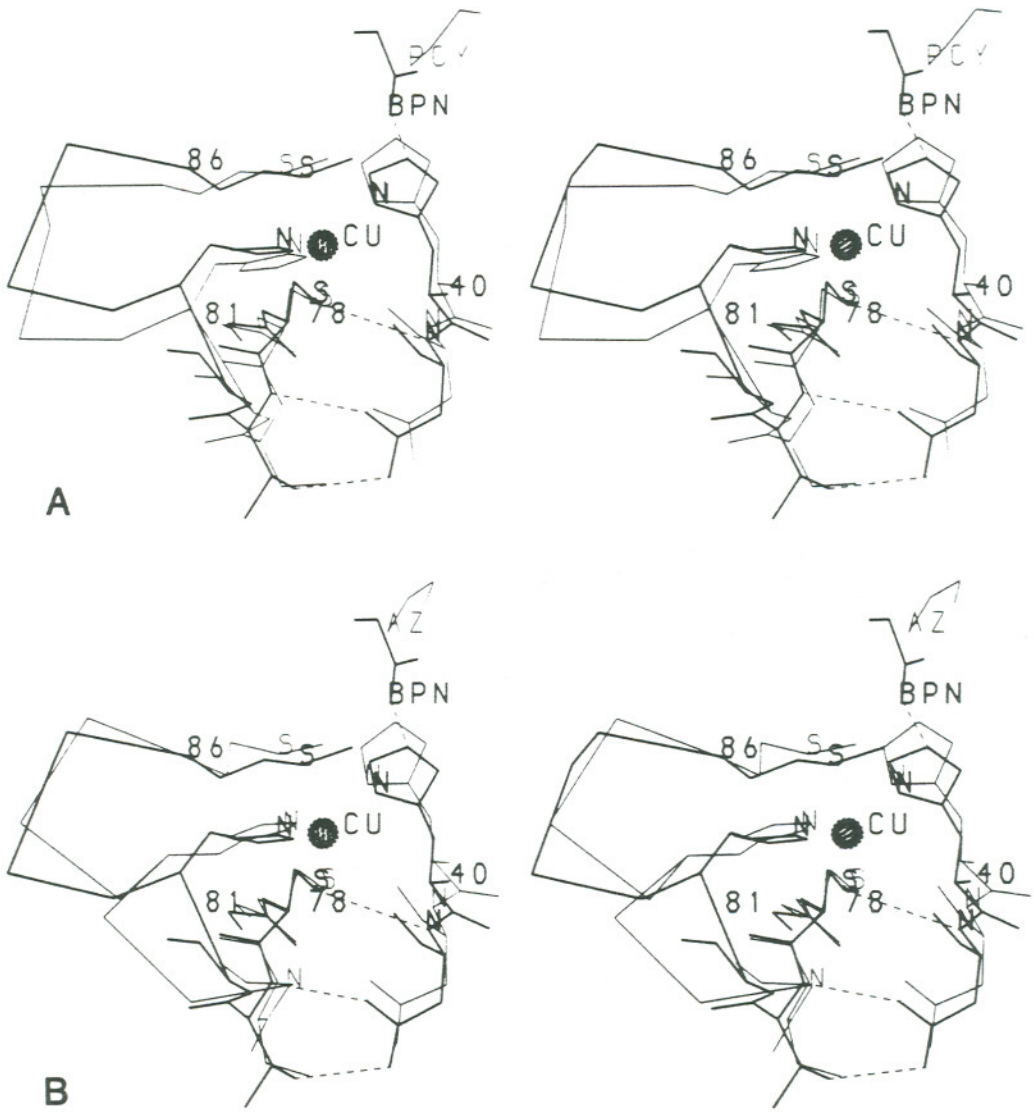
BPN
86
CU
40
81
78
A
BPN
86
CU
40
81
78
A
BPN
86
CU
40
81
78
B
BPN
86
CU
40
81
78
B

Figure 3.1

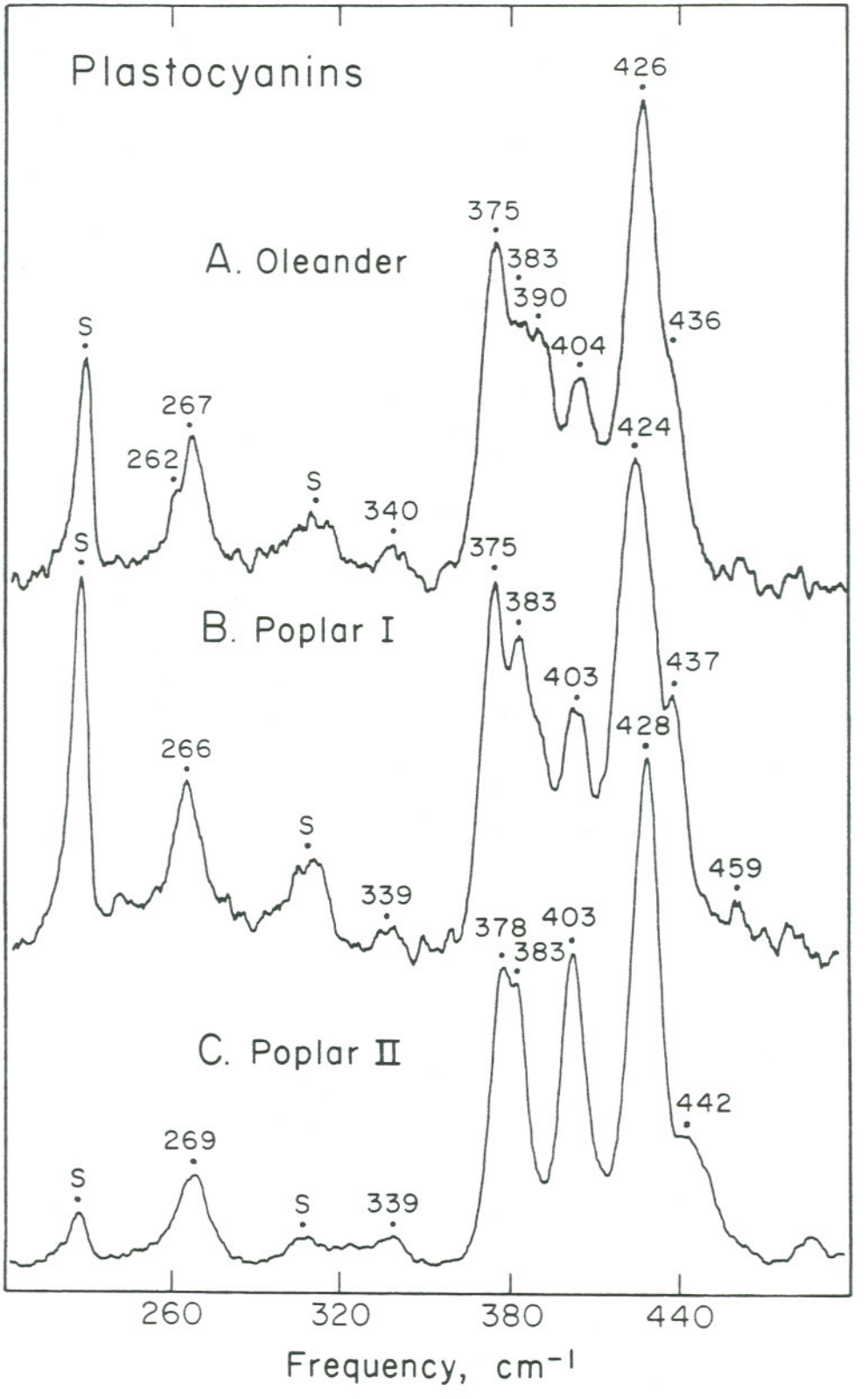
Plastocyanins
A. Oleander
B. Poplar I
C. Poplar II
S
267
262
S
340
375
383
390
404
426
436
424
S
375
383
403
437
428
266
S
339
459
378
403
383
442
269
S
S
339
260
320
380
440
Frequency, cm⁻¹

Figure 3.2

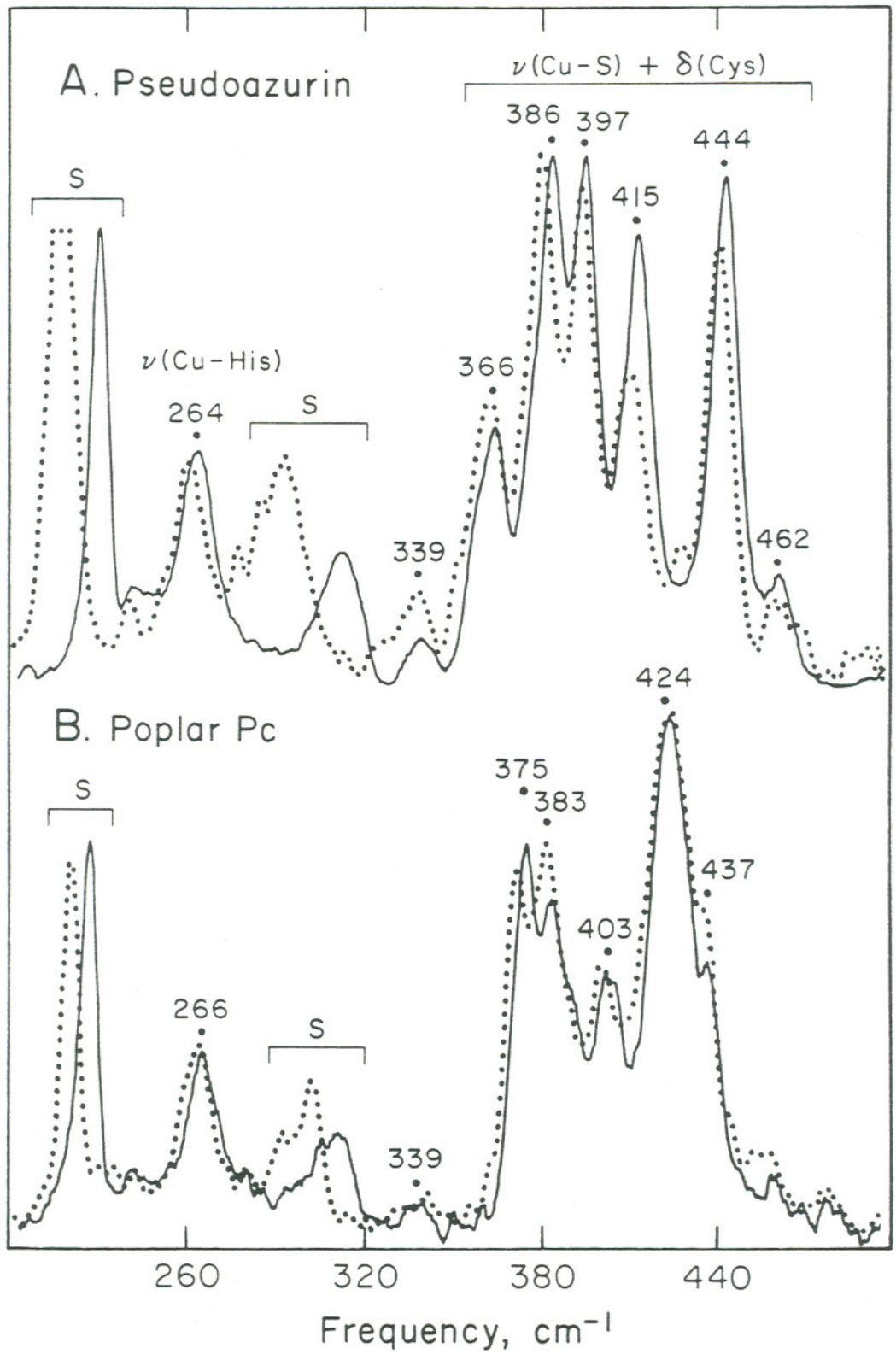
A. Pseudoazurin
ν(Cu-S) + δ(Cys)
386
397
444
415
S
ν(Cu-His)
366
264
S
339
462
B. Poplar Pc
424
375
383
S
437
403
266
S
339
260
320
380
440
Frequency, cm⁻¹

Figure 3.3

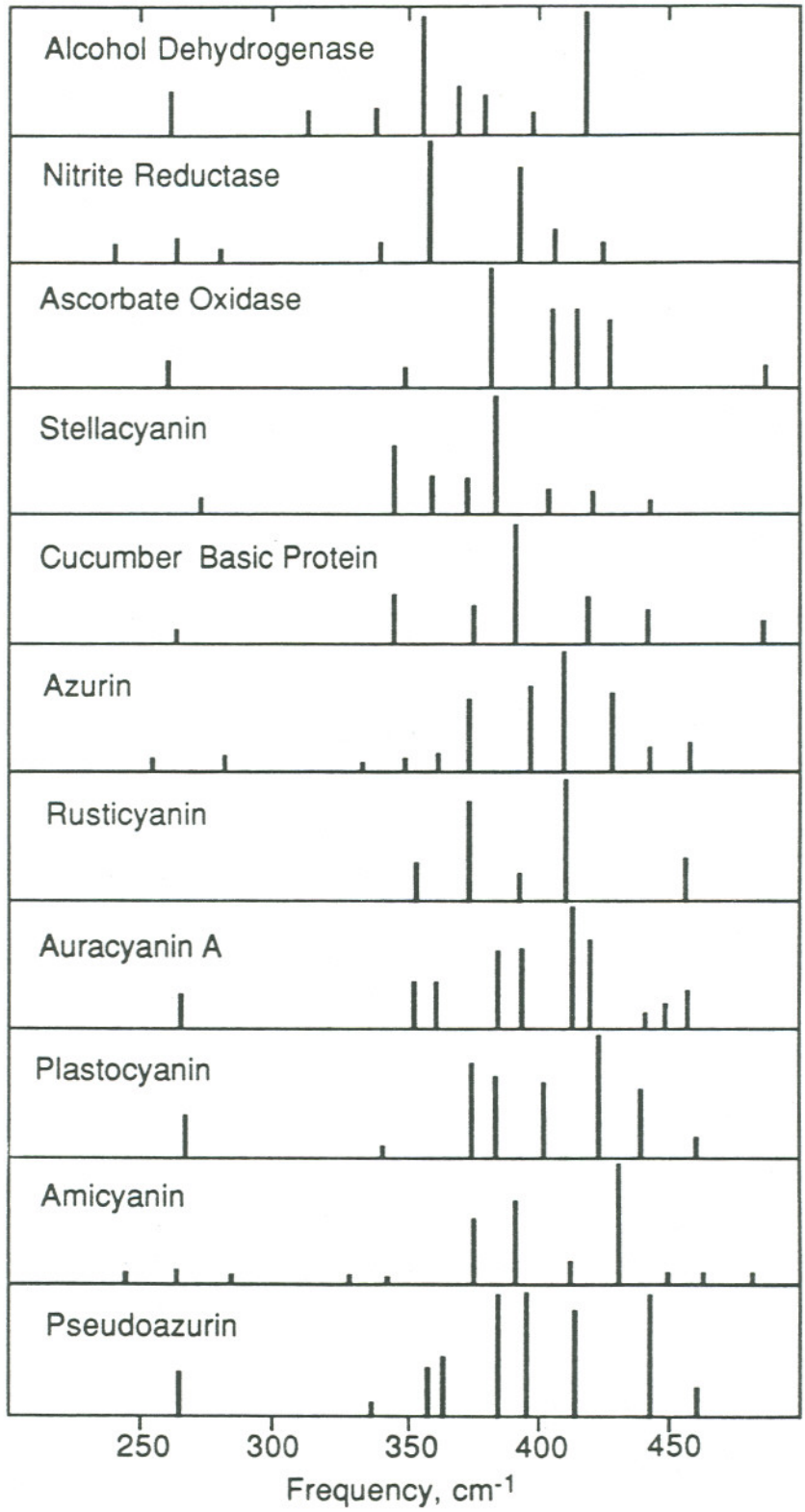
Alcohol Dehydrogenase
Nitrite Reductase
Ascorbate Oxidase
Stellacyanin
Cucumber Basic Protein
Azurin
Rusticyanin
Auracyanin A
Plastocyanin
Amicyanin
Pseudoazurin
250
300
350
400
450
Frequency, cm-1

Figure 3.4

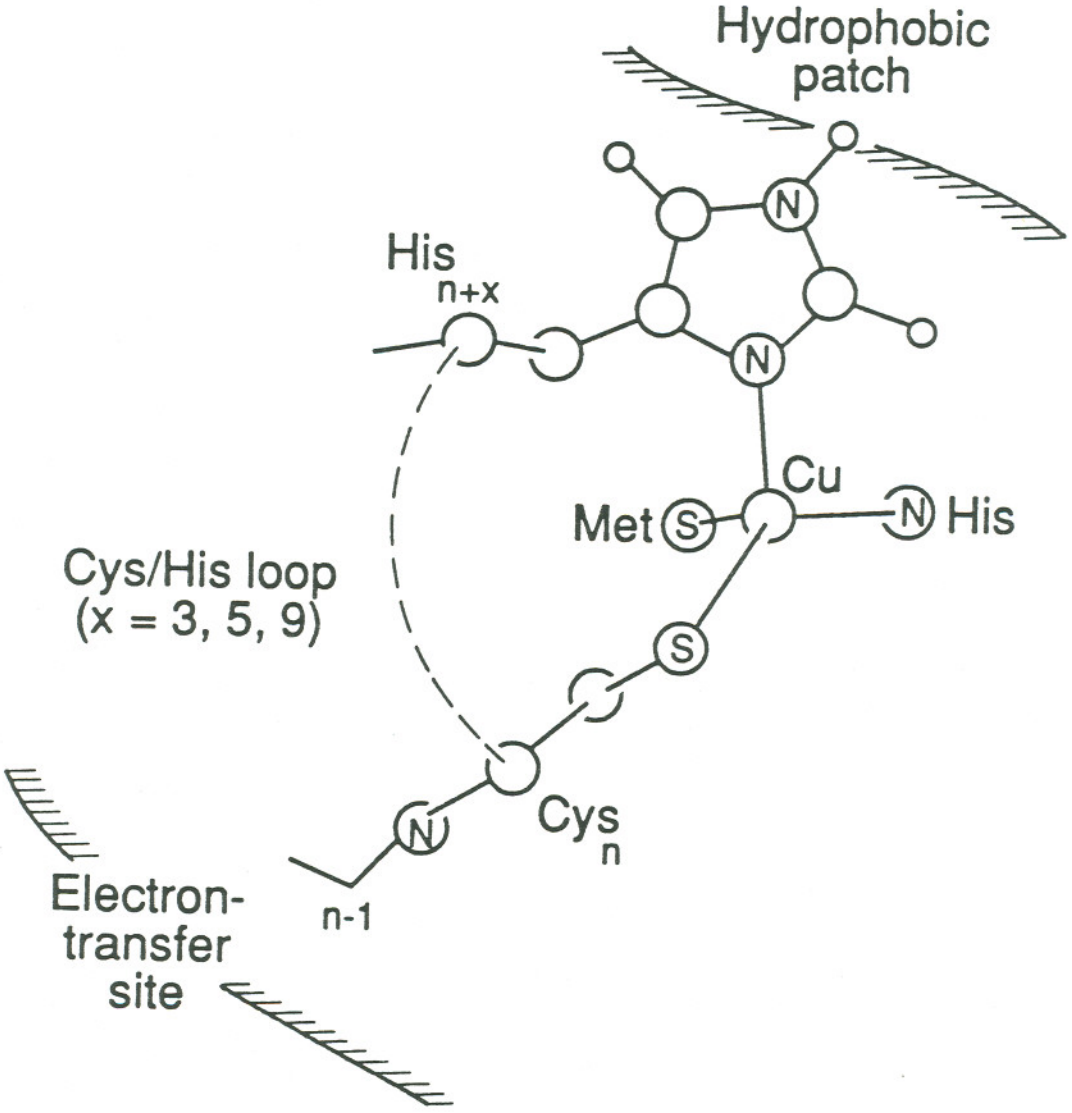
Hydrophobic
patch
His
n+x
N
N
Cu
Met
S
N
His
Cys/His loop
(x = 3, 5, 9)
S
N
Cys
n
n-1
Electron-
transfer
site

Figure 3.5

Chapter 4

RESONANCE RAMAN EXCITATION PROFILES INDICATE MULTIPLE Cys → Cu CT TRANSITIONS IN TYPE 1 COPPER PROTEINS[1]

4.1 Introduction

Type 1 (blue) copper sites are found in both mononuclear and multinuclear copper proteins where their most common function is the catalysis of inter- and intramolecular electron transfer, respectively.[2] X-ray crystal structure determinations for seven different proteins (3 plastocyanins, azurin, pseudoazurin, basic blue protein, and ascorbate oxidase) reveal a highly conserved site with the copper coordinated to one cysteine and two histidines in a nearly trigonal planar array.[2] This unusual trigonal pyramidal geometry includes a short Cu-S(Cys) at a distance of 2.12 $\pm$ 0.05 Å and an axial methionine at a considerably longer distance of 2.6-3.1 Å.[3]

Another striking feature of the type 1 Cu site is its intense absorption (ϵ > 3,000 M^{-1} cm^{-1}) near 600 nm.[4,5] In a recent study of plastocyanin, Gewirth and Solomon[6] proposed detailed assignments of the entire electronic spectrum. The dominant band at 600 nm was ascribed to a charge-transfer transition from the cysteinate S pπ orbital to the $d_{x^2-y^2}$ orbital of Cu(II), with the large intensity deriving from the excellent overlap between ground- and excited-state wave functions. An unresolved band at 535 nm was ascribed to a transition involving pseudo-σ overlap between a cysteinate S p orbital and a Cu d orbital. Two weak features at 430 and 465 nm were attributed to Met → Cu(II) and His → Cu(II) CT, respectively. Finally, the four absorption bands at lower energy (between 650 and 1050 nm) were assigned to ligand-field transitions, particularly on the basis of their MCD behavior. This analysis revealed that the Cu(II)-thiolate interaction

---

[1] As published in the *Journal of the American Chemical Society* **1993,** *115,* 4256-4263.

dominates the electronic spectrum, leading to the possibility of multiple (Cys)S → Cu(II) CT transitions and the probable contribution of Cu ligands to a number of different absorption bands.

An anomalous electronic spectrum is associated with the type 1 Cu site of nitrite reductase (NiR) from *Achromobacter cycloclastes*.[7,8] According to the X-ray crystal structure, the protein has a typical type 1 Cu site with a His_2Cys trigonal planar ligand set which functions to transfer electrons to a type 2 Cu, 12.5 Å away.[9] The type 2 Cu site appears to be responsible for the reduction of NO_2^- to NO or N_2O.[9,10] In the absorption spectrum of NiR, the most intense feature occurs at 458 nm (ϵ = 2,530 M^{-1} cm^{-1}) with additional prominent bands at 385, 585, and 695 nm. This spectrum is unaltered in protein samples that are deficient in type 2 copper.[11] Despite the unusual electronic spectrum associated with the NiR copper site, its EPR and resonance Raman (RR) spectra are otherwise characteristic of a type 1 Cu.[11,12]

A similarly unusual electronic spectrum is observed for a mutant of Cu_2Zn_2-superoxide dismutase (SOD) from *Saccharomyces cerevisiae*. In the native yeast protein, the tetragonal type 2 Cu appears to be coordinated to four His, one of which bridges through imidazolate to a tetrahedral Zn having two other His and one Asp as ligands (Figure 4.5).[13,14] Mutation of His 80 in the zinc site to Cys and replacement of Zn by Cu creates a type 1 Cu site in H80C-Cu_2Cu_2SOD, based on its absorption and EPR spectra.[15] Like NiR, the mutant SOD has several intense CT bands with the strongest occurring at 459 nm ($\epsilon \geq$ 1,460 M^{-1} cm^{-1}) and a somewhat weaker one at 595 nm ($\epsilon \geq$ 1,420 M^{-1} cm^{-1}).[16]

To gain more information about these type 1 Cu sites and to understand the diversity of their absorption spectra, we have undertaken a study of their RR spectra and enhancement profiles. The RR spectra of type 1 Cu proteins exhibit as many as nine resonance-enhanced vibrational fundamentals between 330 and 490 cm^{-1}.[17,18] The multiplicity of spectral features is believed to be due to a kinematic coupling of the Cu-S(Cys) stretch with vibrational motions of the cysteine and histidine ligands. Such coupling, particularly with cysteine ligand deformations, is enhanced by the coplanarity of the Cu-S bond with the C_β, C_α, and N atoms of the cysteine moiety.[3] All of the RR modes show a maximum in intensity as the excitation wavelength approaches 600 nm,

indicating that the Raman enhancement is derived from vibronic coupling with the principal (Cys)S → Cu(II) CT transition.[19,20]

We have found that the RR spectra of NiR and mutant SOD (Cu_2Cu_2-H80C) are similar to those of other type 1 Cu proteins. This observation implies the presence of a coplanar cysteinate ligand with a Cu-S_γ-C_β-C_α dihedral angle close to 180° in these proteins. In addition, the same set of vibrational modes is enhanced by excitation within either the 460- or 600-nm bands, indicating that both absorption bands have substantial (Cys)S → Cu(II) CT character. A careful investigation of the enhancement behavior of two other type 1 Cu proteins, azurin and pseudoazurin, reveals that the electronic transitions in the 460-nm region, although weaker, also contain a substantial contribution from a Cu-cysteinate chromophore. Thus, the 460-nm absorption in type 1 copper proteins is likely to have Cys → Cu(II) CT character in addition to the previously assigned His → Cu(II) CT.[6]

4.2 Experimental Procedures

4.2.1 Protein Samples

Azurin from *Alcaligenes denitrificans* was obtained from a cloned azu gene expressed in *Escherichia coli*[21] and was the gift of Dr. Gerard Canters and Carla Hoitink. Pseudoazurin from *Alcaligenes faecalis* S-6[22] was the gift of Dr. Teruhiko Beppu. Nitrite reductase from *Achromobacter cycloclastes* was purified in its native and type-2-depleted forms as described previously.[11] The H80C mutant of yeast superoxide dismutase was prepared in the apo form and reconstituted with 4 equivalents of copper (in both the Cu and Zn sites) to yield Cu_2Cu_2-H80C.[15,23]

4.2.2 Resonance Raman Spectroscopy

Raman spectra were obtained on a Jarrell-Ash 25-300 spectrophotometer, equipped with an Ortec Model 9302 amplifier/discriminator and an RCA C31034 photomultiplier, and interfaced to an Intel 310 computer. The desired excitation wavelengths were provided by the following lasers: Spectra-Physics 2025-11 Kr, Coherent Innova 90-6 Ar, and Coherent 599-01 Dye (rhodamine 6G). Raman spectra were collected in an ~150° backscattering geometry from samples maintained at ~15 K using a closed-cycle helium refrigerator (Air Products Displex). Accurate peak heights

and peak positions ($\pm$ 1 cm^{-1}) were obtained by ordinate and abscissa expansion, respectively. For the enhancement profiles, all spectra were recorded on the same sample under the same instrumental conditions. Enhancement was measured as the height of the protein peak relative to the height of the ice peak at 230 cm^{-1}, except for mutant SOD where peak areas were measured.

4.3 Results and Discussion

4.3.1 Resonance Raman Spectrum of Pseudoazurin

Excitation of type 1 Cu proteins within the intense, 600-nm (Cys)S → Cu(II) CT band leads to characteristic RR spectra having one-to-two vibrational fundamentals in the 250-280 cm^{-1} region and as many as nine fundamentals in the 330-490 cm^{-1} region.[3] Pseudoazurin from *A. faecalis* is a typical blue copper protein according to its X-ray crystal structure,[24,25] and it exhibits a typical type 1 Cu RR spectrum (Figure 4.1B).[3] In the 330-490-cm^{-1} region, seven distinct peaks are observed at 340, 363, 385, 397, 415, 444, and 460 cm^{-1}. The multiplicity of vibrational modes has been ascribed to kinematic coupling, an admixture of the Cu-S(Cys) stretch with cysteine and histidine ligand deformation modes.[17,18] Such coupling is favored by Cu-S_γ-C_β-C_α and S_γ-C_β-C_α-N dihedral angles being close to 180°,[17,26] as is the case in pseudoazurin and a number of other type 1 Cu proteins.[3] The fact that these vibrational modes occur at a fairly constant set of frequencies in all blue copper proteins is a reflection of the highly conserved ground-state structure of the type 1 Cu site.[3]

In contrast, the RR spectra of different blue Cu proteins show a striking variability in vibrational peak intensities. For example, the strongest feature in the RR spectrum of pseudoazurin is at 397 cm^{-1} (Figure 4.1B), whereas those for azurin and plastocyanin are at 408 and 425 cm^{-1}, respectively.[18] Resonance Raman peak intensities are related to the change in geometry of the copper-cysteinate chromophore in the electronic excited state. The intensity of a particular mode is maximized when the excited-state displacement of atoms occurs along the normal coordinate of the vibration.[27,28] It is likely that differences in protein structure beyond the first coordination sphere in different blue copper proteins affect the excited-state displacements, thereby explaining the variation in RR intensities.[3]

Excitation of pseudoazurin within its 450-nm absorption band (Figure 4.2) leads to the same set of RR frequencies (Figure 4.1A). There are, however, some alterations in RR intensities. For example, the peak at 363 cm^{-1} has increased relative to the other modes. The constancy of frequencies shows that the electronic transitions at 450 and 590 nm arise from a common ground-state structure, i.e., a single type 1 Cu site. The variability in intensities, in this case, suggests that different electronic transitions are responsible for the 450 and 590 nm absorption bands.

4.3.2 Resonance Raman Spectrum of Nitrite Reductase

NiR from *A. cycloclastes* is a trimeric protein containing a type 1 Cu site (Figure 4.3, insert) in the amino-terminal domain of each monomer.[9] There is also a type 2 Cu site at a distance of 12.5 Å that is connected to the type 1 site by a His-Cys sequence where the His is coordinated to the type 2 Cu and the Cys is coordinated to the type 1 Cu. The type 2 site appears to be responsible for binding the nitrite substrate. NiR can be depleted of 80% of its type 2 Cu and lose 80% of its enzymatic activity, and still have an intact type 1 Cu site according to absorption and EPR spectroscopy.[11] The RR spectrum of type-2-depleted NiR (data not shown) is identical to that of the native enzyme (Figure 4.3A). This indicates the RR spectrum of NiR arises solely from the type 1 Cu site. Even though the type 1 Cys ligand is flanked by a His ligand to the type 2 site, there is no apparent change in the type 1 copper cysteinate geometry upon removal of the type 2 copper.

The absorption spectrum of NiR is unusual for a type 1 site in that it exhibits four intense bands at 385, 460, 585, and 695 nm (Figure 4.4). Excitation within the predominant 460-nm absorption band produces the RR spectrum shown in Figure 4.3A. This spectrum is the same as that reported previously for *A. cycloclastes* NiR,[12] and it is characteristic of a type 1 Cu site. It exhibits one strong fundamental at 262 cm^{-1} (a weaker peak at 280 cm^{-1} tends to be obscured by the ice mode) and six distinct fundamentals at 343, 361, 395, 409, 424, and 443 cm^{-1}. Excitation within the 585- and 695-nm absorption bands leads to a similar set of resonance-enhanced spectral features, unchanged in their vibrational energies (Figures 4.3B,C). Thus, the same copper-cysteinate moiety must be contributing to all three of these electronic transitions (Figure 4.4). A previous RR investigation of NiR also assigned the 460-nm absorption as S(Cys)

→ Cu CT, but proposed that two separate Cu-S(Cys) moieties were responsible for the 460- and 585-nm transitions.[12] Those spectra, however, were obtained in glass capillaries and were distorted by the presence of an underlying glass band (between 350 and 520 cm^{-1}) in addition to low signal-to-noise. The present evidence for a single Cu-S(Cys) chromophore is compelling.

An interesting aspect of the RR spectrum of NiR is that the 361-cm^{-1} peak is more enhanced with 477-nm excitation and actually becomes the dominant feature in the RR spectrum (Figure 4.3). This is similar to the behavior of pseudoazurin whose 363-cm^{-1} peak is also the strongest spectral feature with 458- or 488-nm excitation (Figures 4.1, 4.2). In a previous study, we noted that high Raman intensity in the 350-365-cm^{-1} region appeared to correlate with the presence of a long loop of 8 amino acids between the Cys 136 and His 145 ligands of NiR (Han et al., 1991). However, the present findings for pseudoazurin show that enhancement in the 350-365-cm^{-1} region is also dependent on excitation wavelength. It cannot be just a function of loop size since pseudoazurin has only two amino acids in the loop connecting Cys 78 and His 81 ligands.[24]

4.3.3 Resonance Raman Spectrum of Mutant Superoxide Dismutase

In native yeast Cu_2Zn_2SOD,[14] the Zn(II) in each subunit is ligated to His 71, His 80, and Asp 83, with the imidazolate of His 63 bridging the Zn and Cu ions (Figure 4.5). The Zn(II) site has a geometry close to tetrahedral. When the His 80 ligand is converted to Cys by site-directed mutagenesis and the protein is reconstituted with four Cu(II), the resultant protein has the EPR properties of a 1:1 mixture of type 1 and type 2 copper sites.[15,23] The type 1 component, arising from the original zinc site, is responsible for the green color of the mutant protein and yields a RR spectrum typical of a blue copper protein (Figure 4.6). Two vibrational fundamentals appear at 259 and 280 cm^{-1} and six higher-energy fundamentals are seen at 341, 352, 398, 415, 435, and 468 cm^{-1}. In addition, a several less intense bands are observed at even higher energy at 606, 702, 754, and 813 cm^{-1} (Figure 4.6, insert) that are also characteristic of type 1 Cu sites.[18] These bands can be ascribed, respectively, to a combination band (352 + 259 = 611), an overtone (2 × 352 = 704), the C-S stretch of cysteine at 754 cm^{-1}, and another combination band (352 + 468 = 820).

The RR spectrum of H80C-Cu_2Cu_2SOD is clearly indicative of copper cysteinate coordination. The similarity of vibrational frequencies to other type 1 copper sites suggests a number of common structural features. (i) The multiple vibrational modes arise from coupling of the Cu-S(Cys) stretch with Cys and other ligand deformations. (ii) The conserved nature of the Cu-S stretching and Cys bending force constants requires a similarly short Cu-S(Cys) bond length of $\sim 2.12 \pm 0.05$ Å.[3] (iii) The kinematic coupling further requires a coplanar orientation for the Cys 80 ligand with a Cu-S_γ-C_β-C_α dihedral angle close to 180°. (iv) The short Cu-S(Cys) bond implies a trigonal planar array of ligands.[29]

The electronic and RR spectral properties of the type 1 Cu site in H80C-Cu_2Cu_2SOD appear closely related to those of the type 1 Cu site in NiR. The absorption spectrum exhibits two strong components at 458 and 597 nm, with the 458-nm band being slightly more intense (Figure 4.7). Excitation within either absorption band yields the same RR spectrum (Figure 4.6), suggesting that both absorptions involve S(Cys) → Cu(II) CT transitions. The extent of resonance enhancement (as judged by the intensity of the protein Raman peaks relative to the ice mode) is comparable to other type 1 Cu proteins (Figures 4.2, 4.4, 4.7), indicating similar displacements in the electronic excited state. The only differences in the RR spectra of mutant SOD between 647- and 458-nm excitation are increased intensities at 296 and 341 cm^{-1} and decreased intensities at 259 and 280 cm^{-1} (Figure 4.6). An unusual aspect relative to other blue copper proteins is that the RR spectrum of mutant SOD is so strongly dominated by the peak at 352 cm^{-1} at all excitation wavelengths, with only weakly enhanced bands in the 380-480-cm^{-1} region. The RR spectra of NiR also lack intensity in the 420-480-cm^{-1} region, but the effect is considerably more pronounced for mutant SOD.

Two additional mutants of yeast SOD, each with a cysteine in place of a Cu-site histidine (Figure 4.5), were examined. These were H46C-Cu_2Zn_2SOD[15] and H120C-Cu_2Zn_2SOD.[16] Cysteinate coordination of the copper in each mutant is evident from the appearance of a S(Cys) → Cu(II) CT band at 379 nm (ϵ = 1,940 M^{-1} cm^{-1}) and 406 nm (ϵ = 1,120 M^{-1} cm^{-1}), respectively. The high energy of these electronic transitions is suggestive of tetragonal rather than tetrahedral coordination geometry.[30a] For example, tetragonal cupric thiolate complexes often exhibit absorption maxima at 400-430 cm^{-1}

with ϵ = 1,000-6,500 M^{-1} cm^{-1}.[29] Excitation of the H46C mutant at 350.8 nm produced a weak RR spectrum with the most distinct peak at 343 cm^{-1}; excitation of the H120C mutant at 406.7 nm yielded an even weaker RR spectrum with a detectable peak at 367 cm^{-1} (data not shown).[30b] The weak resonance enhancement and large EPR $A_{\|}$ values (Table 4.1) are also consistent with a tetragonal assignment.

4.3.4 Raman Intensities for Type 1 versus Type 2 Copper

The major criterion for distinguishing between type 1 and type 2 copper has been the EPR hyperfine splitting, with small $A_{\|}$ values of 30-70 $\times$ 10^{-4} cm^{-1} defining a type 1 site and larger $A_{\|}$ values of 130-180 $\times$ 10^{-4} cm^{-1} defining a type 2 site (Table 4.1). Crystal structures of proteins and model compounds have revealed that whereas type 2 Cu tends to have four strongly coordinated ligands in a tetragonal array and a Cu-S bond distance $\geq$2.25 Å, type 1 Cu tends to be associated with a trigonal planar ligand set. This decrease in the number of strongly coordinated ligands is presumably responsible for the shortening of the Cu-S bond to ~2.15 Å (Table 4.1) and the change in the EPR hyperfine character. For type 2 Cu, the wavelength of the most intense thiolate $\rightarrow$ Cu(II) CT band is quite variable, with absorption maxima ranging from 380-590 nm (Table 4.1). This electronic transition is somewhat less variable for type 1 Cu with maximum absorption occurring either at 595-665 nm or near 460 nm. Despite the variability in absorption maxima, it appears that type 1 and type 2 Cu sites can be distinguished by their different extents of RR intensity enhancement.

For solids or samples in aqueous solution, Raman intensities can be quantitated relative to the intensity of the 980-cm^{-1} symmetric stretch of a sulfate internal standard. The type 1 copper proteins (**1**-**6**) listed in Table 4.1 have large Raman enhancements with molar scattering intensities of 100-600 relative to sulfate. The molar scattering values $\geq$500 tend to be associated with ϵ values near 5,000 $M^{-1}cm^{-1}$, whereas those in the 120-200 range are associated with ϵ values near 2,500 $M^{-1}cm^{-1}$. This is commensurate with the expectation that Raman intensities for symmetric vibrations are proportional to ϵ^2.[18] The sterically hindered Cu complexes (**8**, **9**) with tris-pyrazolylborate and $SCPh_3$ or SC_6F_5 as ligands are the first small-molecule models in which type-1 Cu properties have been duplicated. Each of these complexes has a CuN_2S cluster in a trigonal planar array

with an unusually short Cu-S bond and narrow hyperfine splitting.[29] These complexes also yield a set of strongly enhanced Raman modes derived from the Cu-SR moiety.[35]

Although the type 2 copper complexes (**10-15**) and proteins (**16-19**) in Table 4.1 exhibit extinction coefficients of similar magnitude to the type 1 complexes (i.e., 1,000-6,000 $M^{-1}cm^{-1}$), they give rise to considerably less RR enhancement of Cu-thiolate vibrational modes. The observed molar scattering values of 10-60 relative to sulfate are 5-10 times smaller than for the corresponding type 1 sites with similar extinction coefficients. Thus, it would appear that the Cu-cysteinate moiety in type 1 Cu undergoes a greater change in geometry in the excited state, leading to more extensive vibronic coupling than is observed for type 2 Cu.

4.3.5 Raman Excitation Profiles

An excitation profile for a particular vibrational mode is obtained by collecting RR spectra at a number of different excitation wavelengths and plotting the vibrational intensity as a function of wavelength. Peaks in the excitation profile are expected to correspond with peaks in the electronic spectrum. If the atoms responsible for the vibrational mode are known, this information can be used to assign the nature of the electronic transition. A typical RR excitation profile for a blue copper protein is shown in Figure 4.8 for azurin from *A. denitrificans*. All of the vibrational features have maximum intensity corresponding to the 619-nm absorption band. Similar findings have been reported previously for this azurin[19] and for stellacyanin.[20] These results show that all of the vibrational modes are associated with the same chromophoric species. Isotope and ligand-substitution experiments,[17,18,49] as well as MCD and single-crystal polarized absorption experiments,[5,6] all point to the Cu-cysteinate moiety as the chromophore responsible for the $\sim$600-nm absorption and, thus, many of the observed RR modes.

Although a strong absorption band near 600 nm (band 2) has been the hallmark for type 1 Cu, there is a 2.5-fold variability in the magnitude of the extinction coefficient (Table 4.2). There appears to be a corresponding, but inverse, variability in the magnitude of the absorption band near 460 nm (band 1), such that ϵ_{460} increases as ϵ_{600} decreases. The ratio of the 460 and 600 nm absorption intensities (R_{abs}) ranges from 0.11 for azurin to 1.34 for NiR (Table 4.2). However, the sum of $\epsilon_{460} + \epsilon_{600}$ is remarkably constant at 4,000-5,000 M^{-1} cm^{-1}. This interrelationship between the two

absorption bands is further supported by our RR data. The Raman spectra for pseudoazurin (Figure 4.1), nitrite reductase (Figure 4.3), mutant SOD (Figure 4.6), and azurin show that the same vibrational modes are observed upon excitation within either absorption band. Furthermore, in the excitation profiles for pseudoazurin (Figure 4.2), nitrite reductase (Figure 4.4), mutant SOD (Figure 4.7), and azurin (Figure 4.8), the intensity of each RR peak tracks both the 460- and 600-nm absorption bands. Given the dominant contribution of the cysteine ligand to the 600-nm absorption and concomitant RR spectrum, it is likely that the 460-nm electronic transition has substantial Cu-cysteinate character, as well.

The excitation profiles also show that the relative intensities of the different RR peaks do vary as a function of excitation wavelength. For example, with 460-nm excitation of pseudoazurin, the 363-cm^{-1} peak exhibits increased intensity relative to the 444-cm^{-1} peak (Figures 4.1, 4.2). Similar relative intensity increases with 460-nm excitation are observed for the 361- versus 395-cm^{-1} peak in nitrite reductase (Figure 4.4), the 341- versus 352-cm^{-1} peak in mutant SOD (Figure 4.7), and the 431- versus 413 cm^{-1} peak in azurin (Figure 4.8). Since RR intensities are determined by changes in the nuclear coordinates of bonded atoms between the ground state and the excited state,[27] the variability in RR intensities indicates that the ~460-nm absorption band arises from a different electronic transition. The constancy of vibrational frequencies suggests a common copper-cysteinate ground state that leads to a somewhat different set of excited-state structures upon absorption of 460- or 600-nm radiation.

4.3.6 Assignment of Electronic Transitions in Type 1 Cu Sites

Previous analysis of type 1 Cu proteins, particularly by CD and MCD spectroscopy, have revealed the presence of at least three electronic transitions between 400 and 550 nm.[5,6] For plastocyanin these have been specifically assigned to Met → Cu(II) CT at 430 nm, His → Cu(II) CT at 465 nm, and Cys → Cu(II) CT at 535 nm. Other type 1 proteins such as pseudoazurin, nitrite reductase, and mutant SOD show markedly increased absorption intensities in this region (Figures 4.2, 4.4, 4.7), leading to the question of whether the plastocyanin assignments are generally applicable to all type 1 copper sites.

The methionine assignment is problematical because excitation within the 430-nm region does not lead to the appearance of any new RR features that could be associated with vibrations of a methionine ligand. Furthermore, replacement of the methionine ligand in *P. aeruginosa* (*P.a.*) azurin by selenomethionine causes no perturbation in the 430-nm spectral region[60] and no change in the RR spectrum.[49] Replacement of the Met 121 ligand in *A. denitrificans* azurin by a ligating glutamine results in increased rather that decreased intensity at 430-460 nm.[54] Removal of the Met 121 ligand in *P.a.* azurin by cleavage of the polypeptide chain after residue 120 also results in a more prominent absorption band at 450 nm.[61] Thus, additional electronic transitions unrelated to methionine are clearly present in this spectral region.

The His → Cu(II) CT assignment at 460 nm is supported by single-crystal studies of plastocyanin which indicate that this absorption band is more polarized in the direction of the two histidine ligands than is the 600-nm absorption band.[5b] New information has been obtained using histidine ligand mutants of *P.a.* azurin. (i) Reconstitution of the His117Gly mutant with exogenous imidazole yields a species almost identical to wild-type in its absorption spectrum,[46,47] RR frequencies (all within 2 cm^{-1}), RR molar scattering intensity ($\sim$600) and relative RR intensities.[48] (ii) Reconstitution of the His117Gly mutant with ^{15}N-imidazole does not cause any detectable isotope shifts in the 350-500-cm^{-1} region. (iii) Replacement of either the His 117 ligand by chloride[47,48] or the His 46 ligand by aspartate[62], causes no decrease in the intensity of the 460-nm absorption band and produces very little change in the RR spectrum. For example, in the RR spectrum of the H117G mutant plus chloride, most of the frequencies are within 2-4 cm^{-1} of wild-type azurin and only 3 of the 11 peaks have changed in intensity. Since the RR spectrum of azurin appears to be dominated by the Cu-cysteinate moiety, it is likely that both the 460- and 600-nm absorption bands have substantial S(Cys) → Cu(II) CT contributions.

The alternative that a His → Cu(II) CT transition at 460-nm adds electron density into cysteine orbitals remains a possible explanation for the RR results. However, the Raman intensity patterns obtained via 460- and 600-nm excitation are strikingly similar. This would require that electron density derived from either a Cys or a His ligand could produce a similar structural change in going from the ground state to the excited state.

Furthermore, the large molar absorptivities at 460 nm ($\epsilon > 1{,}000$ M^{-1} cm^{-1}) for many type 1 copper proteins (Table 4.2) seem more compatible with a Cys → Cu(II) CT assignment. Cupric thiolate complexes typically yield ϵ values of this magnitude (Table 4.1). In contrast, cupric imidazole complexes tend to have weaker absorption bands in this region. For example, the Cu(II) complex with the contrained bidentate ligand, 2,2'-bis(2-imidazolyl)biphenyl, has an imidazole → Cu CT band at 440 nm but its ϵ value is only 260 $M^{-1}cm^{-1}$.[63] In addition, cupric imidazole complexes are very weak Raman scatterers.[64] Yet the RR spectrum of nitrite reductase obtained with 460-nm excitation is as strongly enhanced (molar scattering É 200) as the RR spectra of other type 1 sites obtained with 600-nm excitation (Table 4.1). These results imply that Cys → Cu CT is a major contributor to the 460-nm absorption band in many type 1 copper proteins.

The assignment of a second Cys → Cu CT transition at 460 nm suggests an explanation for the variability and approximate additivity of the ϵ values for the 460- and 600-nm absorption bands (Table 4.2). The actual absorption intensity associated with each band would be expected to depend on the relative alignment of the sulfur p orbitals with respect to the Cu d orbitals for each type 1 Cu site. Perturbations in these alignments would alter the degree of orbital overlap and, thus, alter the relative transition probabilities in different type 1 copper proteins.

4.3.7 Correlation of Electronic, EPR, and Structural Properties

The EPR definition of a type 1 Cu species is the appearance of narrow hyperfine splitting in the $A_{\|}$ region (Table 4.1). This can be ascribed to the influence of a short Cu-S(Cys) bond in a trigonal-pyramidal structure. However, within this category there is surprising variability in the rhombicity of the EPR spectrum, ranging from strongly axial as in plastocyanin to strongly rhombic as in stellacyanin.[4] The rhombic distortion should be reflecting a further loss of symmetry in the type 1 site. A correlation between the occurrence of a rhombic EPR signal and the appearance of the 460-nm absorption band has been noted by Lu et al.[23] As indicated in Table 4.2, type 1 sites with a weak 460-nm band ($\epsilon < 600$ M^{-1} cm^{-1}) and an $R_{abs} \leq 0.12$ have axial EPR spectra. Type 1 sites with a more intense 460-nm band ($\epsilon > 1{,}000$ M^{-1} cm^{-1}) and an $R_{abs} \geq 0.20$ have rhombic EPR spectra.

What is the structural basis for increased rhombicity in EPR spectra and enhanced absorptivity at 460 nm? From single crystal studies of plastocyanin and a model compound, Gewirth et al.[65] suggested that the rhombic distortion was due to a strengthening of the Cu-X(axial ligand) bond. Thus, axial EPR character should be associated with a trigonal planar Cu-NNS site. Rhombic EPR character should be associated with movement of the Cu away from the NNS plane, generating a more tetrahedral coordination geometry. This hypothesis is supported by a comparison of the properties of wildtype *A. denitrificans* azurin and the M121Q mutant in which the axial methionine ligand has been replaced by a glutamine (coordinated to copper through the amide carbonyl group).[54] The M121Q mutant has a rhombic rather than axial EPR spectrum as well as increased absorbance at 460 nm, and the crystal structure indicates that the Cu has moved out of the NNS plane by 0.26 Å compared to 0.12 Å in wildtype (Table 4.2).

The other crystallographic data in Table 4.2 also support the correlation between EPR rhombicity and a strengthening of the Cu-X(axial ligand) bond. Thus, short Cu-S(Met) distances (<2.8 Å) are observed for the rhombic sites in pseudoazurin, cucumber basic protein, and nitrite reductase. Longer Cu-S(Met) distances are observed for the axial sites in azurin (3.13 Å) and plastocyanin[66] from Enteromorpha prolifera (2.92 Å). Although the Cu-S(Met) distance of 2.82 Å for Populus nigra plastocyanin (Table 4.2) is somewhat borderline (Table 4.2), the uncertainty in Cu-ligand bond distances is $\pm$ 0.05 Å even in high-resolution protein crystal structures.[3] The Cu$\cdots$(NNS) distances in listed in Table 4.2 are more variable, but do indicate a trend towards longer distances in the rhombic category. Thus, the high 460-nm absorbance of rhombic type 1 Cu sites is most likely due to stronger coordination of the axial ligand.

The changes in the alignment of copper and sulfur orbitals associated with the conversion from trigonal planar to a tetrahedral geometry would be expected to affect absorption energies as well as intensities. This is indeed observed (Table 4.2). The proteins in the axial EPR category have their average absorption maxima at 462 and 603 nm, whereas those in the rhombic EPR category have their average absorption maxima at 452 and 598 nm. Similar trends are apparent in the set of Met 121 ligand mutants from *P.a.* azurin.[61] Replacement of Met 121 with Leu, Ala, Thr, Val, Ile, or Trp yields

an axial EPR spectrum consistent with weak or absent axial ligation and a trigonal planar geometry. This group has R_{abs} values ranging from 0.09 to 0.15 and average absorption maxima at 460 and 625 nm. Replacement of Met 121 with Asn, Asp, Gln, Cys, or His yields a rhombic EPR spectrum consistent with stronger axial ligation and a more tetrahedral geometry. The R_{abs} values for this group range from 0.15 to 0.48 and the average absorption maxima are at 450 and 610 nm. Thus, increased energies for the Cu-cysteinate electronic transtions are yet another indicator of tetrahedral character in type 1 copper proteins.

4.4 Conclusions

1. The RR spectra of NiR and mutant SOD (H80C) are typical of type 1 Cu sites, indicating that both have a short Cu-S(Cys) bond of $\sim$2.1 Å. The large number of vibrational modes between 340 and 415 cm^{-1} is due, in part, to the kinematic coupling of ν(Cu-S) with Cys deformation modes and is, thus, indicative of a coplanar cysteine.

2. In the electronic spectra, ϵ_{460} varies from 300 M^{-1} cm^{-1} in plastocyanin to 1,180 in pseudoazurin and 2,530 in NiR, while the ϵ_{600} varies from 5,200 M^{-1} cm^{-1} in plastocyanin to 2,900 in pseudoazurin and 1,890 in NiR. This inverse relationship in ϵ values suggests that a common chromophoric group may be responsible for the two electronic transitions.

3. The 460- and the 600-nm electronic transitions give rise to the same RR frequencies and, thus, can be ascribed to the same Cu-cysteinate ground-state structure. Their variable Raman intensities require different excited state structures. Both absorptions are likely to have substantial (Cys)S $\rightarrow$ Cu(II) CT character.

4. Increased intensity at 460 nm and increased rhombicity in the EPR spectrum both appear to be correlated with a more tetrahedral site where the Cu has moved away from the NNS ligand plane and towards the axial ligand.

5. Since the 460- and 600-nm copper-cysteinate transitions are observed in the electronic spectra of all type 1 Cu proteins, the definition of a type 1 Cu site should be expanded to include the occurrence of two absoption bands at 460 and 600 nm.

References

1. (a) Oregon Graduate Institute of Science and Technology. (b) University of California, Los Angeles. (c) University of Virginia.
2. Adman, E. T. *Adv. Protein Chem.* **1991,** *42,* 145-197.
3. Han, J.; Adman, E. T.; Beppu, T.; Codd, R.; Freeman, H. C.; Huq, L.; Loehr, T. M.; Sanders-Loehr, J. *Biochemistry* **1991,** *30,* 10904-10913.
4. Adman, E. T. In *Metalloproteins*; Harrison, P., Ed.; Verlag Chemie: Weinheim, FRG, 1985; Part I, pp 1-42.
5. (a) Solomon, E. I.; Baldwin, M. J.; Lowery, M. D. *Chem. Rev.* **1992**, *92*, 521-542. (b) Penfield, K. W.; Gay, R. R.; Himmelwright, R. S.; Eickman, N. C.; Norris, V. A.; Freeman, H. C.; Solomon, E. I. *J. Am. Chem. Soc.* **1981**, *103,* 4382-4388.
6. Gewirth, A. A.; Solomon, E. I. *J. Am. Chem. Soc.* **1988,** *110,* 3811-3819.
7. Iwasaki, H.; Matsubara, T. J. *Biochemistry* **1972,** *71,* 645-652.
8. Liu, M.-Y.; Liu, M.-C.; Payne, W.; LeGall, J. *J. Bacteriol.* **1986,** *166,* 604-608.
9. Godden, J. W.; Turley, S.; Teller, D. C.; Adman, E. T.; Liu, M. Y.; Payne, W. J.; LeGall, J. *Science* **1991,** *253,* 438-442.
10. Hulse, C. L.; Tiedje, J. M.; Averill, B. A. *Anal. Biochem.* **1988,** *172,* 420-426.
11. Libby, E.; Averill, B. A. *Biochem. Biophys. Res. Commun.* **1992,** *187,* 1529-1535.
12. Dooley, D. M.; Moog, R. S.; Liu, M. Y.; Payne, W. J.; LeGall, J. *J. Biol. Chem.* **1988,** *263,* 14625-14628.
13. Getzoff, E. D.; Tainer, J. A.; Weiner, P. K.; Kollman, P. A.; Richardson, J. S.; Richardson, D. C. *Nature (London)* **1983,** *306,* 287-290.
14. Valentine, J. S.; Pantoliano, M. W. In *Copper Proteins*; Spiro, T. G., Ed.; Wiley: New York, 1981; pp 291-357.
15. Lu, Y.; Gralla, E. B.; Roe, J. A.; Valentine, J. S. *J. Am. Chem. Soc.* **1992,** *114,* 3560-3562.
16. Lu, Y. Ph.D. Dissertation, University of California: Los Angeles, 1992.

17. Nestor, L.; Larrabee, J. A.; Woolery, G.; Reinhammar, B.; Spiro, T. G. *Biochemistry* **1984,** *23,* 1084-1093.

18. Blair, D. F.; Campbell, G. W.; Schoonover, J. R.; Chan, S. I.; Gray, H. B.; Malmstrom, B. G.; Pecht, I.; Swanson, B. I.; Woodruff, W. H.; Cho, W. K.; English, A. M.; Fry, H. A.; Lum, V.; Norton, K. A. *J. Am. Chem. Soc.* **1985,** *107,* 5755-5766.

19. Ainscough, E. W.; Bingham, A. G.; Brodie, A. M.; Ellis, W. R.; Gray, H. B.; Loehr, T. M.; Plowman, J. E.; Norris, G. E.; Baker, E. N. *Biochemistry* **1987,** *2,* 71-82.

20. Musci, G.; Desideri, A.; Morpurgo, L.; Tosi, L. J. *Inorg. Biochem.* **1985,** *23,* 93-102.

21. Hoitink, C. W. G.; Woudt, L. P.; Turenhout, J. C. M.; Van de Kamp, M.; Canters, G. W. *Gene* **1990,** *90,* 15-20.

22. Kakutani, T.; Watanabe, H.; Arima, K.; Beppu, T. *J. Biochem. (Tokyo)* **1981,** *89,* 463-472.

23. Lu, Y.; LaCroix, L. B.; Lowery, M. D.; Solomon, E. I.; Bender, C. J.; Peisach, J.; Row, J. A.; Gralla, E. G.; Valentine, J. S. *J. Am. Chem. Soc.* **1993,** in press.

24. Petratos, K.; Dauter, Z.; Wilson, K. S. *Acta Crystallogr.* **1988,** *B44,* 628-636.

25. Adman, E. T.; Turley, S.; Bramson, R.; Petratos, K.; Banner, D.; Tsernoglou, D.; Beppu, T.; Watanabe, H. *J. Biol. Chem.* **1989,** *264,* 87-99.

26. Han, S.; Czernuszewicz, R. S.; Spiro, T. G. *J. Am. Chem. Soc.* **1989,** *111,* 3496-3504.

27. Nishimura, Y.; Hirakawa, A. Y.; Tsuboi, M. In *Advances in Infrared and Raman Spectroscopy*; Clark, R. J. H., Hester, R. E., Eds.; Heyden: London, 1978; Vol. 5, pp 217-275.

28. Shin, K.-S.; Zink, J. I. *Inorg. Chem.* **1989,** *28,* 4358-4366.

29. (a) Kitajima, N. *Adv. Inorg. Chem.* **1992,** *38,* in press. (b) Kitajima, N.; Fujisawa, K.; Tanaka, M.; Moro-oka, Y. *J. Am. Chem. Soc.* **1992**, *114,* 9232-9233.

30. (a) Lever, A. B. P. In *Inorganic Electronic Spectroscopy*; Elsevier: Amsterdam, 1984; pp 303-308. (b) Andrew, C. R.; Yeom, H.; Valentine, J. S.; Sanders-Loehr, J., unpublished results.

31. Sharma, K. D.; Loehr, T. M.; Sanders-Loehr, J.; Husain, M.; Davidson, V. L. *J. Biol. Chem.* **1988,** *263,* 3303-3306.

32. Maret, W.; Shiemke, A. K.; Wheeler, W. D.; Loehr, T. M.; Sanders-Loehr, J. *J. Am. Chem. Soc.* **1986,** *108,* 6351-6359.

33. Maret, W.; Kozlowski, H. *Biochim. Biophys. Acta* **1987,** *912,* 329-337.

34. Brader, M. L.; Borchardt, D.; Dunn, M. F. *J. Am. Chem. Soc.* **1992,** *114,* 4480-4486.

35. Spiro, T. G. Personal communication.

36. Thompson, J. S.; Marks, T. J.; Ibers, J. A. *J. Am. Chem. Soc.* **1979,** *101,* 4180-4192.

37. Anderson, O. P.; Becher, J.; Frydendahn, H.; Taylor, L. F.; Toftlund, H. *J. Chem. Soc. Chem. Commun.* **1986,** 699-701.

38. Jensen, R. W.; Becher, J.; Toftlund, H. In *Spectroscopy of Biological Molecules*; Alix, A. J. P., Bernard, L., Manfait, M., Eds.; John Wiley: New York, 1985; pp 205-207.

39. Sharma, K. D.; Sanders-Loehr, J.; Toftlund, H., unpublished results.

40. Taylor, M. R.; Glusker, J. P.; Gabe, E. J.; Minkin, J. A. *Bioinorg. Chem.* **1974,** *3,* 189-205.

41. Tosi, L.; Garnier-Suillerot, A. *J. Chem. Soc. Dalton* **1982,** 103-108.

42. Hughey, J. L., IV; Fawcett, T. G.; Rudich, S. M.; Lalancette, R. A.; Potenza, J. A.; Schugar, H. J. *J. Am. Chem. Soc.* **1979,** *101,* 2617-2623.

43. Birker, P. J. M. W. L.; Freeman, H. C. *J. Am. Chem. Soc.* **1977,** *99,* 6890-6899.

44. Tosi, L.; Garnier, A. *Biochem. Biophys. Res. Commun.* **1979,** *91,* 1273-1279.

45. Bharadwaj, P. K.; Potenza, J. A.; Schugar, H. J. *J. Am. Chem. Soc.* **1986,** *108,* 1351-1352.

46. den Blaauwen, T.; van de Kamp, M.; Canters, G. W. *J. Am. Chem. Soc.* **1991,** *113,* 5050-5052.

47. den Blaauwen, T.; Canters, G. W. *J. Am. Chem. Soc.* **1993,** *115,* 1121-1129.

48. (a) Han, J.; Loehr, T. M.; Sanders-Loehr, J.; den Blaauwen T.; Canters, G. W., unpublished results. (b) Sanders-Loehr, J. In *Bioinorganic Chemistry of Copper*; Karlin, K. D.; Tyeklar, Z., Eds.; Chapman & Hall, New York, 1993; pp. 51-63.

49. Thamann, T. J.; Frank, P.; Willis, L. J.; Loehr, T. M. *Proc. Natl. Acad. Sci. USA* **1982,** *79,* 6396-6400.

50. Katoh, S.; Shiratori, I.; Takamiya, A. *J. Biochem. (Tokyo)* **1962,** *51,* 32.

51. Guss, J. M.; Bartunik, H. D.; Freeman, H. C. *Acta Cryst. B* **1992**, *48,* 790-811.

52. Baker, E. N. *J. Mol. Biol.* **1988,** *203,* 1071-1095.

53. Husain, M.; Davidson, V. L. *J. Biol. Chem.* **1985,** *260,* 14626-14629.

54. Romero, A.; Hoitink, C. W. G.; Nar, H.; Huber, R.; Messerschmidt, A.; Canters, G. W. *J. Mol. Biol.* **1993**, in press.

55. McManus, J. D.; Brune, D. C.; Han, J.; Sanders-Loehr, J.; Meyer, T. E.; Cusanovich, M. A.; Tollin, G.; Blankenship, R. E. *J. Biol. Chem.* **1992,** *267,* 6531-6540.

56. Sakurai, T.; Sawada, S.; Nakahara, A. *Inorg. Chim. Acta* **1986,** *123,* L21-L22.

57. Guss, J. M.; Freeman, H. C. Personal communication.

58. Blake, R. C., II; Shute, E. A. *J. Biol. Chem.* **1987,** *262,* 14983-14989.

59. Adman, E. T. Personal communication.

60. Frank, P.; Licht, A.; Tullius, T. D.; Hodgson, K. O.; Pecht, I. *J. Biol. Chem.* **1985,** *260,* 5518-5525.

61. Karlsson, B. G.; Nordling, M.; Pascher, T.; Tsai, L.-C.; Sjαlin, L.; Lundberg, L. G. *Protein Eng.* **1991,** *4,* 343-349.

62. (a) Chang, T. K.; Iverson, S. A.; Rodrigues, C. G.; Kiser, C. N.; Lew, A. Y. C.; Germanas, J. P.; Richards, J. H. *Proc. Natl. Acad. Sci. USA* **1991,** *88,* 1325-1329. (b) Dave, B. P., Germanas, J. P.; Czernuszewicz, R. S., personal communication.

63. Knapp, S.; Keenan, T. P.; Zhang, X., Fikar, R., Potenza, J. A.; Schugar, H. J. *J. Am. Chem. Soc.* **1990**, *112,* 3452-3464.

64. Larrabee, J. A.; Spiro, T. G. *J. Am. Chem. Soc.* **1980**, *102,* 4217-4223.

65. Gewirth, A. A.; Cohen, S. L.; Schugar, H. J.; Solomon, E. I. *Inorg. Chem.* **1987,** *26,* 1133-1146.

66. Collyer, C. A.; Guss, J. M.; Sugimura, Y.; Yoshizaki, F.; Freeman, H. C. *J. Mol. Biol.* **1990,** *211,* 617-632.

Table 4.1. Properties of Cupric Thiolate Complexes

compound[a]	Cu-S distance, Å	EPR[b] $A_{\parallel}$	S → Cu CT[c] λ_{max}	ϵ	Raman intensity[d]
		Type 1 Cu sites			
1 amicyanin		50	595	4,610	500
2 azurin	2.13	60	619	5,100	~650
3 pseudoazurin	2.16	55	593	2,900	~130
4 nitrite reductase	2.15	69	458	2,530	~200
5 SOD-Cu_2Cu_2-(H80C)		15	595	>1,420	~150
6 LADH-Cu		50	623	2,450	~120
7 $Cu_2(insulin)_6(SC_6F_5)_2$		27	630	1,800	[e]
8 $Cu(Pz)_3(SCPh_3)$	2.12	74	625	6,600	[e]
9 $Cu(Pz)_3(SC_6F_5)$	2.18	54	665	5,960	[e]
		Type 2 Cu sites			
10 $Cu(Pz)_3(SC_6H_4NO_2)$		171	588	3,900	[e]
11 Cu(diimino-)(S-pyrazole-)$_2$	2.25	137	535	3,000	20
12 Cu(thiosemicarbazone)$_2$	2.26		469	6,300	60
13 Cu(tetraazo-)$(SC_6H_4CO_2)$	2.36		418	1,100	
14 Cu(N_2S_2-penicillamine)	2.28		518	4,250	[e]
15 Cu(diamino-)$(SCH_2CH$-)$_2$	2.25	182	400	>1,000	10
16 SOD-Cu_2Zn_2-(H46C)		151	379	1,940	~20
17 SOD-Cu_2Zn_2-(H120C)		175	406	1,250	~15
18 azurin-(H117G) + His		156	400	~2,800	~50
19 LADH-Cu + imidazole		127	480	~2,000	~20

Table 4.1 (continued):

[a] Compounds and data from following sources: **1**. *Paracoccus denitrificans* (ref 31). **2**. *A. denitrificans* (ref 19), Raman spectrum of *P. aeruginosa*. **3**. *A. faecalis* S-6 (ref 22, 24). **4**. *A. cycloclastes* (ref 11, 59). **5**. *S. cerevisiae* (ref 16 and this work). **6**. Cu-substituted liver alcohol dehydrogenase (ref 32, 33). **7**. Insulin complexed to Cu and benzenethiolate (ref 34). **8,9**. Cu[HB(3,5-$iPr_2pz)_3$](L) where L = $SCPh_3$ or SC_6F_5 (ref 29), Raman spectrum (ref 35). **10**. Cu[HB(3,5-$Me_2pz)_3(SC_6H_4NO_2)$ (ref 36). **11**. Cu[2,2'-bis-(1-phenyl-3-methyl-5-thiopyrazol-4-ylmethyleneamino)biphenyl] (ref 37), Raman spectrum (ref 38,39). **12**. Cu[3-ethoxy-2-oxobutyraldehyde bis(thiosemicarbazone)] (ref 40), Raman spectrum (ref 41). **13**. Cu complex with a tetraazocylcotetradecane and $(o\text{-}SC_6H_4CO_2)^-$ (ref 42). **14**. $[(Cu^{II})_6(Cu^{I})_8$(D-penicillamine$)_{12}Cl]^{5-}$ (ref 43,44). **15**. Cu[$SCH_2CH(CO_2CH_3)NHCH_2\text{-}]_2$ (ref 45), Raman on Cu[$SC(CH_3)_2CH_2NHCH_2\text{-}]_2$ (ref 39). **16,17**. *S. cerevisiae* (ref 16, 30b). **18**. *P. aeruginosa* azurin mutant (H117G) plus exogenous histidine (ref 46-48). **19**. Cu-substituted LADH plus exogenous imidazole (ref 32). [b] $A_{\parallel}$ in $cm^{-1} \times 10^{-4}$. [c] λ_{max} in nm, ϵ in $M^{-1}\ cm^{-1}$ per Cu. [d] Intensity of strongest RR peak relative to intensity of 980-cm^{-1} peak of sulfate (accuracy $\pm$ 20%). Data obtained with excitation close to λ_{max} and calculated per mole of Raman scatterer. Approximate intensity ($\sim$) obtained relative to 230-cm^{-1} ice mode and normalized to value for sulfate, based on liquid and frozen solution data for amicyanin (accuracy $\pm$ 30%). [e] RR spectrum observed, but molar scattering intensity not quantitated.

Table 4.2. Properties of Type 1 Copper Sites

EPR spectrum[a]	absorption band near 460 nm[b] λ_{max}	absorption band near 460 nm[b] ϵ	absorption band near 600 nm[b] λ_{max}	absorption band near 600 nm[b] ϵ	R_{abs} ($\epsilon_{460}/\epsilon_{600}$)	Cu-X (axial) distance, Å[c]	Cu···(NNS) distance, Å[d]
axial							
$Cu(Pz_3)(SCPh_3)$,**8**[e]	440	340	625	6600	0.05	2.03(N)	0.20
$Cu(Pz)_3(SC_6F_5)$,**9**[e]	420	630	665	5960	0.11	2.04(N)	0.34
plastocyanin[f]	460	590	597	4300	0.12	2.82(S)	0.36
azurin[g]	460	580	619	5100	0.11	3.13(S)	0.12
amicyanin[h]	464	520	595	4610	0.11		
rhombic							
azurin(M121Q)[i]	452	1200	610	6000	0.20	2.27(O)	0.26
stellacyanin[j]	450	1100	608	4080	0.27		
auracyanin A[k]	454	900	596	3000	0.30		
pseudoazurin[l]	450	1180	593	2900	0.41	2.76(S)	0.43
cucumber basic protein[m]	448	1240	593	2900	0.43	2.62(S)	0.39
rusticyanin[n]	445	1000	600	2100	0.47		
SOD-Cu_2Cu_2(H80C)[o]	459	>1460	595	>1420	1.03		
nitrite reductase[p]	458	2530	585	1890	1.34	2.62(S)	0.50

Table 4.2 (continued):

[a]Axial versus rhombic character of X-band EPR spectra described in ref 23. [b]λ_{max} in nm, ϵ in M^{-1} cm^{-1} per type 1 Cu. [c]Distance to axial ligand, X = N(Pz), S(Met), or O(Gln). [d]Distance of Cu from plane of three ligands; N = His, S = Cys in proteins. [e]Cu[HB(3,5-$iPr_2pz)_3$](L) (ref 29). [f]Spinach, optical and EPR (ref 50); P. nigra X-ray structure at 1.33 Å resolution (ref 51). [g]*A. denitrificans* (ref 19, 52). [h]*P. denitrificans* (ref 53). [i]*A. faecalis* S-6 mutant (ref 54). [j]*Rhus vernicifera* (ref 20). [k]*Chloroflexus aurantiacus* (ref 55). [l]*A. faecalis* S-6 (ref 22, 24). [m](refs 56, 57). [n]*Thiobacillus ferroxidans* (ref 58). [o]*S. cerevisiae* (ref 16). [p]*A. cycloclastes* (refs 11, 59).

FIGURE LEGENDS

Figure 4.1. Resonance Raman spectra of pseudoazurin from *A. faecalis*. Spectra were obtained from 1.5 mM protein in 0.02 M phosphate, 0.04 M KCl (pH 6.3) using 488.0- and 593-nm excitation (60 mW) with a resolution of 5 cm^{-1}, scan rate of 0.5 cm^{-1}/s, and accumulation of 10 scans.

Figure 4.2. Absorption spectrum (—) and RR excitation profiles (---) for 363- and 444-cm^{-1} modes of pseudoazurin. Raman data were obtained as in Figure 1, and peak heights were measured relative to the height of the 230-cm^{-1} ice mode.

Figure 4.3. Resonance Raman spectra of nitrite reductase from *A. cycloclastes*. Spectra were obtained from a sample 0.59 mM in type 1 Cu in 0.05 M MES (pH 6.4) in D_2O using 476.5-, 589-, and 676.4-nm excitation (~120 mW) with a resolution of 8 cm^{-1}, scan rate of 1 cm^{-1}/s, and accumulation of 15 scans. S denotes peak from frozen solvent and is set offscale in the lower two spectra. The insert shows the coordination of the type 1 Cu site (Godden et al., 1991).

Figure 4.4. Absorption spectrum (—) and RR excitation profiles (---) for 361- and 395-cm^{-1} modes of nitrite reductase. Raman data were obtained as in Figure 4.3, and peak heights were measured relative to the height of the 230-cm^{-1} ice mode.

Figure 4.5. Metal site coordination of superoxide dismutase.

Figure 4.6. Resonance Raman spectra of mutant superoxide dismutase (H80C-Cu_2Cu_2) from *S. cerevisiae*. Spectra were obtained from 0.75 mM protein (1.5 mM in type 1 Cu) in 0.1 M acetate (pH 5.5) using 457.9-, 599-, and 647.1-nm excitation (~65 mW) with a resolution of 7.5 cm^{-1}, scan rate of 0.5 cm^{-1}/s, and accumulation of 4, 4, and 16 scans, respectively. The insert shows the overtone region of the same sample obtained as above with 610-nm excitation (80 mW) and 17 scans.

Figure 4.7. Absorption spectrum (—) and RR excitation profiles (---) for 341- and 352-cm^{-1} modes of mutant superoxide dismutase. Raman data were obtained as in Figure 4.6, and peak areas were measured relative to the area of the 230-cm^{-1} ice mode. The overlapping peaks at 341 and 352 cm^{-1} were resolved by curve-fitting (Galactic LabCalc), and the areas relative to the ice peak were measured using a planimeter.

Figure 4.8. Absorption spectrum (—) and RR excitation profiles (---) for 413- and 431-cm^{-1} modes of azurin from *A. denitrificans*. The Raman spectrum in the insert was obtained on 2 mM protein in 0.02 M Tris-Cl (pH 8.4) using 609-nm excitation (60 mW), a resolution of 5 cm^{-1}, scan rate of 0.5 cm^{-1}/s, and accumulation of 8 scans. Raman spectra at other excitation wavelengths were similarly collected, and peak heights were measured relative to the height of the 230-cm^{-1} ice mode. The enhancement in the 400-500-nm region has been multiplied by a factor of 10.

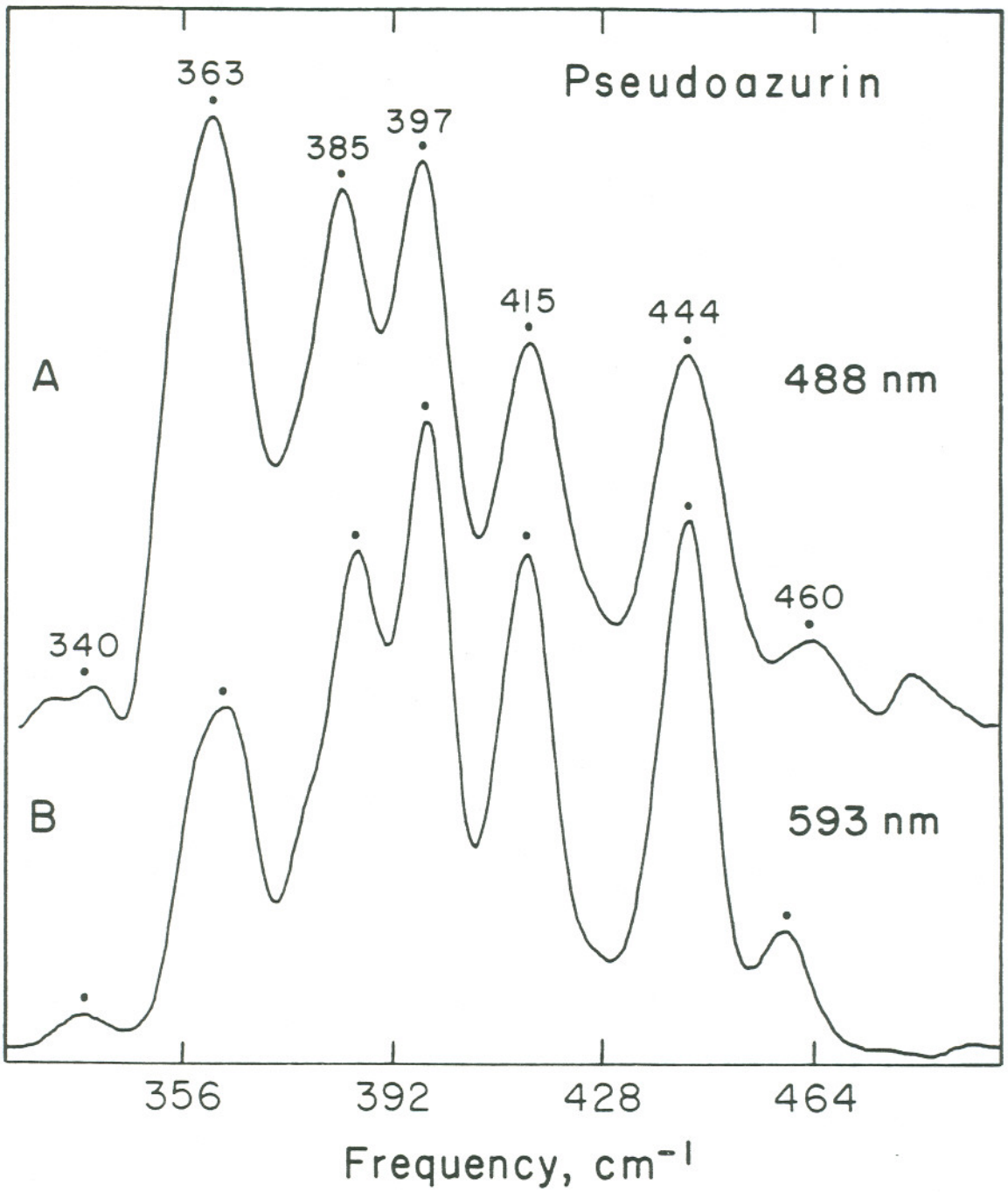
Pseudoazurin
363
385
397
415
444
460
340
A
488 nm
B
593 nm
356
392
428
464
Frequency, cm⁻¹

Figure 4.1

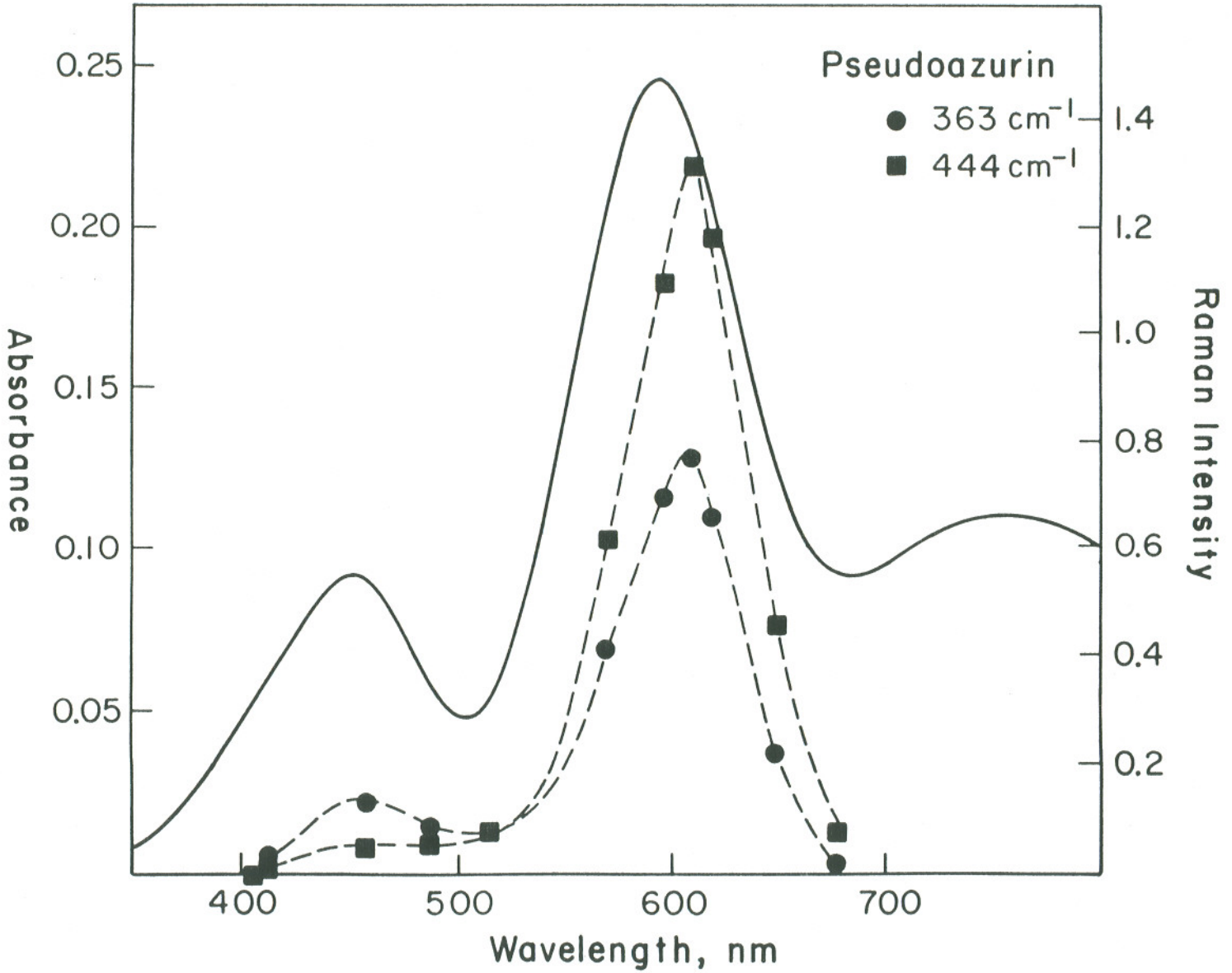
Pseudoazurin
363 cm⁻¹
444 cm⁻¹
Absorbance
Raman Intensity
Wavelength, nm
0.25
0.20
0.15
0.10
0.05
1.4
1.2
1.0
0.8
0.6
0.4
0.2
400
500
600
700

Figure 4.2

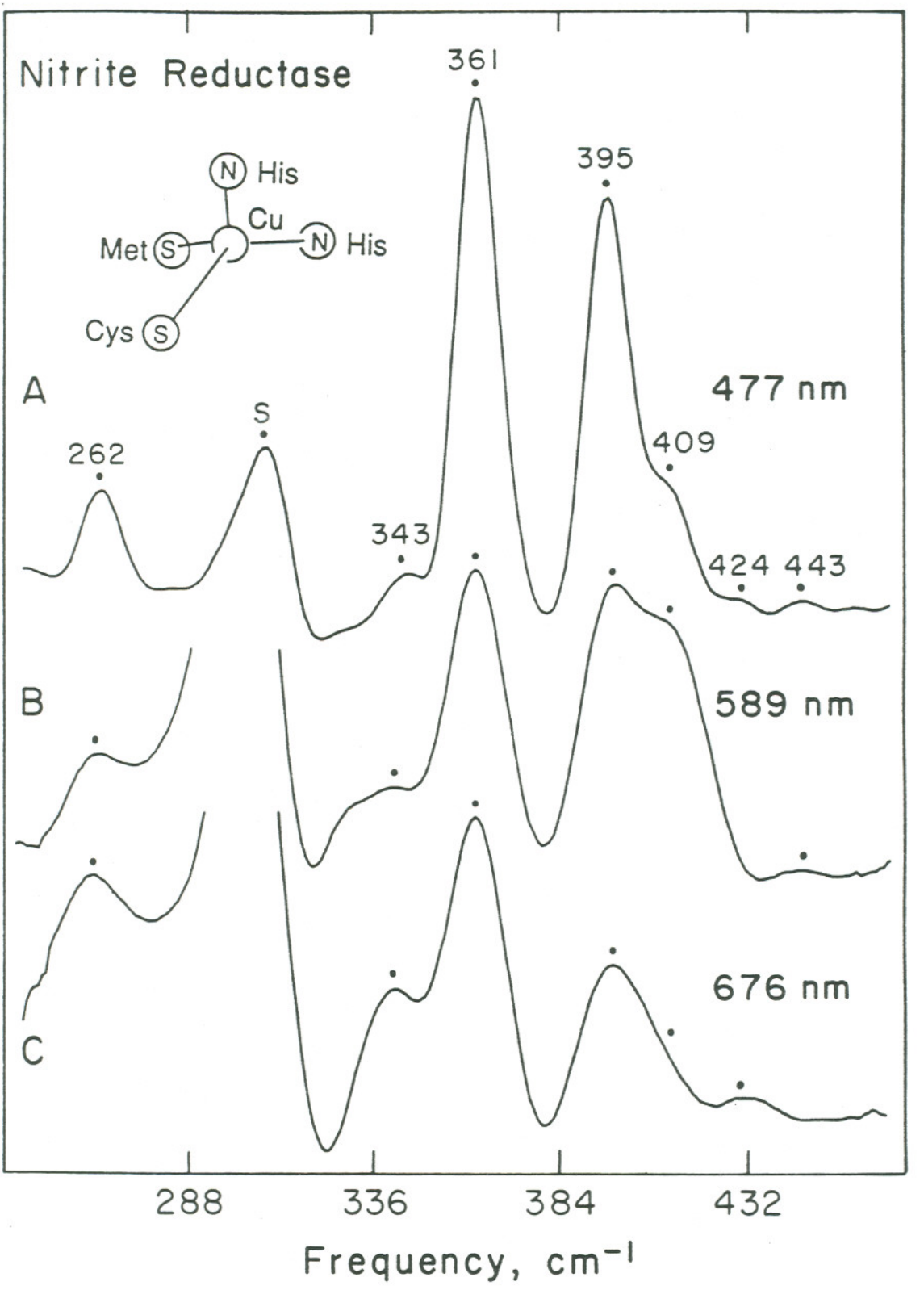
Nitrite Reductase
361
395
N His
Cu
Met S
N His
Cys S
A
477 nm
S
262
409
343
424 443
B
589 nm
676 nm
C
288
336
384
432
Frequency, cm⁻¹

Figure 4.3

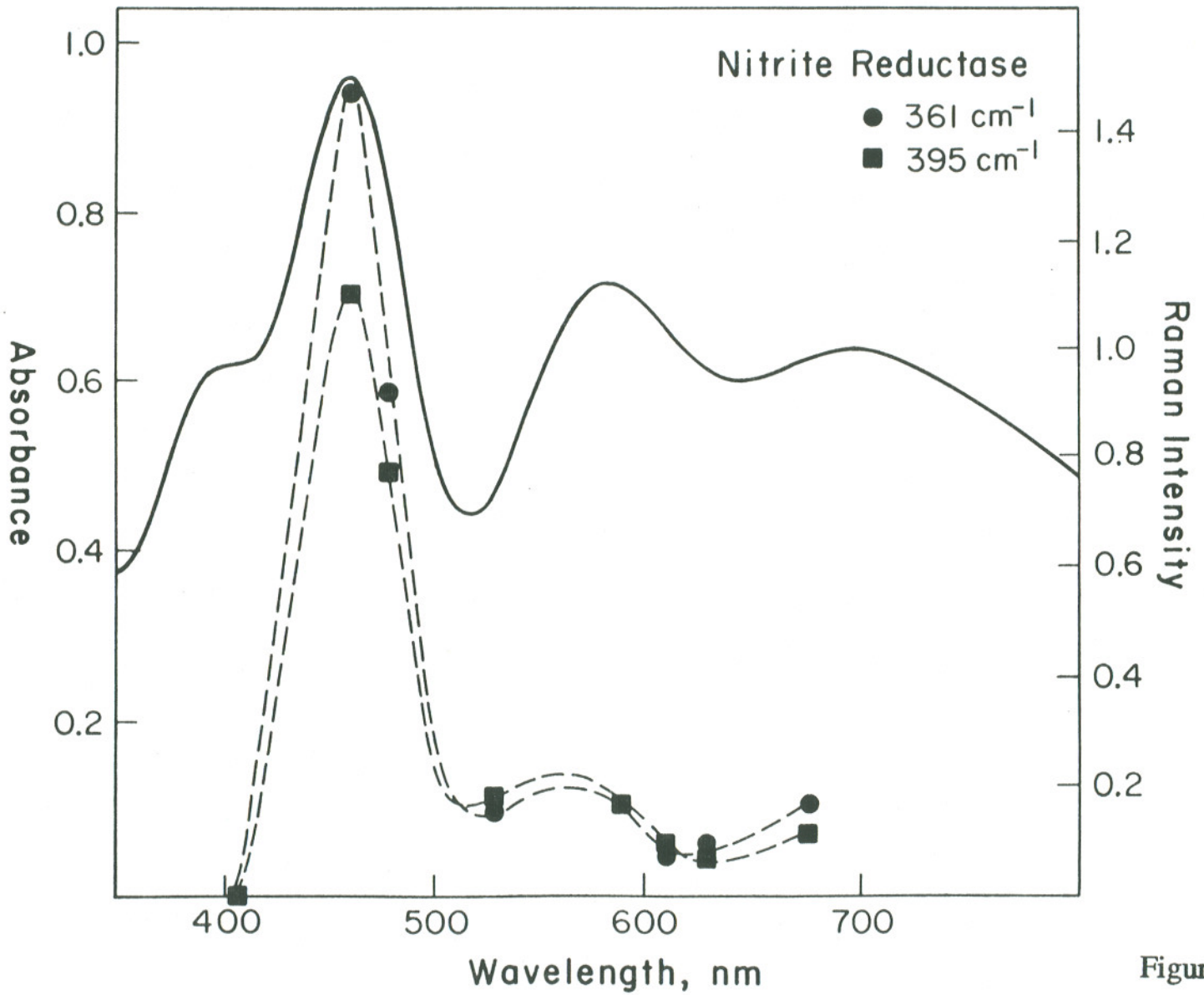
Nitrite Reductase
361 cm⁻¹
395 cm⁻¹
Absorbance
Raman Intensity
Wavelength, nm
1.0
0.8
0.6
0.4
0.2
1.4
1.2
1.0
0.8
0.6
0.4
0.2
400
500
600
700

Figure 4.4

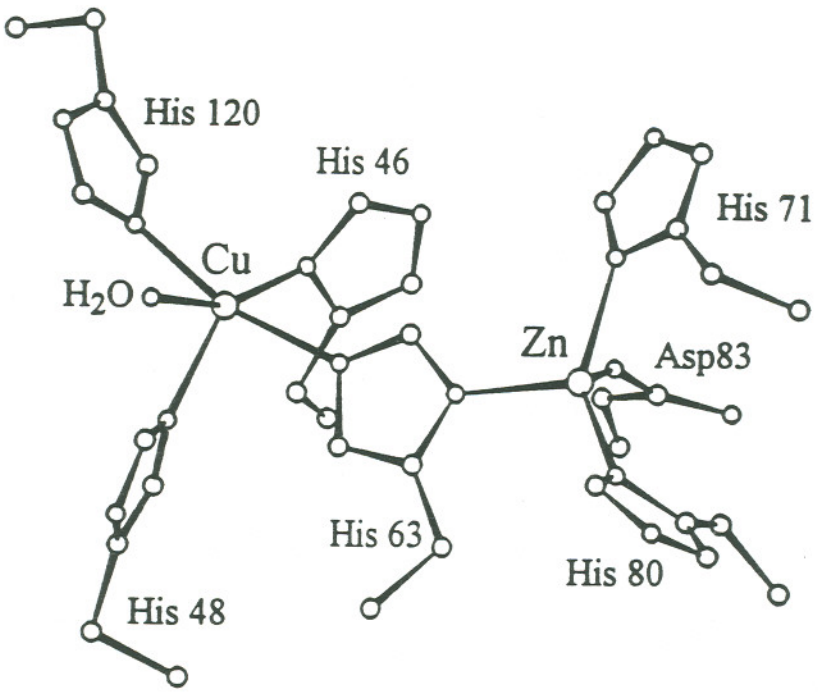

Figure 4.5

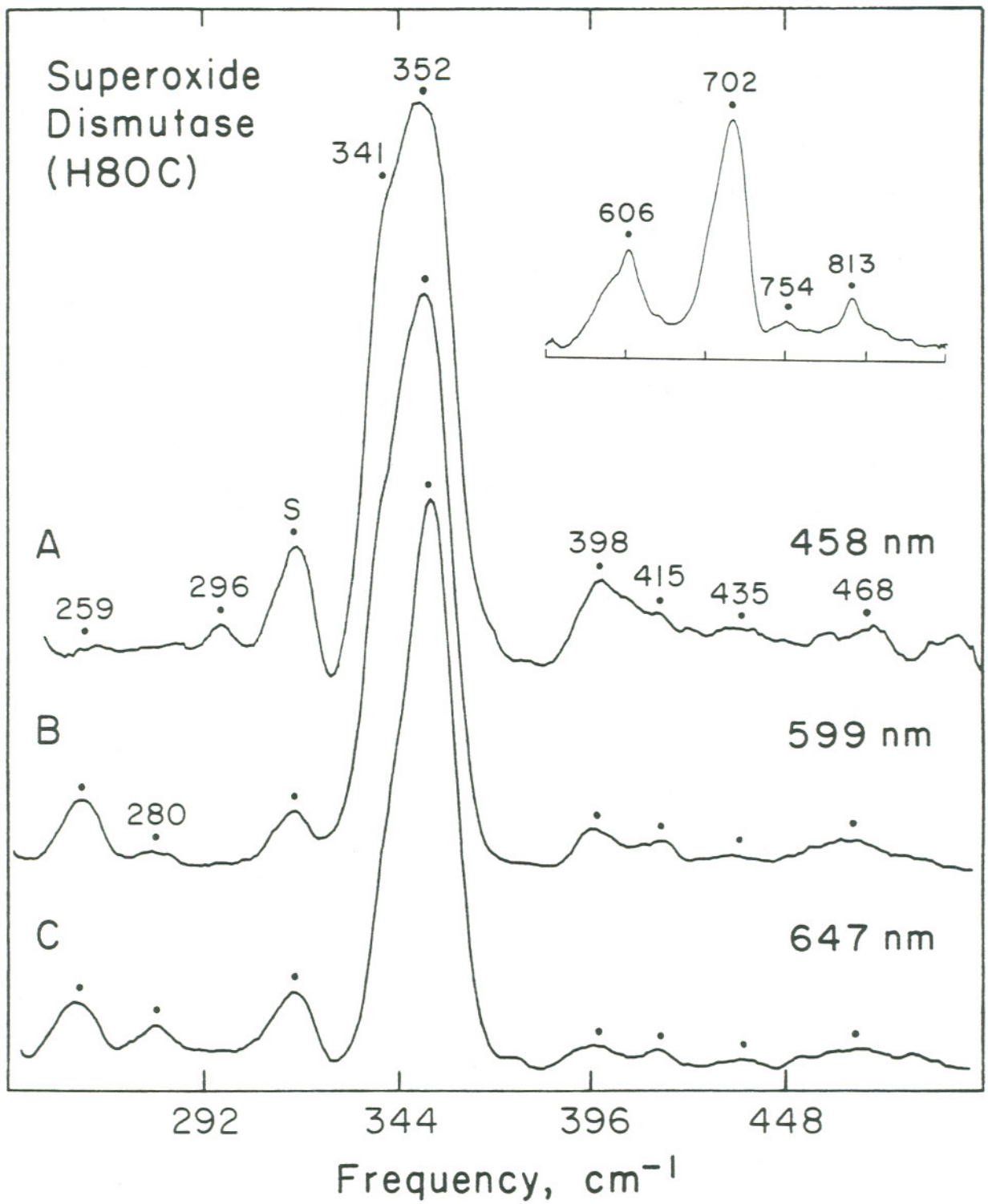
Superoxide
Dismutase
(H80C)
352
341
702
606
754
813
S
A
259
296
398
415
435
468
458 nm
B
280
599 nm
C
647 nm
292
344
396
448
Frequency, cm⁻¹

Figure 4.6

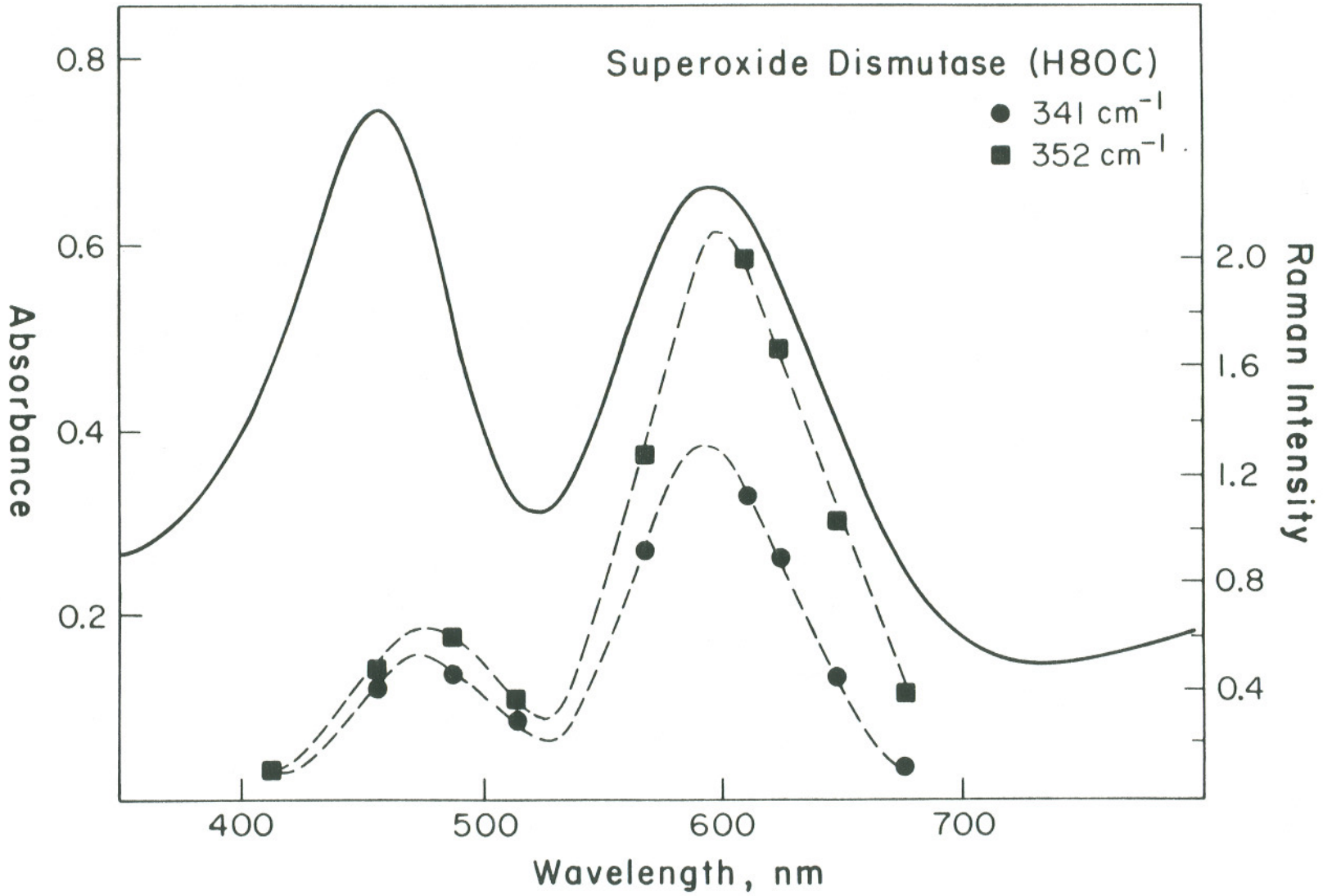
Superoxide Dismutase (H80C)
341 cm⁻¹
352 cm⁻¹
Absorbance
Raman Intensity
0.8
0.6
0.4
0.2
2.0
1.6
1.2
0.8
0.4
400
500
600
700
Wavelength, nm

Figure 4.7

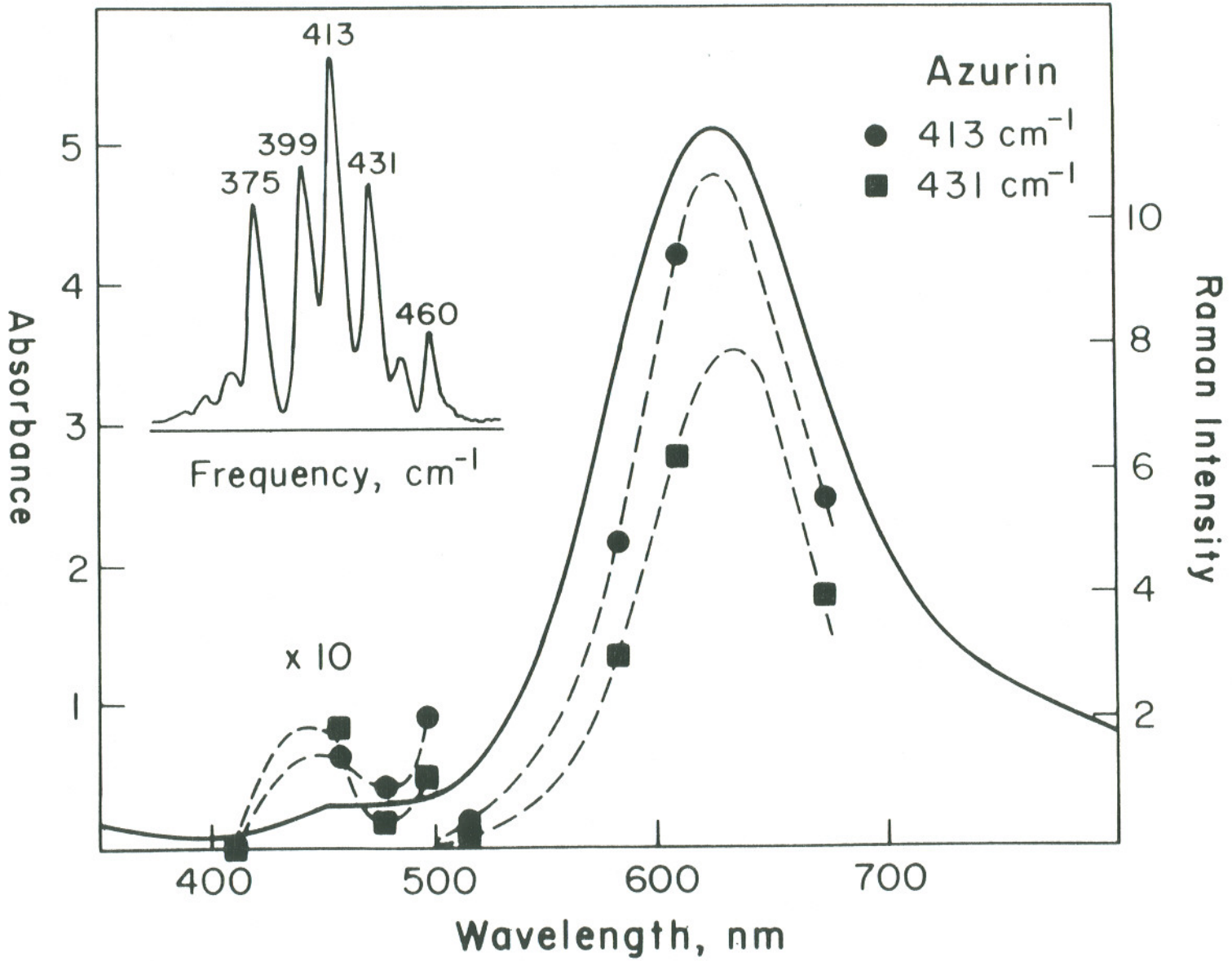
Azurin
413 cm⁻¹
431 cm⁻¹
413
399
375
431
460
Frequency, cm⁻¹
x 10
Absorbance
Raman Intensity
Wavelength, nm
400
500
600
700
1
2
3
4
5
2
4
6
8
10

Figure 4.8

Chapter 5

ASSIGNMENT OF THE RAMAN SPECTRUM OF AZURIN THROUGH ISOTOPE LABELING AND METAL-SITE MUTATION[1]

5.1 Introduction

The understanding of the structure and function of type 1 Cu proteins (cupredoxins) has been greatly enhanced in the last several years. A highly conserved Cu site is demonstrated by high resolution X-ray crystal structural analysis of seven different cupredoxins (Adman, 1991a). The Cu is strongly coordinated by one cysteine (S) and two histidines (NN) and it sits close to the plane of the trigonal SNN array (Figure 5.1). The Cu-S(Cys) bond is abnormally short ($\sim$2.15 Å) compared to the regular Cu-thiolate complexes. Structural studies of the plastocyanin and azurin apo-proteins reveal that this unique Cu site is preformed by the polypeptide of the protein (Garrett et al., 1984; Baker et al., 1991). Nature designed this specific site to satisfy both Cu(+2) and Cu(+1) states for use as an electron transfer center (Sykes, 1991). One noticeable structural difference among the known proteins is the variation of Cu site geometry between trigonal planar and distorted tetrahedral, in which Cu is pulled out of the plane by the 4th axial ligand (Karlsson et al., 1991; Han et al., 1993; Romero et al., 1993)

The existence of a conserved Cu site in type 1 Cu proteins is proved by the high similarity of the RR spectra of these proteins (Han et al., 1991). In all cases, excitation within the S(Cys) → Cu(II) CT band near 600 nm produces strong enhancement of 4 or more fundamental vibrational modes in the 330 to 500-cm^{-1} region, plus one or two weak modes between 250-310 cm^{-1}. $^{63/65}$Cu isotope studies suggest that the multiplicity of

[1]These experiments were performed in collaboration with Tanneke den Blaauwen and Gerard W. Canters of Leiden University who provided the azurin samples.

observed modes comes from the coupling of the Cu-S(Cys) stretch with ligand internal deformations (Blair et al., 1985; Nestor et al., 1984). The Cu-S(Cys) stretch contributes most significantly to the strong RR bands. The remainder of the modes are enhanced due to their fractional Cu-S(Cys) stretching character (kinematic coupling) or to Cu cysteinate excited state delocalization (vibronic coupling). RR intensity studies confirm the importance of the Cu-S(Cys) moiety in both absorption and Raman spectra (Han et al., 1993). In addition to the strong blue band near 600 nm, which is identified as a S(Cys) → Cu CT band, the absorption band near 450 nm has a large Cys → Cu CT component as well. The transition of Cu site geometry from trigonal planar to more tetrahedral appears correlated with increased intensity of the 450 nm absorption band (Lu, 1992; Lu et al., 1993; Han et al., 1993).

Protein engineering now enables us to study protein structure and function in terms of specific amino acids (Adman, 1991b). Azurin from *Pseudomonas aeruginosa* (Figure 5.1) is the first type 1 Cu protein to be studied extensively by site-directed mutagenesis. A recent study of the azurin mutant, Cys112Asp, proves the critical role of the Cys112 ligand in the formation of the type 1 Cu center and the unusual absorption and EPR spectral properties (Mizoguchi et al., 1992). Studies of two other ligand mutants, His117Gly and His46Asp, prove that the two His ligands are not required for the spectroscopic properties of the type 1 Cu center. Upon addition of an exogenous ligand such as azide to the His117Gly mutant, a type 1 Cu site similar to that of WT azurin is identified by EPR and absorption spectra (den Blaauwen and Canters, 1993; den Blaauwen et al., 1993). Replacement of His46 by Asp also generates a type 1 Cu site similar to that of WT azurin, with only a slight change in Cu site geometry from trigonal planar towards tetrahedral as indicated by EPR and absorption spectra (Chang et al., 1991; Dave et al., 1993). However, the His ligands are needed for maintaining the Cu^{2+} oxidation state. Therefore, the two His ligands are important to the function of the protein (Guss et al., 1986; Sykes, 1991).

Azurin has eleven resonance enhanced Raman bands in the 200-500 cm^{-1} region. Two weak bands are at lower energy between 250-300 cm^{-1}, and the rest of the bands are in 350-500 cm^{-1} region. The most intense band is at 408 cm^{-1}, accompanied by other intense bands near 400 cm^{-1}. Kinematic and vibronic couplings of ligand internal modes

with the Cu-S(Cys) stretch explain why a single Cu-S(Cys) bond leads to such a rich RR spectrum (Han et al., 1991). To understand whether the three ligands, Cys112, His117, and His46, contribute equally to the RR spectrum, and to assign the RR spectrum of azurin, we investigated the RR spectra of (i) isotopically labeled wild-type (WT) azurin prepared from cells grown with ^{14}N or ^{15}N ammonium chloride, (ii) WT azurin incubated in H_2O or D_2O, and (iii) the His117Gly mutant in ^{63}Cu or ^{65}Cu plus exogenous imidazole.

We have found that among the eleven RR bands, only three (including the most intense band at 408 cm^{-1}) show significant Cu isotope contribution. These are likely to have the greatest Cu-ligand stretching character. Most of the other bands are cysteine ligand deformation modes as indicated by the $^{14/15}N$ isotope experiments. The coplanarity of the Cys side chain atoms with the Cu-S(Cys) bond (Figure 5.2) accounts for the extensive coupling of Cys deformation modes with Cu-S stretching (Nestor et al., 1984, Han et al., 1991). Studies with $^{32/34}S$ labeled azurin showed that the peak at 408 cm^{-1} has the most Cu-S(Cys) stretching character (Dave et al., 1993). The His117 ligand is responsible for one weak mode at 284 cm^{-1}, but it is not a significant contributor to the RR spectrum. In addition, studies on the His46Asp mutant yield no evidence that the Cu ligand His46 contributes to any of the RR bands (Dave et al., 1993). These studies make it clear that cysteine is the essential ligand that gives rise to the RR spectrum of azurin, as well as to its unique absorption and EPR spectra.

5.2 Experimental Procedures

5.2.1 Materials

Imidazole (Im) and NaN_3 were purchased from E. Merck AG, Darmstadt, Germany. N-methylimidazole (N-MeIm) and 2-methylimidazole (2-MeIm) were purchased from Sigma Chemical Co., St Louis, Mo. 4-methylimidazole (4-MeIm) was purchased from BASF, Germany. Structural formulas for these Im derivatives are shown in Figure 5.3. Metallic copper ^{63}Cu (99.7%) and ^{65}Cu (99.2%) were purchased from Intersales-Holland BV, The Netherlands, and converted to $Cu(NO_3)_2$ by dissolving 10 mg Cu in 50 ml 70% HNO_3. The Cu solutions were diluted to 5 ml and adjusted to pH 2 before being added to protein samples.

5.2.2 Preparation of WT Azurin Labeled with ^{15}N or D

The ^{15}N-enriched azurin was obtained by growing the protein on ^{15}N-ammonium ion as the sole source of nitrogen for the organism. Details of the procedure and protein purification were described previously (van de Kamp et al., 1992). The ^{15}N-enriched azurin contains ^{15}N in all side chains as well as in the main chain of the protein. For WT azurin in D_2O, a 2-mM protein solution was diluted 100-fold in 2 mM Tris-HCl in 99.7% D_2O (pH reading 8.5) and incubated for 16 h at 20°C, and 48 h at 4°C. The solution was then concentrated to 3 mM (Centricon-10, Amicon), diluted 100-fold in 20 mM MES in 99.7% D_2O (pH reading 5.2), and reconcentrated. Protein concentrations were estimated from $\epsilon_{289} = 9{,}800\ M^{-1}cm^{-1}$ (van de Kamp et al., 1990)

5.2.3 Preparation of ^{65}Cu, ^{63}Cu, or Deuterium-Labeled Azurin H117G(Im)

The apo-H117G mutant of *Pseudomonas aeruginosa* azurin was constructed through site-directed mutagenesis as described previously (den Blaauwen, et al., 1991; den Blaauwen and Canters, 1993). A stoichiometric amount of ^{63}Cu or ^{65}Cu was added to 0.1 mM apo-H117G in 20 mM MES (pH 5.0) and a yellowish-green solution was obtained. The absorption at 420 nm, which was monitored as a measure of Cu^{2+} binding, achieved a maximum during the 30 min incubation. A 30-fold excess of Im was then added, and a blue-colored solution was obtained. The samples were concentrated to 2 mM by ultrafiltration (Centricon-10, Amicon). For H117G(Im) in D_2O, the apo-H117G solution was exchanged with D_2O in the same procedures as that of WT azurin in D_2O. The protein was then reconstituted with natural abundance copper and imidazole after dilution in MES buffer and reconcentrated to 3 mM.

5.2.4 Preparation of Azurin H117G with Exogenous Ligands

The apo-H117G mutant was reconstituted with Cu (natural abundance) and 2-MeIm, N-MeIm, or 4-MeIm as described for the Cu isotopes. For the H117G(H_2O) sample, no exogenous ligand was added. For the less stable sample of H117G(N_3^-), the Cu complex of H117G was first formed and concentrated to ~2 mM. Then a 10-fold excess of azide was added to the solution. The sample was loaded on to the Raman sample holder and frozen within 5 min. In the cases where no exogenous ligand was added to azurin H117G, the Cu is assumed to be coordinated to one or more solvent molecules and is referred to as H117G(H_2O).

5.2.5 Resonance Raman Spectroscopy and Isotope Shifts

RR spectra were obtained with a computer-interfaced Jarrell-Ash spectrophotometer using a Spectra Physics 2025-11 Kr-laser for 647.1-nm excitation at 15 K, as described previously (Han et al., 1991). To measure the small isotope shifts accurately, samples were run sequentially under identical conditions. No changes were made to any spectrometer settings, the laser line was not retuned and the slit width was kept constant. To increase the spectral resolution, the slit width was set at 5 cm^{-1}, a lower limit for observing protein RR spectra due to the lower signal/noise. Peak positions and isotope shifts were determined by abscissa expansion. Also, we used the auto fitting routine in the LabCalc program (see Chapter 2) to resolve overlapped bands with small isotope shifts. Each set of data was repeated at least once by an independent experiment to check spectral reproducibility. In this way, a shift as small as 0.5 cm^{-1} could be verified as a real frequency change. Absolute peak frequencies are accurate to only ± 1 cm^{-1} owing to uncertainties in the precise location of the laser line (Loehr and Sanders-Loehr, 1993).

5.3 Results

5.3.1 RR Spectrum of WT Azurin

Excitation within the intense (Cys)S → Cu(II) CT band near 625 nm gives the strongly enhanced Raman spectrum shown in Figure 5.4A. A total of 11 bands were observed in the 200-500 cm^{-1} region (Table 5.1), which is the location of fundamental vibrations of Cu-ligand bond stretching and ligand internal deformations. The strongest band is at 408 cm^{-1}, accompanied by three other strong bands at 372, 400, and 428 cm^{-1}. This group of intense bands is centered near 400 cm^{-1}, which is the expected frequency for the Cu-S(Cys) stretch according to normal coordinate analysis (Nestor et al., 1984). Another 5 weak but relatively well-resolved modes are observed at 348, 441, 456, 476, and 494 cm^{-1}, concentrated largely in the high-energy side of the spectrum. Two weak and broad modes are observed at 267 and 284 cm^{-1}, isolated at the low energy side of the spectrum. The RR spectrum of azurin is typical of type 1 Cu proteins and is among those having the largest number of resonance-enhanced bands (Han et al., 1991).

5.3.2 RR Spectra of H/D-Labeled WT and H117G(Im) Azurin

When WT azurin is equilibrated in D_2O, most of the bands shift by -1 to -2 cm^{-1} (Table 5.2). The 284-cm^{-1} band has the largest shift of -2 cm^{-1}. Similar results have been reported previously for *P. aeruginosa* azurin by Blair et al. (1985) and are also shown in Table 5.2. In our experiment we added a 2-day incubation at pH 8.5 because H-exchange is base-catalyzed and occurs more rapidly as the pH is raised. However, the observed D-isotope shifts are not significantly greater than those reported by Blair et al. (1985) who performed only a 24-hour incubation in D_2O at 4°C and at pH 6.0.

The H117G azurin mutant was incubated in D_2O (pH reading 8.5) as the apoprotein, then reconstituted with Cu and Im (pH reading 6.0). Deuterium isotope shifts for this sample are also listed in Table 5.2. They are very close to those of the WT protein indicating that *(i)* the amide NH of His117 is not a significant contributor to the WT spectrum and *(ii)* removal of Cu does not increase the extent of D exchange.

5.3.3 RR Spectra of $^{63/65}$Cu-Labeled H117G(Im) Azurin

Samples were prepared through reconstitution of ^{63}Cu or ^{65}Cu into the apo-H117G mutant, followed by addition of exogenous Im. The RR spectrum of H117G(Im) with natural abundance copper is shown in Figure 5.4A and Table 5.1. The spectrum is nearly identical to that of WT protein, indicating that the Cu site structure and environment are very much conserved in the H117G mutant. It also shows that the Cu can bind Im as an exogenous ligand in the same manner that it coordinates the imidazole of His117 in the WT protein. RR spectroscopy verifies the recovery of the type 1 Cu site by addition of exogenous Im (den Blaauwen and Canters, 1993), as has also been indicated by absorption and EPR spectral studies (den Blaauwen et al., 1991). The only noticeable differences are the increased intensity in the 400-cm^{-1} shoulder and a -3-cm^{-1} shift in the 284-cm^{-1} peak.

RR spectra of $^{63/65}$Cu labeled azurin H117G(Im) are shown in Figure 5.4B. As we can see from the overplot, the isotope effects are very small and most of bands do not shift in ^{65}Cu. Band frequencies and isotope shifts are listed in Tables 5.1 and 5.2. Using a curve-fitting program (Chapter 2), we found that the 372- and 408-cm^{-1} bands shift -0.5 and -0.6 cm^{-1} respectively, in ^{65}Cu. The shifts are consistently detected and are considered real shifts. The 429- and 441-cm^{-1} bands have small shifts which are

within the experimental error of ± 0.5 cm^{-1} and, thus, are not considered significant. The 281-cm^{-1} band shifts about -1.5 cm^{-1}, and it is difficult to determine the shift more accurately due to the shape of the band. The 456-, 478-, and 494-cm^{-1} bands clearly do not shift in ^{65}Cu. In addition, the strong 400-cm^{-1} shoulder does not shift by curve fitting analysis and the apparent difference at 400 cm^{-1} in the overplot is due to an intensity increase rather than a frequency shift. This increase is most likely due to intensity borrowing from the 408 cm^{-1} peak as it shifts 0.6 cm^{-1} to lower energy (for details, see Chapter 2). Finally, the 266-cm^{-1} band appears to shift 0.5 cm^{-1} to higher energy in ^{65}Cu. Similar results have been observed for WT azurin (Blair et al., 1985) and are listed in Table 5.2, as well.

5.3.4 RR Spectra of $^{14/15}N$-labeled WT Azurin

The ^{14}N- or ^{15}N-labeled WT azurin was prepared by growing the protein on ^{14}N- or ^{15}N-ammonium chloride. Thus, all nitrogen atoms in the protein are labeled. RR spectra of $^{14/15}N$-labeled azurin are shown in Figure 5.4C. The observed frequency shifts are listed in Table 5.2. The 372- and 408-cm^{-1} bands, which also have Cu-isotope effects, shift -0.9 and -1.4 cm^{-1}, respectively, in ^{15}N-azurin. The 428-, 441-, 456-, and 476-cm^{-1} bands, which have no Cu isotope effects, show the largest shifts of -2.6 to -3.7 cm^{-1}. These bands are weak, but well resolved. In addition, the 348- and 400-cm^{-1} bands, which have no Cu isotope effect, also show large $^{14/15}N$ isotope shifts of -2.5 and -2.7 cm^{-1}, respectively. The 494-cm^{-1} band shows a small shift of -0.4 cm^{-1} that is probably not significant. On the low frequency side of the spectrum, the 284-cm^{-1} band shifts -2 cm^{-1}, and the 267-cm^{-1} band shows no change. Thus, ten out of eleven modes shift in ^{15}N-azurin. It is clear that one or more nitrogen atoms are largely involved in these vibrations. Figure 5.5 summarizes the isotope shifts obtained in azurin and azurin mutants. It is interesting to see the remarkably different patterns of $^{63/65}Cu$ and $^{14/15}N$ isotope effects on the RR bands.

5.3.5 RR Spectra of H117G Azurin with Exogenous Ligands

Samples were prepared by reconstitution of apo-H117G protein with natural abundance Cu, followed by addition of exogenous ligand. When no exogenous ligand is added, the resultant H117G(H_2O) is actually a mixture of type 1 and type 2 Cu species that can be probed by excitation at 647 and 413 nm, respectively (den Blaauwen et al.,

1993). The RR spectrum of the type 1 form of H117G(H_2O) is shown in Figure 5.6B and the band frequencies are listed in Table 5.1. The spectrum is quite similar to that of WT azurin, showing eleven bands. Among these, the five bands between 420-500 cm^{-1}, plus one at 345 cm^{-1}, show no change in frequencies and intensities compared to the spectrum of H117G(Im) in Figure 5.4A. The most significant changes are that the 372- and 400-cm^{-1} bands shift to 367 and 397 cm^{-1}, respectively, with dramatic increases in intensity, while the band at 406 cm^{-1} decreases in intensity. In the low frequency region, the 264-cm^{-1} band shifts to 260 cm^{-1} and the 284-cm^{-1} band diminishes in intensity. In addition, a new mode at 302 cm^{-1} shows up and this band is relatively intense and sharp compared to the 267- and 284-cm^{-1} bands in WT azurin. Similar results to that of H117G(H_2O) are observed in azurin H117G(N_3^-), where N_3^- takes the place of the His117 ligand (Table 5.1). The fact that the RR spectrum is largely unaffected by the loss of an imidazole ligand tells us that His117 is not a major contributor to the RR spectrum. The most important change is the loss of the 284-cm^{-1} band in the absence of the His117 ligand. This band is closely related to the Cu-N(His117) interaction. The shift in intensity from the 406-cm^{-1} band to the bands at 397 and 367 cm^{-1} is associated with a lengthening of the Cu-S(Cys) bond (den Blaauwen et al., 1993).

The RR spectra of H117G with alkylated imidazoles, 2-MeIm and N-MeIm, are shown in Figures 5.4C and D. The frequencies of these spectra, together with the data for the 4-MeIm adduct, are given in Table 5.1. The spectrum of H117G(4-MeIm) is very close to that of H117G(N-MeIm). The spectrum of H117G(2-MeIm) is essentially identical to that of H117G(Im) and WT azurin. For the N-MeIm and 4-MeIm adducts, the majority of the bands above 300 cm^{-1} maintain the same frequencies and intensities, showing that these bands are not sensitive to changes in the imidazole ring. The most noticeable changes relative to WT azurin occur in the low frequency region. The 264-cm^{-1} band shifts to 259 cm^{-1}, the 284 cm^{-1} band diminishes in intensity, and the 372-cm^{-1} band broadens revealing a new feature at 368 cm^{-1} in the N-MeIm case. These results show that RR spectrum senses no effect of the protein backbone beyond the imidazole ring of His117 and that the 2-MeIm is bound in the same orientation as unmethylated imidazole, however, the N-MeIm and 4-MeIm derivatives have slightly altered configurations.

5.4 Discussion

The RR spectrum of type 1 Cu proteins is characterized by the high intensity and the multiplicity of bands near 400 cm^{-1}. The assignment of the observed bands has been the subject of many studies. In 1978, the first two crystal structures of type 1 Cu proteins, plastocyanin and azurin, were determined and the Cu ligand set (Cys, 2His, and Met) and Cu coordination geometry were established. A short Cu-S(Cys) bond of 2.13 Å was also discovered. With the structural information and the observed RR spectrum, normal coordinate analysis could be used to calculate the expected frequencies and to assign the bands in detail.

A five-atom model CuSS*NN of the type 1 Cu site was examined in detail in a normal coordinate analysis by Thamann et al. (1982). Their analysis revealed considerable mixing of Cu-S and Cu-N vibrational modes and excluded the contribution of S*(Met) ligand to the spectrum in 200-500 cm^{-1} region. However, their analysis considered only point masses, and did not allow for mixing of Cu-L stretching motions with internal ligand vibrational modes. Therefore, the detailed assignments were not realistic. Isotope studies, including H/D and $^{63/65}Cu$ exchange on a large number of type 1 Cu proteins, provided strong evidence of coupling of Cu-L vibrations with internal ligand motions (Nestor et al., 1984; Blair et al., 1985; Nestor et al., 1986). An improved normal coordinate analysis for a CuSS*$[N(Im)]_2$ model, using ligand effective masses, was performed by Nestor et al., (1984). Their study concluded that the Cu-S stretch was the only vibration expected near 400 cm^{-1}, the Cu-N(His) stretches should be in the low frequency region of 230-310 cm^{-1}, and the weakly bonded Cu-S*(Met) stretch should be at a even lower frequency. The observed multiple bands near 400 cm^{-1} were assigned to His and Cys internal ligand deformations and their high intensity was the result of coupling with the Cu-S(Cys) stretching motion.

The normal coordinate analysis of Nestor et al. (1984) provided a rough picture of the RR spectrum of type 1 Cu proteins. However, detailed assignment of ligand modes could not be made because they did not know what atoms should be included in the normal coordinate analysis calculation. The aim of the present investigation was to determine whether the His and Cys ligands contribute equally to the RR spectrum of azurin and what ligand atoms are involved in the coupling.

5.4.1 Cu-Ligand Stretches

The use of isotopic pairs of heavy metals in vibrational spectroscopy was first reported by Nakamoto and co-workers (Nakamoto et al., 1969). The metal isotope labeling method provides definitive band assignments of metal ligand vibrations. Only the vibrations involving the motion of the metal atom are shifted by metal isotope substitution. However, if the metal-ligand vibrations are coupled with ligand internal vibrations, the latter also become metal isotope sensitive (Mohan et al., 1975). Thus, it is possible that the observed shift for a particular band may be smaller than calculated if this mode does not correspond to a pure stretching mode.

Table 5.3 presents the calculated isotope shifts for a specific stretching mode of an isolated two-atom oscillator in the Cu site of azurin. The calculated isotope shift of the Cu-N(Im) stretch can be approximated by using a mass of 14 for the nitrogen atom alone, or a mass of 68 if the entire imidazole ring is taken as a point mass. As we can see, the calculated shifts are very sensitive to the mass used.

In the spectrum of H117G(Im) reconstituted with ^{63}Cu or ^{65}Cu, three bands at 281, 372, and 408 cm^{-1} show significant ^{65}Cu isotope effects (Figure 5.5, Table 5.2). The $\sim$284-cm^{-1} band has been previously assigned to Cu-N(His) stretch on the basis that the observed frequency and isotope shift are close to the expected values for a Cu-Im vibration (Nestor et al., 1984; Blair et al., 1985). However, the observed -1.5 cm^{-1} shift (Table 5.2) is smaller than the calculated value of -2.3 cm^{-1} (Table 5.3). The observed isotope shifts of -0.5 and -0.6 cm^{-1} for bands at 372 and 408 cm^{-1} (Table 5.2) are also smaller than the -2.1 cm^{-1} expected for an isolated Cu-S stretching mode at 408 cm^{-1} (Table 5.3). Even the aggregate shift of -1.1 cm^{-1} is substantially less than -2.1 cm^{-1}. These results tell us that there are no pure Cu-L stretching modes and, rather, that the Cu must be involved in a number of different vibrations. These additional vibrations are likely to be predominantly ligand internal modes that have a small amount of Cu-L stretching character, such that the remainder of the change of the Cu mass is divided among them. Many of these vibrational modes will undergo a Cu isotope shift of less than 0.5 cm^{-1} which is below the limit of detectability in our RR experiments. The modes with no detectable Cu-isotope effect very likely originate from ligand atoms further away from the Cu, such as the cysteine side chain, histidine ring, and even

peptide bond atoms.

The RR spectrum of $^{32/34}$S-labeled WT azurin has been studied by Czernuszewicz and co-workers (Dave et al., 1993). Among the eleven bands between 200 and 500 cm^{-1}, only the bands at 408 and 428 cm^{-1} show significant sulfur isotope effects (Figure 5.5, Table 5.2). The strongest band at 408 cm^{-1} shifts -4 cm^{-1} in ^{34}S which is 50% of the calculated value of -8.1 cm^{-1} for a pure Cu-S mode (80% of calculated value if one considers -SCH_2 as a point mass; Table 5.3). The intense band at 428 cm^{-1} shifts -2 cm^{-1} in ^{34}S. The S-C_β stretch mode at 750 cm^{-1} shifts about -3 cm^{-1} in ^{34}S, which is smaller than the expected value of -7 cm^{-1}. The rest of the bands either do not shift at all or they shift only insignificantly. The results tell us that only two bands in 200-500 cm^{-1} region have significant sulfur contribution and suggest that the most intense 408-cm^{-1} band has the greatest amount of Cu-S(Cys) stretching character.

It is expected that excitation within the (Cys)S → Cu CT band will enhance primarily the Cu-S(Cys) stretch. Thus, it is logical that the feature with the greatest RR intensity (the peak at 408 cm^{-1}) also has the greatest Cu-S stretching character. The short Cu-S(Cys) bond of ~2.15 Å in azurin causes this mode to appear at 408 cm^{-1}, a much higher energy compared to the ~300 cm^{-1} frequency for the typically longer Cu-SR bonds of ~2.3 Å in model complexes (Han et al., 1993). The fact that the only 408-cm^{-1} mode senses the $^{32/34}$S-isotope substitution among the three Cu-sensitive modes suggests that only the 408-cm^{-1} mode has a significant contribution of the Cys ligand. The other two Cu-sensitive bands at 284 and 372 cm^{-1} are probably not sulfur related, and their assignments will be discussed in detail in the following sections.

5.4.2 Histidine Ligand Modes

The involvement of one or more nitrogen atoms in the RR spectrum of azurin is demonstrated by the large isotope effects when all of the nitrogens in the protein are substituted with ^{15}N (Figure 5.5, Table 5.2). There are a total of five nitrogen atoms in the Cu ligands, as shown in Figure 5.1. Two N_δ nitrogens from His117 and His46 are directly bound to Cu. Two other N_ϵ nitrogens from His117 and His46 are within the Im rings. The fifth nitrogen is the Cys amide nitrogen. This nitrogen is not directly connected to Cu, but is associated with the Cu-S(Cys) framework. Here, we first discuss the contributions of the two His ligands to the RR spectrum of azurin.

5.4.2.1 His and Cu-Im Complexes

RR studies of His and His-containing polypeptides have been accomplished using UV laser sources (Tsuboi et al., 1987; Ashikawa and Itoh, 1979; Colombo et al., 1974). The important results are as follows: *(i)* All in-plane Im ring vibrations observed, as well as predicted by normal coordinate analysis, are in the 600-1600 cm^{-1} region. There are no in-plane modes < 600 cm^{-1}. *(ii)* The Im ring does have a pair of out-of-plane ring deformation modes which fall in the 400-600 cm^{-1} region (Colthup et al., 1980). These bands are expected to shift significantly in D_2O, because of coupling with the N-H out-of-plane bend. *(iii)* These modes are not sensitive to the polypeptide backbone conformations. Therefore, it is safe to expect that vibrational frequencies will be the same in free His and in a protein.

A number of metal-Im complexes have been studied by IR and Raman spectroscopy. Typically, all of the Cu-N(Im) stretching modes (symmetric and asymmetric) occur below 310 cm^{-1} and shift by -3 to -4 cm^{-1} when ^{65}Cu is substituted for ^{63}Cu (Hodgson et al., 1980; Cornilsen and Nakamoto, 1974; Larrabee and Spiro, 1980). The Raman-active ν_s(Cu-N) mode occurs between 245 and 288 cm^{-1} for a series of $Cu(Im)_2L_2$ and $Cu(Im)_4$ complexes with underivatized or methylated imidazoles (Larrabee and Spiro, 1980). Other bands are observed at lower frequency and are assigned to δ(M-N-CH). This bending mode involves one of the carbon atoms, which can be deuterated (M-N-CD), and the mass effect on δ(M-N-C) of 8 cm^{-1} (Hodgson et al., 1980) is greater than on ν(M-N) which shifts only 1 to 2 cm^{-1} upon deuteration (Hodgson et al., 1980; Larrabee and Spiro, 1980). Therefore, the bending mode can be identified and distinguished from ν(M-N).

In Cu-Im complexes, the Im → Cu charge transfer (LMCT) absorptions have been used to characterize Cu coordination geometry (Fawcett et al., 1980). For tetragonal Cu(II)-Im complexes, three LMCT absorptions are observed in the 220-330 nm region. These absorptions are expected to be red shifted as the Cu site geometry changes from tetragonal to tetrahedral. Such LMCT absorptions should make it possible to identify Cu(II)-N(Im) stretch and Im ring vibrations by RR spectroscopy. Unfortunately, the resonance-enhancement is so weak that these modes cannot be detected in proteins using excitation within the Im → Cu CT band (Larrabee and Spiro, 1980; Caswell and Spiro,

1986). Thus, metal-Im vibrations in proteins are only detected when they are coupled to a stronger chromophore.

5.4.2.2 M-Im Vibrations in Proteins

Imidazole groups have important ligand roles when a metal is complexed by His-containing peptides. His ligation has been well characterized by X-ray crystallographic studies of proteins such as azurin (Adman et al., 1978; Baker 1988; Adman, 1991a), superoxide dismutase (Richardson et al., 1975; Tainer et al., 1982; Parge et al., 1992), hemocyanin (Volbeda and Hol, 1988; Magnus et al., 1993), and hemoglobin (Shaanan, 1982). In the case of oxyhemocyanin, the M-N(Im) stretching modes are detected at 230, 269, and 313 cm^{-1} due to resonance-enhancement with a peroxide → Cu(II) CT band (Larrabee et al., 1977; Larrabee and Spiro, 1980). No other Im modes were observed in the 200-500 cm^{-1} region. Similarly, in heme proteins, the axial Fe-N(His) bond stretches are detected through resonance with the porphyrin electronic transitions. The Fe-N(His) stretch occurs at $\sim$220 cm^{-1} in ferrous hemoglobin and myoglobin, and at $\sim$240-270 cm^{-1} in peroxidases (Teraoka and Kitagawa, 1981). In contrast, in the respiratory protein, hemerythrin, in which five histidines are ligated to an oxo-bridged dinuclear iron center, no Fe-N(His) vibrations have ever been detected (Sanders-Loehr, 1989).

5.4.2.3 Cu-Im Vibrations in Azurin

In azurin, Cu is coordinated by His117 and His46 and the Cu-N(His) bonds are both $\sim$2.0 Å (Nar et al., 1991), which are within the normal range of 2.0 $\pm$ 0.1 Å of Cu(II)-Im complexes. Therefore, we expect the frequency of ν(Cu-N) to be at $<$300 cm^{-1}, as observed in other metal-His containing proteins. The 284-cm^{-1} band is the only band showing a Cu isotope effect in this region, indicating a Cu-ligand vibration. This band also undergoes a -2-cm^{-1} shift in ^{15}N-labeled azurin (Table 5.2), which is in good agreement with the -2-cm^{-1} value calculated for a unit mass change on both N_ϵ and N_δ (Table 5.3). A similar shift of -2 cm^{-1} is observed when H117G is reconstituted with ^{15}N-imidazole (Andrew et al., 1993). These results lead us to assign the band at 284 cm^{-1} to the Cu-N(Im) stretch of an imidazole at the His117 site. The His117 assignment is supported by the fact that 284-cm^{-1} band disappears when the His117 ligand is removed (Figure 5.6B), but is still present when the His46 ligand is replaced by Asp

(Figure 5.6E).

Further evidence for a Cu-N(Im) stretching mode at 284 cm^{-1} is the fact that this band shows no sensitivity to sulfur isotope (Figure 5.5). In addition, it shows a -2-cm^{-1} shift in D_2O (Table 5.3). NMR studies of azurin have shown that the N_ϵ-hydrogen of the Im ring of His117 does exchange with deuterium (van de Kamp et al., 1992). However, the observed deuterium shift is larger than the -1.0-cm^{-1} value calculated for exchange of a single hydrogen on the Im ring (Table 5.3). This may be due to the exchange of additional hydrogen, e.g., at the C2 position on the imidazole ring (Nestor et al., 1984). Alternatively, the unusually large D effect may reflect a change in H-bond strength, since the N_ϵ proton of His117 is H-bonded to a water molecule in azurin (Figure 5.1). Our assignment of the 284-cm^{-1} band to a Cu-N(Im) stretch agrees with the previous predictions of Nestor et al. (1984) and Blair et al. (1985) which were based on Cu and D isotope data. However, given the fact that the 284-cm^{-1} band does not change in the His46Asp mutant (Figure 5.6E), the assignment of this mode to a symmetric Im-Cu-Im stretch (Blair et al., 1985) is no longer appropriate.

It appears that the Cu-N(Im) stretch of the His117 ligand at 284 cm^{-1} is the only histidine mode that is resonance-enhanced in the 200-500 cm^{-1} region of the RR spectrum. When apoH117G is reconstituted with Cu and ^{15}N-labeled imidazole, the only two peaks exhibiting any detectable ^{15}N-isotope dependence between 200 and 1500 cm^{-1} are the peaks at 284 and 658 cm^{-1}, which shift by -2 and -1 cm^{-1}, respectively (Andrew et al., 1993). These are also the only two peaks that are affected by histidine ligand replacement. Thus, upon substitution of His117 with H_2O, only the 284-cm^{-1} peak disappears (Figure 5.6B). Even less spectral change occurs when His46 is replaced by Asp (Figure 5.6E); only the peak at 658 cm^{-1} disappears (Dave et al., 1993). The increased intensity at 398 cm^{-1} is due to a slight lengthening of the Cu-S(Cys) bond (Dave et al., 1993) and there is a possible frequency shift from 348 to 337 cm^{-1}. However, there is no indication of any vibrational modes of the His46 ligand in the 200-500-cm^{-1} region of the RR spectrum.

In the crystal structure of azurin (Figure 5.1), both of the imidazole rings are tilted approximately 30° relative to the NNS ligand plane. Thus, it is not clear what structural or electronic basis exists for resonance enhancement of the Cu-N(His) stretch

of His117, but not His46. It may be that subtle differences in orbital overlap affect vibronic coupling with the (Cys)S → Cu CT transition. Thus, modifications of the imidazole ring in imidazole complexes of H117G azurin also affect the enhancement of the vibration of ~284 cm^{-1}. This mode is observed with 2-MeIm and N-polyvinylIm, but not with 4-MeIm or N-MeIm (Figure 5.6, Table 5.1). Comparison of the structures of the alkylated imidazoles (Figure 5.3) also does not reveal any obvious structural basis for the observed RR differences. Most likely there is a slight variability in the orientation of exogenous imidazoles in the H117 site.

The involvement of His ligands in the RR spectrum of type 1 Cu proteins has long been debated. Electronic spectra of type 1 Cu proteins generally show absorption near 450 nm, in addition to the strong S(Cys) → Cu CT band at ~600 nm. The 450-nm absorption band was assigned to a His → Cu(II) CT transition on the basis of polarized single-crystal absorption spectroscopy (Penfield et al., 1981). However, we determined that excitation within the 450-nm absorption band leads to the same set of RR modes as is observed with 600-nm excitation (Han et al., 1993). Thus, both electronic transitions must have primarily Cys(S)→ Cu CT character. This conclusion is further supported by the present findings that no histidine vibrational fundamental (other than the Cu-N(Im) stretch at 284 cm^{-1}) is resonance-enhanced. The extensive RR spectral features in azurin must, thus, be due to the cysteinate ligand. The Cu-N(Im) stretch of His117 is most likely enhanced via vibronic coupling with the Cys(S) → Cu CT transition. This finding is in keeping with the vibrational studies of metal-Im complexes in proteins discussed earlier where metal-Im stretching modes are also enhanced via coupling to a stronger chromophore.

5.4.3 Cysteine Ligand Modes

5.4.3.1 Cysteine Vibrations

Our attention now focuses on the Cys ligand and vibrations associated with it. Free cysteine is a non-linear molecule consisting of 14 atoms. For a non-linear molecule, there are 3N-6 normal vibrations, where N is the number of atoms in the molecule (Colthup et al., 1980). One therefore expects that cysteine has a total of 36 normal vibrations. The vibrational spectrum of cysteine has been reported and a normal coordinate analysis has also been performed (Susi et al., 1983). A total of 35 modes are

observed between 100 and 3200 cm^{-1}. The majority of these bands are bond stretching and angle bending motions, and most of the stretching modes are located in the high frequency region between 1000-3200 cm^{-1}. Of the 35 observed vibrations, only 8 are at lower energy between 100 and 500 cm^{-1}, which is the region of interest in the discussion of the fundamental vibrations of type 1 Cu proteins. As an analogue of cysteine, the Raman spectrum of 1-propanethiol has also been fully discussed (Li et al., 1992).

Band frequencies and band assignments for both L-cysteine and 1-propanethiol in 100-500 cm^{-1} region are listed in Table 5.4. It can be seen that most of these modes are due to the angle bending involving the heavy atoms S, N, and C and the torsional motions involving atoms C and H. The frequencies of the angle bending modes are likely to be found between 250 and 450 cm^{-1}, and the frequencies of the torsional modes are generally at even lower energy near 200 cm^{-1}. It is noteworthy that the assignments for cysteine in Table 5.4 are for the dominant vibrational motion, but that most are actually mixtures of 2-3 different vibrational motions. For example, the $\delta(S\text{-}C_\beta\text{-}C_\alpha)$ bend accounts for 49% of the potential energy distribution at 118 cm^{-1}, 11% at 207 cm^{-1}, and 14% at 444 cm^{-1}, whereas the $C_\beta\text{-}C_\alpha\text{-}N$ bend contributes 31% at 444 cm^{-1} and 14% at 535 cm^{-1}.

5.4.3.2 Cu-SR Complexes

The cysteine ligand modes are less well documented in Cu-SR complexes than for uncoordinated ligands. Most of these complexes have a metal site geometry that is either trigonal bipyramidal or tetragonal with a normal Cu(II)-S bond distance $\geq$ 2.25 Å (Kitajima et al., 1992; Kitajima, 1993). Although these complexes generally have large extinction coefficients ($\geq$ 1,000 $M^{-1}cm^{-1}$), they exhibit much lower molar Raman scattering intensities than type 1 Cu proteins, a feature presumably related to the absence of the short Cu-S(Cys) bond (Han et al., 1993). In 1990, Kitajima and co-workers reported the first successful synthesis of tetrahedral Cu(II)-thiolato complexes (Kitajima et al., 1990 and 1992), which are the only low molecular compounds closely mimicking the Cu site in type 1 Cu proteins. In these compounds, Cu is coordinated to tris-pyrazolylborate and SR (R = CPh_3, C_6F_6, or $C(CH_3)_3$). Especially noteworthy is the Cu(II)-S bond distance of 2.12-2.18 Å, which is clearly shorter than that in other Cu-SR complexes, making these complexes more suitable models for type 1 Cu proteins.

The RR spectrum of the Cu-$SC(CH_3)_3$ complex of Cu(II)[$HB(3,5\text{-}iPr_2pz)_3$] exhibits a set of resonance-enhanced vibrational modes, similar to that of a type 1 Cu protein (Qiu et al., 1992). The most intense band is at 435 cm^{-1}, with several other weaker bands at lower energy. All these bands are shifted to lower frequency when S-$C(CD_3)_3$ is used as a ligand. Based on normal coordinate analysis, the band at 435 cm^{-1} is assigned as having the greatest Cu-S stretching character. However, the sensitivity of all modes to deuterium substitution shows that they are all mixed modes and that C-H motions must also be considered. Results on this model compound demonstrate that a single thiolate ligand can produce as many as five resonance-enhanced vibrations and that the RR spectrum is extremely sensitive to the changes in the R group of the thiolate ligand.

5.4.3.3 Cu-Cysteinate Modes in Azurin

The contribution of the two His ligands, His117 and His46, to the RR spectrum of azurin has been fully discussed in section 5.4.2 (Histidine Ligand Modes). Of the 11 bands observed in the 200-500 cm^{-1} region, only the mode at 284 cm^{-1} is assignable to Cu-N(His117) stretching. Previous studies of azurin substituted with selenomethionine demonstrated that the methionine ligand also does not contribute to the low frequency RR spectrum (Thamann et al., 1982). Thus, the majority of bands is most likely due to the cysteine ligand.

The large isotope effects seen in the RR spectrum of ^{15}N-labeled azurin provide, for the first time, direct evidence that cysteine side chain atoms including the amide nitrogen contribute significantly to the RR spectrum. As can be seen in Figure 5.1, there are five nitrogen atoms within the Cu site. Out of the 5 nitrogen atoms, the four nitrogens from His117 and His46 are not important to the RR spectrum. This leaves the nitrogen from the Cys amide group as the only candidate. Of the 11 RR bands of azurin, 10 show significant ^{15}N-effects (Figure 5.5, Table 5.2). However, only one band at 284 cm^{-1} exhibits ^{15}N-isotope dependence when apoH117G is reconstituted with Cu and ^{15}N-labeled imidazole. The high sensitivity of the RR spectrum towards ^{15}N-isotope labeling implies the large participation of the Cys side chain including the amide group in the spectrum.

Vibrational spectral studies of free cysteine and its analogue provide us with vibrational modes in the 100 to 500 cm^{-1} region and serve as the basis for the discussion of cysteine vibrations in the protein. However, the band frequencies will most likely be different when cysteine is coordinated to the metal in the protein, because the $-NH_2$ and -C=O groups of the Cys become part of the peptide bond. Each amide bond now has partial double bond character, and the vibrations involving these amide bonds are expected to have higher frequencies. In addition, the Cys side chain atoms are more firmly positioned by the protein environment. The sulfur is coordinated to a bound copper rather than a mobile hydrogen. H-bonding to the sulfur and to the amide nitrogen further increases the structural rigidity. These structural differences strongly affect the degree of coupling of atomic motions and, thus, the observed vibrational frequencies. Therefore, comparisons of band frequencies of the Cu-S(Cys) structural unit in the protein with those of free cysteine are really no longer appropriate.

The fact that the Raman spectrum of azurin is resonance-enhanced by coupling to the S → Cu CT band provides another source of uncertainty in band assignments. The Cu-S moiety not only adds a new component for coupling with stretching and bending motions, but may also change the vibrational intensities of modes with which it is coupled. Because many of the bands in free cysteine will be altered as a result of the formation of the Cu-S(Cys) bond, we do not have a well-established reference system. The following discussion of the assignments of the Cys-related vibrations (Table 5.4) is therefore based on the isotope effects, band frequencies and intensities, as well as information from free cysteine.

5.4.3.4 The Cu-S Stretch 408 cm^{-1}

The dominant 408-cm^{-1} band in the RR spectrum of azurin (Fig. 5.4) has been assigned to ν[Cu-S(Cys)] based on the Cu and sulfur isotope data discussed section 5.4.1 (Cu-Ligand Stretches). The fact that many type 1 Cu proteins show their most intense RR band as high as 400 cm^{-1} is largely the result of the unusually short Cu-S(Cys) bond. Nevertheless, the smaller-than-expected sulfur isotope shift (Table 5.3) reveals that this is not a pure Cu-S mode and must contain other vibrational components in addition to the Cu-S stretch.

5.4.3.5 The S-C_β Stretch at 750 cm^{-1}

Most type 1 Cu proteins show a fundamental vibration near 750 cm^{-1} that is more intense than any of the overtones or combination bands in the 700-900-cm^{-1} region (Blair et al., 1985). The -3-cm^{-1} shift of this mode in ^{34}S-labeled azurin identifies it as having a significant S-C_β(Cys) stretching component (Dave et al., 1993). It is of interest that the ν(S-C) vibrational frequency for azurin is considerably higher than the 691 and 650-cm^{-1} values assigned for L-cysteine and 1-propanethiol, respectively (Table 5.4). It is likewise higher than ν(S-C) at 653 cm^{-1} for the Fe-cysteinate moiety in oxidized rubredoxin (Czernuszewicz et al., 1986). However, none of these other assignments have been verified by sulfur isotope substitution. The S-C_β-C_α bend in azurin is also likely to be at higher energy than in L-cysteine where it accounts for 49% of the PED at 118 cm^{-1} and 14% of the PED at 444 cm^{-1} (Susi et al., 1983). Angle bending modes are generally found at half the mean stretching frequency of the bonds forming the angle. Thus, for azurin with ν(S-C_β) at 750 cm^{-1} and ν(C_β-C_α) at 975 cm^{-1}, the predominant δS-C_β-C_α mode is likely to be closer to 400 cm^{-1} (Blair et al., 1985).

5.4.3.6 The Intense Bands at 372, 400, and 428 cm^{-1}

The RR spectrum of WT azurin shows three additional intense bands at 372, 400 (shoulder), and 428 cm^{-1}. The high intensities of these bands indicate either kinematic coupling with the Cu-S(Cys) stretch or vibronic coupling with the (Cys)S → Cu(II) CT transition. These bands are likely due to angle deformations involving S, C, and N atoms of the cysteine ligand. Possible candidates are δ(Cu-S-C_β), δ(S-C_β-C_α), and δ(C_β-C_α-N). Among them, the δ(Cu-S-C_β) mode involves the heavy Cu atom and its frequency is thus expected to be the lowest. By the above criterion, one would predict the frequency of δ(Cu-S-C_β) to be near 300 cm^{-1} if ν(Cu-S) is at 408 cm^{-1} and ν(S-C_β) is at 750 cm^{-1}. When considering the isotope effect of the δ(Cu-S-C_β) mode, a large displacement of the Cu atom and only a small $^{32/34}$S isotope shift are expected. Of the three bands, the 372-cm^{-1} band is the only one showing significant Cu contribution and little sulfur and nitrogen isotope effects (Fig. 5.5). Therefore, we assign the 372-cm^{-1} band as predominantly δ(Cu-S-C_β).

The 428-cm^{-1} band shows a -2 cm^{-1} shift in ^{34}S, and no significant Cu involvement (Fig. 5.5). Therefore, we assign it predominantly to the δ(S-C_β-C_α).

However, this band shifts by -3.8 cm^{-1} in ^{15}N-labeled azurin, indicating coupling with a vibrational motion of the Cys amide nitrogen. The 400-cm^{-1} band does not shift with either Cu or S isotopes, but shifts by -2.7 cm^{-1} in ^{15}N-labeled azurin. Thus, we assign it predominantly to $\delta(C_\beta\text{-}C_\alpha\text{-}N)$, which senses the mass change on the amide nitrogen. It is somewhat surprising for $\delta(S\text{-}C_\beta\text{-}C_\alpha)$ with its large S atom to be at higher energy than $\delta(C_\beta\text{-}C_\alpha\text{-}N)$. However, the energy of $\delta(S\text{-}C_\beta\text{-}C_\alpha)$ could be increased by the unusually large $S\text{-}C_\beta$ bond strength, as evidenced by its 750-cm^{-1} vibrational frequency.

The high intensities of these bands may be due to kinematic coupling with Cu-S(Cys) stretch. Such coupling is expected to be dependent on the conformation of the Cys side chain. For example, coupling of ν(Cu-S) with $\delta(S\text{-}C_\beta\text{-}C_\alpha)$ or $\delta(C_\beta\text{-}C_\alpha\text{-}N)$ will be maximal when the Cu-S-C_β-C_α and S-C_β-C_α-N dihedral angles are at $\sim 180°$ and minimal at $\sim 90°$ (Han et al., 1989). In azurin, these two angles were found to be 169° and 173°, respectively, leaving the atoms Cu, S, C_β, C_α and N in an essentially coplanar conformation (Han et al., 1991). Moreover, in a detailed analysis of all available crystal structures of proteins containing type 1 Cu sites, we noted that a coplanar Cu-S-C_β-C_α-N network was a fully conserved feature (Han et al., 1991). Thus, maximal coupling of Cys internal modes with the Cu-S stretch would be achieved. Therefore, we observe additional enhanced bands, rather than a single strong band from the Cu-S(Cys) stretch, in all type 1 Cu proteins. A similar type of coupling has been suggested for the RR spectra of iron-sulfur proteins, such as $Fe_2S_2(Cys)_4$ plant ferredoxins and $Fe_4S_4(Cys)_4$ high-potential iron proteins (Backes et al., 1991), which contain one or more Fe-S-C_β-C_α dihedral angles near 180°. This coplanar Cys side chain conformation explains the observation of multiple intense RR bands in metal-cysteinate proteins.

5.4.3.7 Previous Assignments of the Bands Near 400 cm^{-1} in Azurin

The assignments of the intense bands at 372, 400, 408 and 428 cm^{-1} have been discussed previously, based on Cu-isotope data and temperature dependence of the relative intensities of the bands (Blair et al., 1985). In that study, bands at 408 and 400 cm^{-1} were assigned to the coupled Cu-S stretch and the S-C_β-C_α angle bend. The 408-cm^{-1} band was assigned as the in-phase mode, which would have large Cu isotope effect because the Cu-S distance increased as the S-C_β-C_α angle became larger. The 400-cm^{-1} band was assigned as the out-of-phase mode, which would involve a large

displacement of the sulfur atom, and exhibit a smaller Cu isotope effect. Recent studies of $^{32/34}$S-labeled WT azurin suggest that the 408-cm^{-1} band is predominantly a Cu-S(Cys) stretching mode (Dave et al., 1993). Also, the assignment of 400-cm^{-1} band as the out-of-phase mode is no longer appropriate, because the 400-cm^{-1} band does not show any noticeable sulfur isotope effect. To interpret the 372- and 428-cm^{-1} bands, Cys ligand deformations involving the C_α atom and amide NH group were suggested by Blair and co-workers (1985), but the assignments could not be established at that time. Our nitrogen isotope data along with the sulfur isotope data enable us to assign the four intense bands with considerably less ambiguity.

5.4.3.8 The Weak Bands at 348, 441, 456, 476, and 494 cm^{-1}

The low intensities of these bands indicate only weak coupling with the Cu-S(Cys) moiety. This group of bands shows no changes in band frequency or band intensity upon removal or replacement of either of the His ligands (Fig. 5.6). They are furthermore insensitive to Cu and sulfur isotope substitution. However, these bands show remarkable ^{15}N-isotope effects in ^{15}N-labeled azurin (Figure 5.5, Table 5.2). It is obvious that motion of the cysteine amide nitrogen contributes to these modes. As seen in Figure 5.2, the possible internal ligand coordinates are $\delta(C_\beta\text{-}C_\alpha\text{-}CO)$, $\delta(N\text{-}C_\alpha\text{-}CO)$, $\delta(C_\alpha\text{-}N\text{-}CO')$, and τ(N-H) (torsional motions with other atoms). Most of these vibrations involve the amide nitrogen to some extent, and may account for the large $^{14/15}$N isotope effects. The atoms in these modes are connected to the Cu-S bond through one or more intervening bonds and are farther away from the two His ligands. Therefore, these vibrations are not sensitive to $^{63/65}$Cu, $^{32/34}$S, or changes in the His ligand. All of the above bands, except the 348-cm^{-1} band, are located between 420 and 500 cm^{-1}, and their frequencies are higher than those of $\delta(Cu\text{-}S\text{-}C_\beta)$ and $\delta(S\text{-}C_\beta\text{-}C_\alpha)$ modes. The higher frequency of these bands could be explained as a result of the partial double bond character of the amide bonds in the protein and also as a result of the lighter atoms involved in the motions (Fig. 5.2).

5.4.3.9 The 267-cm^{-1} Band

The 267-cm^{-1} band is weak and broad. It does not originate from either of the two His ligands because it appears unchanged when either is removed by site-directed mutagenesis. It shows no isotope effects in H/D, $^{32/34}$S- , and $^{14/15}$N-labeled azurin.

Therefore, it is unlikely to be H-bond related, nor a vibrational mode involving cysteine sulfur or nitrogen. The 267-cm^{-1} band shifts to higher frequency when ^{63}Cu is substituted for ^{65}Cu (Table 5.2). The reason for this up-shift is not known, but it has been observed in both WT and H117G(Im) azurins. In considering the low frequency, this band is likely a torsional motion involving the Cu, C_α-H, and/or C_β-H moieties.

5.5 Deuterium Isotope Effects

All of the type 1 Cu proteins that have been investigated by RR spectroscopy show extensive spectral shifts when the proteins are equilibrated in D_2O (Nestor et al., 1984; Blair et al., 1985). In the case of azurin, almost every fundamental in the 200-500 cm^{-1} region shifts by -1 to -2 cm^{-1} in D_2O (Table 5.2). These isotope effects were originally attributed to the influence of the imidazole ligands on the RR spectrum. However, recent work has shown that neither His117 nor His46 contributes significantly to any modes other than the peak at 284 cm^{-1}. An alternative explanation of the D-isotope effect was that it was due to hydrogen bonding of the cysteine sulfur ligand to backbone amide NH groups (Figure 5.1), in which the strength of the hydrogen bond is different for NH versus ND (Mino et al., 1987). Support for this hypothesis came from the observation of D-isotope shifts of similar magnitude in iron-sulfur proteins where the crystal structures had also shown extensive H-bonding of S ligands (Mino et al., 1987). Such H-bonding could also explain why some peaks appeared to upshift rather than downshift or underwent intensity changes.

There are, however, several problems with the H-bonding hypothesis. One is that NMR studies of azurin (exchanged with D_2O in the same manner as our Raman samples) have failed to detect any indication of D-exchange in the amide NH's of Asn47 and Phe114 (van de Kamp et al., 1992). These are the residues that are H-bonded to the S of Cys112 in the X-ray crystal structure (Baker, 1988). Another problem is that according to the H-bonding hypothesis, the modes with the greatest Cu-S stretching character should undergo the largest shifts in D_2O. This is clearly not the case. The 408-cm^{-1} mode of azurin, which has the largest S-isotope dependence, has one of the smaller D-isotope dependencies (Table 5.2).

The overall pattern of D-shifts for azurin actually most closely resembles the

pattern of N-isotope shifts (Table 5.2). However, the D shifts are only about half as large as those in the ^{15}N-substituted protein. These findings would be consistent with the amide NH of the Cys ligand being responsible for both the ^{15}N- and D-isotope effects. Unfortunately, the Cys112 amide group also appears to be resistant to D-exchanges according to the NMR experiments (van de Kamp et al., 1992). If only partial D exchange were occurring, the D spectra should have exhibited more peak broadening and should have been more sensitive to the use of different pHs and protein samples (apo vs. Cu) for D exchange. We are left with the conclusion that the D-isotope effects may be due to small protein structural perturbations in D_2O that affect the conformation of the cysteinate ligand.

5.6 Conclusions

Studies of azurin through isotopic labeling and metal-site mutations have brought a new and more detailed understanding to the RR spectra of type 1 Cu sites. We conclude that the entire Cu-S(Cys) moiety, rather than Cu-His, is the essential contributor to the RR spectrum of type 1 Cu proteins. Newly proposed assignments of the RR bands of azurin are summarized in Table 5.4. Although most of the bands cannot be assigned precisely, we are able to give plausible explanations that are in agreement with our present data. Our results will further help the interpretation of RR spectra of other type 1 Cu proteins.

(1) The strongest Raman band (at 408 cm^{-1} in azurin) has the greatest Cu-S(Cys) bond character and is predominantly the Cu-S(Cys) stretch. The frequencies of this maximum-intensity band correlate with the Cu-S(Cys) bond distances, however, the latter lie outside of present-day crystallographic accuracy.

(2) A second set of intense RR bands is likely the result of angle bending motions, such as δ(Cu-S-C_β), δ(S-C_β-C_α), and δ(C_β-C_α-N). These modes gain their intensity by strong kinematic and vibronic coupling with ν[Cu-S(Cys)]. The coupling is promoted by the coplanar conformation of the Cu-S-C_β-C_α-N grouping. Because the frequencies are highly dependent on the dihedral angles of Cu-S-C_β-C_α and S-C_β-C_α-N, the relatively constant set of frequencies in all type 1 Cu proteins implies a strong conservation of the coplanar cysteine conformation.

(3) Only one weak band (at 284 cm^{-1} in azurin) can be ascribed to the Cu-N(His) interaction.

(4) The other weakly enhanced Raman bands are due to vibrations of Cys side chain atoms, including atoms as far away as the amide NH- and CO groups.

(5) This study clearly shows that the Cu-S(Cys) moiety is the key feature to a successful interpretation of type 1 Cu protein RR spectrum. However, a conclusive and complete assignment of all the bands still cannot be achieved with present data. Clearly, more experiments will be needed (see Chapter 6). Finally, a rigorous normal coordinate analysis for the entire site will have to be performed for the complete assignments of RR spectrum of type 1 Cu proteins.

References

Adman, E. T. (1991a) Adv. Protein Chemistry 42, 145-197.

Adman, E. T. (1991b) Current Opinion in Structural Biology 1, 895-904.

Adman, E. T., Stenkamp, R. E., Sieker, L. C., and Jensen, L. H. (1978) J. Mol. Biol. 123, 35-47.

Andrew, C. R., Han, J., Canters, G. W., den Blaauwen, T., Loehr, T. M., and Sanders-Loehr, J. (1993) unpublished results.

Ashikawa, I. and Itoh, K. (1979) Biopolymers 18, 1859-1876.

Backes, G., Mino, Y., Loehr, T. M., Meyer, T. E., Cusanovich, M. A., Sweeney, W. V., Adman, E. T., and Sanders-Loehr, J. (1991) J. Am. Chem. Soc. 113, 2055-2064.

Baker, E. N. (1988) J. Mol. Biol. 203, 1071-1095.

Baker, E. N., Anderson, B. F., Blackwell, K. E., Kingston, R. L., Norris, G. E., and Shepard, W. E. B. (1991) J. Inorg. Biochem. 43, 162.

Blair, D. F., Campbell, G. W., Schoonover, J. R., Chan, S. I., Gray, H. B., Malmstrom, B. G., Pecht, I., Swanson, B. I., Woodruff, W. H., Cho, W. K., English, A. M., Fry, H. A., Lum, V., and Norton, K. A. (1985) J. Am. Chem. Soc. 107, 5755-5766.

Caswell, D. S. and Spiro, T. G. (1986) J. Am. Chem. Soc. 108, 6470-6477.

Chang, T. K., Iverson, S. A., Rodrigues, C. G., Kiser, C. N., Lew, A. Y. C., Germanas, J. P., and Richards, J. H. (1991) Proc. Natl. Acad. Sci. USA 88, 1325-1329.

Colombo, L., Blekmann, P., Schrader, B., Schneider, R., and Plesser, T. (1974) J. Chem. Phys. 61, 3270.

Colthup, B. C., Daly, L. H., and Wiberley, S. E. (1980) Introduction to Infrared and Raman Spectroscopy, 3rd ed., Academic Press, New York.

Cornilsen, B. C. and Nakamoto, K. (1974) J. Inorg. Nucl. Chem. 36, 2467-.

Czernuszewicz, R. S., Le Gall, J., Moura, I., and Spiro, T. G. (1986) Inorg. Chem. 25, 696-700.

Dave, B. C., Germanas, J. P., and Czernuszewicz, R. S. (1993) J. Am. Chem Soc., submitted.

den Blaauwen, T. and Canters, G. W. (1993) J. Am. Chem. Soc. 115, 1121-1129.

den Blaauwen, T., Hoitink, C. W. G., Canters, G. W., Han, J., Loehr, T. M., and Sanders-Loehr, J. (1993) Biochemistry, submitted.

den Blaauwen, T., van de Kamp, M., and Canters, G. W. (1991) J. Am. Chem. Soc. 113, 5050-5052.

Fawcett, T. G., Bernarducci, E. E., Krogh-Jespersen, K. K., and Schugar, H. J. (1980) J. Am. Chem. Soc. 102, 2598-2604.

Garrett, T. P. J., Clingeleffer, D. J., Guss, J. M., Rogers, S. J., and Freeman, H. C. (1984) J. Biol. Chem. 259, 2822-2825.

Guss, J. M., Harrowell, P. R., Murata, M., Norris V. A., and Freeman, H. C. (1986) J. Mol. Biol. 192, 361-387.

Han, J., Adman, E. T., Beppu, T., Codd, R., Freeman, H. C., Huq, L., Loehr, T. M., and Sanders-Loehr, J. (1991) Biochemistry 30, 10904-10913. Chapter 4 in this work.

Han, J., Loehr, T. M., Lu, Y., Valentine, J. S., Averill, B. A., and Sanders-Loehr, J. (1993) J. Am. Chem. Soc. 115, 4256-4263. Chapter 5 in this work.

Han, S., Czernuszewicz, R. S., and Spiro, T. G. (1989) J. Am. Chem. Soc. 111, 3496-3504.

Hodgson, J. B., Percy, G. C., and Thornton, D. A. (1980) J. Mol. Struct. 66, 81-92.

Karlsson, B. G., Nordling, M., Pascher, T., Tsai, L.-C., Sjölin, L., and Lundberg, L. G. (1991) Protein Engineering, 4, 343-349.

Kitajima, N. (1993) Adv. Inorg. Chem. 39, 1-77

Kitajima, N., Fujisawa, K., and Moro-oka, Y. (1990) J. Am. Chem. Soc. 112, 3210-3212.

Kitajima, N., Fujisawa, K., Tanaka, M., and Moro-oka, Y. (1992) J. Am. Chem. Soc. 114, 9232-9233.

Larrabee, J. A. and Spiro, T. G. (1980) J. Am. Chem. Soc. 102, 4217-4223.

Larrabee, J. A., Spiro, T. G., Ferris, N. S., Woodruff, W. H., Maltese, W. A., and Kerr, M. S. (1977) J. Am. Chem. Soc. 99, 1979-1980.

Li, H., Wurrey, C. J., and Thomas, Jr. G. J. (1992) J. Am. Chem. Soc. 114, 7463-7469.

Loehr, T. M. and Sanders-Loehr, J. (1993) Methods Enzymol. 226, 431-470.

Lu, Y. (1992) Ph.D. Dissertation, University of California--Los Angeles.

Lu, Y., Lacroix, L. B., Lowery, M. D., Solomon, E. I., Bender, C. J., Peisach, J., Row, J. A., Gralla, E. G., and Valentine, J. S. (1993) J. Am. Chem. Soc. in press.

Magnus, K. A., Ton-That, H., and Carpenter, J. E. (1993) in Bioinorganic Chemistry of Copper (Karlin, K. D. and Tyeklar, Z., Eds.) pp 143-150, Chapman and Hall, New York.

Mino, Y., Loehr, T. M., Wada, K., Matsubara, H., and Sanders-Loehr, J. (1987) Biochemistry 26, 8059-8065.

Mizoguchi, T. J., Di Bilio, A. J., Gray, H. B., and Richards, J. H. (1992) J. Am. Chem. Soc., 114, 10076-10078.

Mohan, N., Müller, A., and Nakamoto, K. (1975) in Adv. in IR and Raman Spectroscopy, 1, 173-226.

Nakamoto, K., Shobatake, K., and Hutchinson, B. (1969) Chem. Commun. 1451.

Nar, H., Messerschmidt, A., Huber, R., van de Kamp, M., and Canters, G. W. (1991) J. Mol. Biol. 221, 765-772.

Nestor, L., Larrabee, J. A., Woolery, G., Reinhammar, B., and Spiro, T. G. (1984) Biochemistry 23, 1084-1093.

Nestor, L., Reinhammar, B., and Spiro, T. G. (1986) Biochim. Biophys. Acta 869, 286-292.

Parge, H. E., Hallewell, R. A., and Tainer, J. A. (1992) Proc. Natl. Acad. Sci. USA 89, 6109-6113.

Penfield, K. W., Gay, R. R., Himmelwright, R. S., Eickman, N. C., Norris, V. A., Freeman, H. C., and Solomon, E. I. (1981) J. Am. Chem. Soc. 103, 4382-4388.

Qiu, D., Kilpatrick, L., and Spiro, T. G. (1992) J. Inorg. Biochem. 47, 56; and personal communication.

Richardson, J. E., Thomas, K. A., Rubin, B. H., and Richardson, D. C. (1975) Proc. Natl. Acad. Sci. USA 72, 1349-1353.

Romero, A., Hoitink, C. W. G., Nar, H., Huber, R., Messerschmidt, A., and Canters, G. W. (1993) J. Mol. Biol., in press.

Sanders-Loehr, J. (1989) in Iron Carriers and Iron Proteins (Loehr, T. M., Ed.) pp 373-466, VCH, New York.

Shaanan, B., (1982) Nature, 296, 683-684.

Susi, H., Byler, D. M., and Gerasimowicz, W. V. (1983) J. Mol. Struc. 102, 63-79.

Sykes, A. G. (1991) in Adv. Inorg. Chem. 36, 377-408.

Tainer, J. A., Getzoff, E. D., Beem, K. M., Richardson, J. S., and Richardson, D. C. (1982) J. Mol. Biol. 160, 181-217.

Teraoka, J., and Kitagawa, T. (1981) J. Biol. Chem. 256, 3969-3977.

Thamann, T. J., Frank P., Willis, L. J., and Loehr, T. M. (1982) Proc. Natl. Acad. Sci. USA 79, 6396-6400.

Tsuboi, M., Nishimura, Y., Hirakawa, A. Y. and Peticolas, W. L. (1987) in Biological Applications of Raman Spectroscopy (Spiro, T. G., Ed.) Vol 2, pp 181-209, Wiley, New York.

van de Kamp, M., Canters, G. W., Wijmenga, S. S., Lommen, A., Hilbers, C. W., Nar, H., Messerschmidt, A., and Huber, R. (1992) Biochemistry 31, 10194-10207.

van de Kamp, M., Hali, F. C., Rosato, N., Finazzi-Agro, A., and Canters, G. W. (1990) Biochim. Biophys. Acta 1019, 283-292.

Volbeda, A. and Hol, W. G. J. (1988) Prog. Clin. Biol. Res. 274, 291-308.

Table 5.1. Resonance Raman Spectra of WT and Mutant Azurins[a]

Sample	Frequency (cm^{-1})											
WT	267	284		348	372	400	408	428	441	456	476	494
H117G(Im)	266	281		348	372	400	408	429	441	456	478	494
H117G(2-MeIm)	265	283		347	373	400	406	429	443	455	477	495
H117G(4-MeIm)	259			349	373	400	407	429	443	455	477	494
H117G(N-MeIm)	259		304	347	368/374	400	408	429	441	455	478	494
H117G(N-polyvinylIm)	267	283		348	372	400	407	429		455	477	494
H117G(N_3^-)	260		305	346	362	389	402	428	440	455	478	493
H117G(H_2O)	260		302	345	367	397	406	428	442	455	477	493
H46D[b]	267	281	300	326/337	376	399	410	426	438	453	472	493

[a]RR spectra for all species were obtained with 647.1-nm excitation (as in Fig. 5.4). [b]Data of Dave et al. (1993).

Table 5.2. Isotope Shifts of RR Frequencies in WT and Mutant Azurins from *P. aeruginosa*[a]

RR mode[b]	$^{63/65}$Cu		$^{14/15}$N	H/D			$^{32/34}$S
	H117G(Im)	WT[c]	WT	WT[c]	WT[d]	H117G(Im)	WT[e]
267	+0.5	+1	0	0	0	-1	0
284	-1.5	~0	-2	-5	-2	+2	0
348	0	~0	-2.5	-2	0	0	0
372	-0.5	-0.6	-0.9	-0.9	-1	-1	0
400	~0	-0.6	-2.7		-2	-2	0
408	-0.6	-0.6	-1.4	-1	-1	-1	-4
428	(-0.3)	(-0.2)	-3.8	-1.2	-1.5	-2.5	-2
441	(-0.4)	n.d.	-3	-1.5	-1.8	-2	0
456	0	0	-2.6	0	-0.7	-1	0

(continued)

Table 5.2, continued:

RR mode[b]	$^{63/65}$Cu		$^{14/15}$N	H/D			$^{32/34}$S
	H117G(Im)	WT[c]	WT	WT[c]	WT[d]	H117G(Im)	WT[e]
476	0	0	-2.8	-1.0	-1.5	-3	0
494	0	0	(-0.4)	+1.3	0	-2	0

[a]Frequency shift in cm^{-1} from lighter mass to heavier mass. Values in parentheses are within the experimental error of ± 0.5 cm^{-1}. [b]Value for WT azurin. [c]Shifts reported by Blair et al. (1985). [d]This work. [e]Shifts reported by Dave et al. (1993) for cells grown on ^{32}S or ^{34}S labeled Na_2SO_4.

Table 5.3. Calculated Isotope Shifts for the Stretching Mode of a Two-Atom Oscillator Using a Localized Point Mass Approximation[a]

Oscillator[b]	Isotope Shift ($\Delta\nu$) at Different Frequencies (ν)		
	284 cm^{-1}	408 cm^{-1}	428 cm^{-1}
$^{63/65}$Cu-N	-0.8	-1.1	-1.2
$^{63/65}$Cu-ImH	-2.3	-3.3	-3.4
Cu-$^{14/15}$N	-7.9	-11.3	-11.9
Cu-$^{14/15}$N-ImH	-2.0	-2.8	-3.0
Cu-ImH/D	-1.0	-1.4	-1.5
Cu-Im/MeIm	-12	-17	-18
$^{63/65}$Cu-S	-1.5	-2.1	-2.2
Cu-$^{32/34}$S	-5.6	-8.1	-8.5
Cu-$^{32/34}SCH_2^-$	-3.5	-5.0	-5.2

[a]ν and ν^* correspond to vibrational frequencies of light and heavy isotopes, respectively. $\Delta\nu = \nu^* - \nu$ calculated based on ν and $\nu/\nu^* = (\mu^*/\mu)^{1/2}$ where $\mu = (m_a \times m_b)/(m_a + m_b)$. In the point mass approximation, an entire moiety (e.g., imidazole ring) is assumed to behave as a single oscillator (e.g., mass of 68).

[b]The two masses yielding an isotope shift are separated by a slash mark. Isotopic substitutions for ImH were calculated assuming two exchangeable N's, but only one exchangeable H.

Table 5.4. Raman Fundamental Vibrations and Proposed Assignments for Cysteine, 1-Propanethiol, and Azurin

L-cysteine[a]		1-propanethiol[b]		WT azurin[c]	
$\nu(cm^{-1})$	Assignment	$\nu(cm^{-1})$	Assignment	$\nu(cm^{-1})$	Assignment
691	$\nu(S\text{-}C_\beta)$	650	$\nu(S\text{-}C)$	750	$\nu(S\text{-}C_\beta)$
498	$\tau(N\text{-}H_3)$			494	$\tau(N\text{-}H)$
				476	$S(C_\alpha\text{-}N\text{-}CO')$
				456	$\delta(C_\beta\text{-}C_\alpha\text{-}CO)$
441	$\delta(C_\beta\text{-}C_\alpha\text{-}N)$	413	$\delta(C\text{-}C\text{-}C)$	441	$\delta(N\text{-}C_\alpha\text{-}CO)$
364	$\delta(C_\beta\text{-}C_\alpha\text{-}CO)$			428	$\delta(S\text{-}C_\beta\text{-}C_\alpha)$
298	$\tau(C\text{-}S\text{-}H)$	284	$\delta(S\text{-}C\text{-}C)$	408	$\nu(Cu\text{-}S)$
268	$\delta N\text{-}(C_\alpha\text{-}CO)$	240	$\tau(C\text{-}H_{3)}$	400	$\delta(C_\beta\text{-}C_\alpha\text{-}N)$
				372	$\delta(Cu\text{-}S\text{-}C_\beta)$

(continued)

Table 5.4, continued:

L-cysteine[a]		1-propanethiol[b]		WT azurin[c]	
$\nu(cm^{-1})$	Assignment	$\nu(cm^{-1})$	Assignment	$\nu(cm^{-1})$	Assignment
210	$\tau(COO^-)$	190	τ(C-S)	348	
148	$\tau(COO^-)$	137	τ(C-C)	284	ν(Cu-N)(His117)
118	$\delta(S\text{-}C_\beta\text{-}C_\alpha)$			267	[$\tau(Cu\text{-}S\text{-}C_\beta\text{-}H_2)$]

[a]Data from Susi et al. (1983). ν, δ, and τ donote stretching, bending, and torsion, respectively. [b] Data from Li et al. 1992). [c]Data and proposed assignments from this work. Assignments in brackets are more tentative.

FIGURE LEGENDS

Figure 5.1. Type 1 Cu site of *P. aeruginosa* azurin. The Cu is coordinated by His117(N), His46(N), and Cys112(S) and sits close to the SNN trigonal plane. The His117 ring is nearly co-planar to the SNN plane. The His46 ring is nearly perpendicular to the SNN plane. H-bonds to Cu ligands are indicated by --- . Figure provided by Dr. E. N. Baker for *A. denitrificans* azurin.

Figure 5.2. (A) Structure of the Cu-Cys moiety of the type 1 Cu site (adapted from Nestor et al., 1984). (B) Diagram showing the coplanarity of Cys ligand. The planes containing Cu-S-C_b, S-C_b-C_a, and C_b-C_a-N are all congruent with one another. Thus, the dihedral angles for Cu-S-C_b-C_a and S-C_b-C_a-N are both close to 180° (Han et al., 1991). The amide bond of the Cys has partial double bond character.

Figure 5.3. Structural formulas of Cu-site ligands for WT azurin (His) and the H117G mutant (Im, 2-MeIm, N-MeIm, or 4-MeIm).

Figure 5.4. Resonance Raman spectra of *P. aeruginosa* azurin. (A) Wild-type azurin (—) and azurin H117G(Im) (---). (B) ^{63}Cu (—) and ^{65}Cu (---) labeled azurin H117G(Im). (C) ^{14}N (—) and ^{15}N (---) labeled wild-type azurin. Spectra were obtained from ~2 mM protein in 20 mM MES (pH 6.0) at 15 K using 647.1 nm excitation (70-100 mW) with a resolution of 5 cm^{-1}, scan rate of 0.5 cm^{-1}/s, and accumulation of 4-9 scans. Listed frequencies are for WT azurin.

Figure 5.5. Isotope shifts in the resonance Raman spectra of WT and mutant azurins. Data are from Table 5.2. Positive shifts and shifts less than 0.5 cm^{-1} have been omitted.

Figure 5.6. Resonance Raman spectra of mutant azurins. (A) WT azurin. (B) H117G(H_2O). (C) H117G(2-MeIm). (D) H117G(N-MeIm). (E) His46Asp azurin (data from Dave et al., 1993). Spectral conditions for A-D are the same as Figure 5.4.

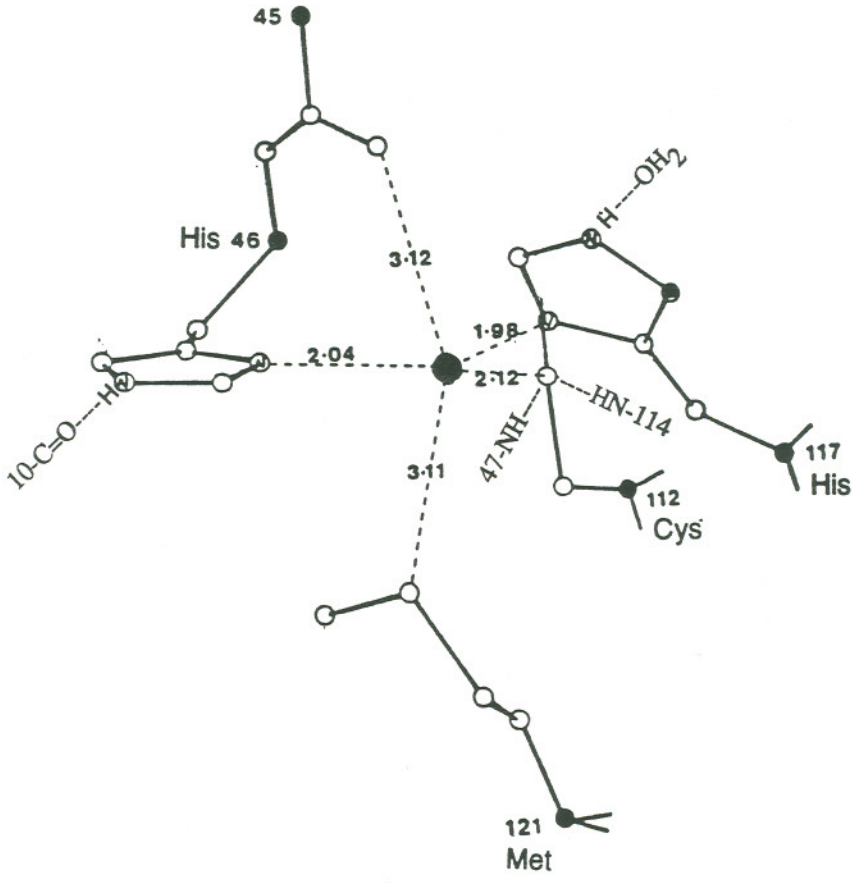
45
His 46
3·12
1·98
2·04
2·12
3·11
10-C=O---H
47-NH
HN-114
117
His
112
Cys
121
Met

Figure 5.1

A

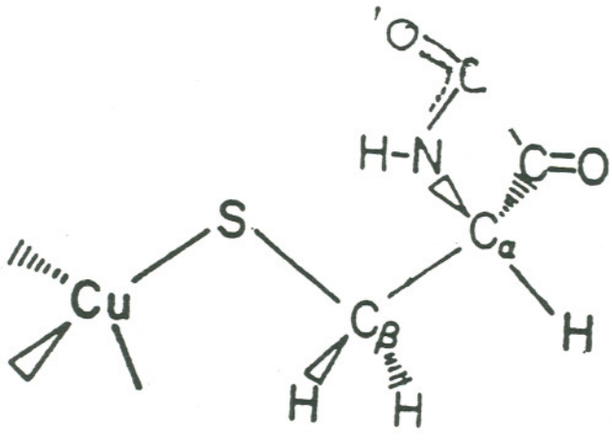

B

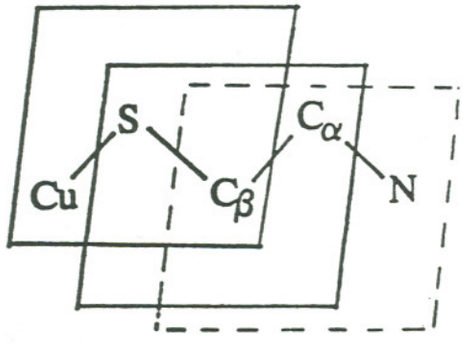

Figure 5.2

Cu-His

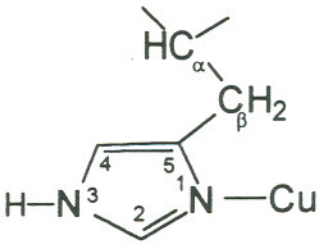

Cu-Im

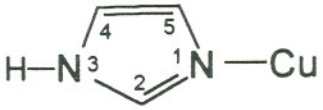

Cu-2-MeIm

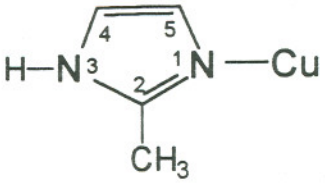

Cu-N-MeIm

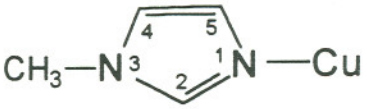

Cu-4-MeIm

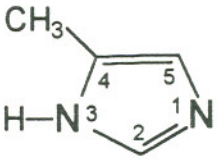

Figure 5.3

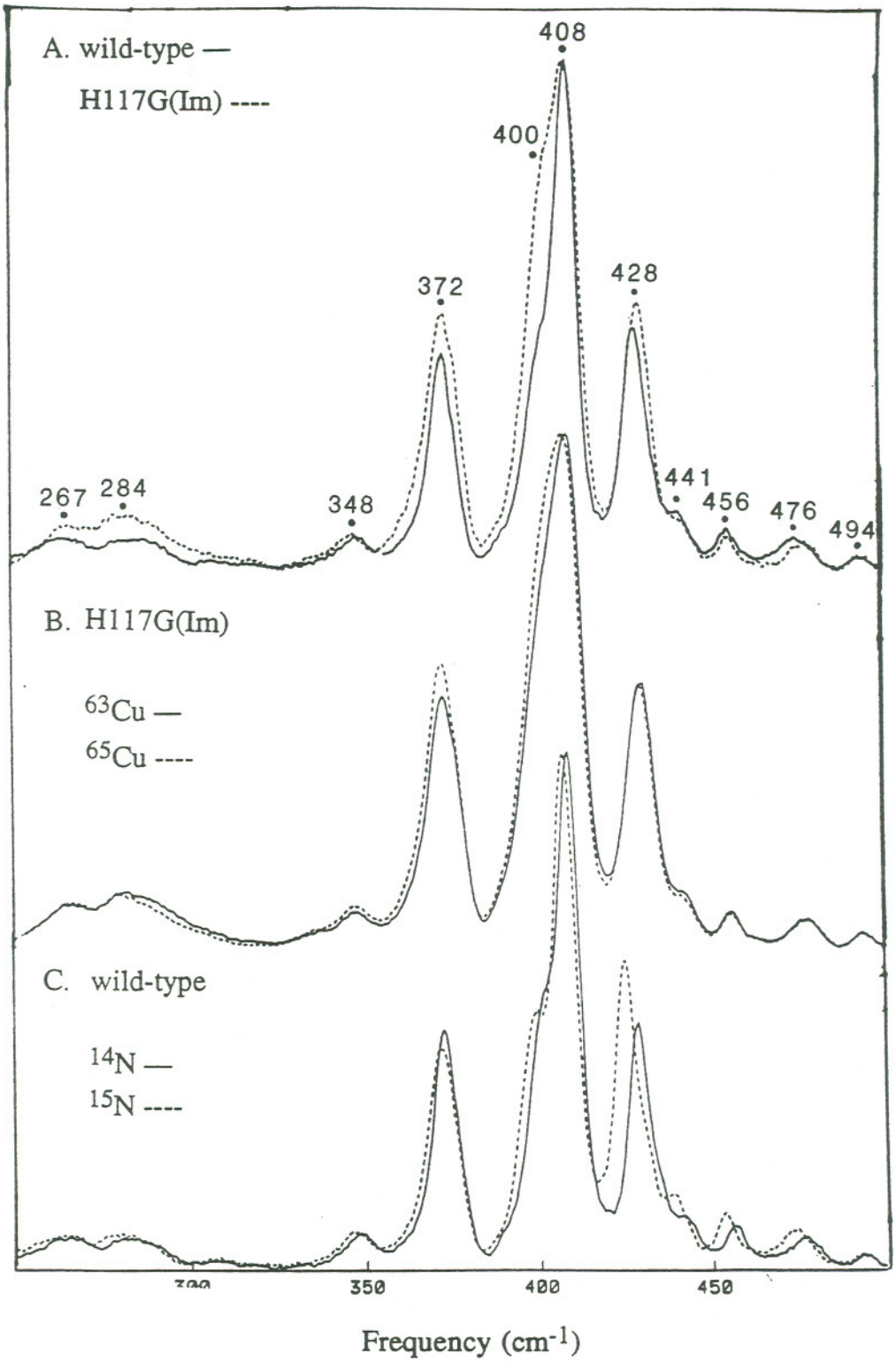
A. wild-type —
H117G(Im) ----
408
400
372
428
267
284
348
441
456
476
494
B. H117G(Im)
63Cu —
65Cu ----
C. wild-type
14N —
15N ----
350
400
450
Frequency (cm-1)

Figure 5.4

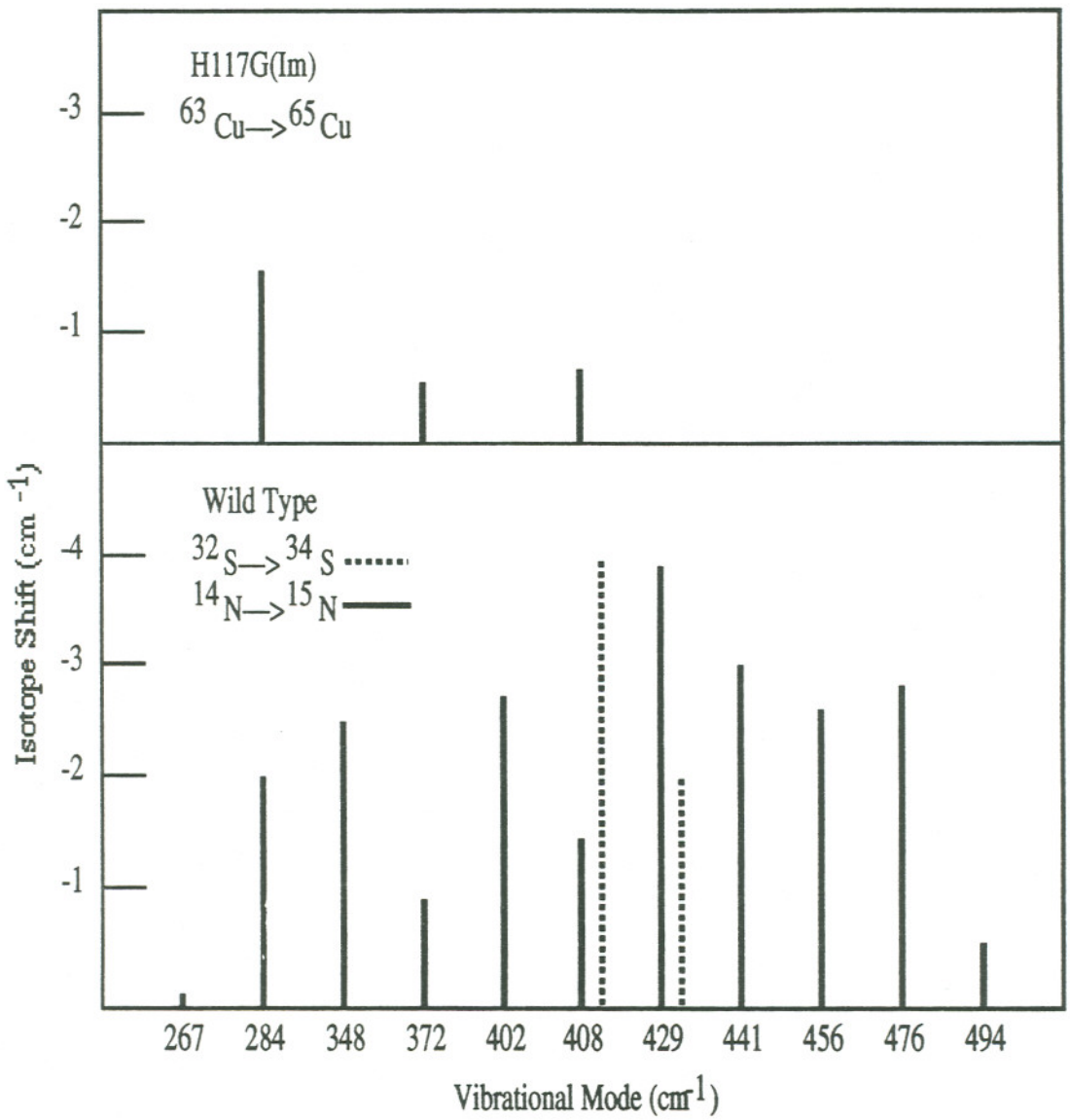
H117G(Im)
63 Cu—>65 Cu
-3
-2
-1
Wild Type
32 S—> 34 S
14 N—> 15 N
-4
-3
-2
-1
Isotope Shift (cm -1)
267
284
348
372
402
408
429
441
456
476
494
Vibrational Mode (cm-1)

Figure 5.5

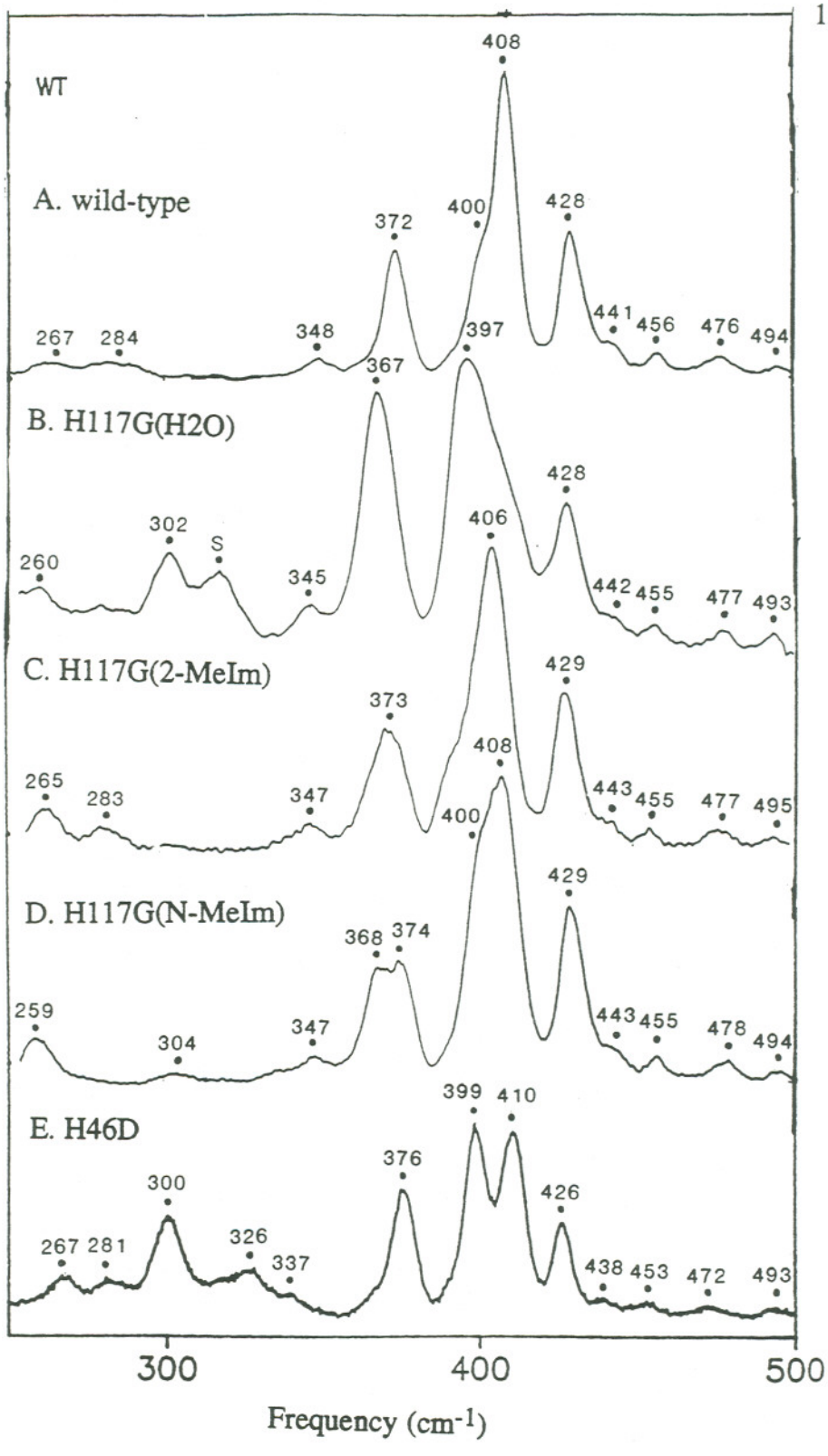
WT
A. wild-type
408
372
400
428
267
284
348
397
441
456
476
494
B. H117G(H2O)
367
428
302
S
406
260
345
442
455
477
493
C. H117G(2-MeIm)
429
373
408
265
283
347
400
443
455
477
495
D. H117G(N-MeIm)
429
368
374
259
304
347
443
455
478
494
E. H46D
399
410
376
300
426
267
281
326
337
438
453
472
493
300
400
500
Frequency (cm-1)

Figure 5.6

Chapter 6

FUTURE DIRECTIONS

Type 1 Cu proteins are electron transfer proteins with molecular weights of 12,000-15,000 Da. These relatively small Cu proteins are widely studied and are well characterized structurally and spectroscopically. The physical properties of type 1 Cu proteins are briefly reviewed in Chapter 1. In addition, a comparison of type 1 and type 2 Cu proteins is addressed in order to clarify the unusual character of type 1 Cu sites. Resonance Raman spectral studies of type 1 Cu proteins formed the major part of this research, and they are presented and discussed in Chapters 2, 3, 4, and 5. We believe that the structural basis for understanding the RR spectra of type 1 Cu proteins has been greatly enhanced by these studies.

There are still many unanswered questions about type 1 Cu proteins. For example, knowledge of factors influencing the redox potential of type 1 Cu protein is very limited. Also, the origin of the $\sim$460 nm absorption band is an unsettled issue. Finally, although the RR spectra of type 1 Cu proteins are well studied, the complete assignments of the Raman bands will require a large amount of future work. Moreover, despite the common properties found among type 1 Cu proteins, understanding the special characteristics of individual proteins, such as stellacyanin and nitrite reductase, would certainly enrich our understanding of type 1 Cu proteins.

6.1 Redox Potentials of Type 1 Cu Proteins

A systematic study of the redox potentials of type 1 Cu proteins is a challenging task. Despite the fact that all type 1 Cu proteins are known to have a common Cu site with three strong ligands, S(Cys), N(His), and N(His), the redox potentials of these proteins are surprisingly different, ranging from 180 mV in stellacyanin to 680 mV in rusticyanin (Adman, 1985). In contrast to most of the other type 1 Cu proteins,

stellacyanin does not have Met at the axial position. Instead, an amide carbonyl group is suspected as a ligand at the axial position (Thomann et al., 1991). EPR studies indicate that stellacyanin has a rhombic Cu site (Chapter 4), which may be due to a strong interaction with -CO. It seems that even though the Met ligand is not a structural prerequisite of the type 1 Cu site, it may be important in determining the E° value (Gray and Malmström, 1983).

However, very little is known about the E° properties of type 1 Cu proteins. Many factors can influence E° such as the Cu site ligands, Cu site geometry, the effective charge on Cu, the environment of Cu, hydrogen bonds near the Cu site, and the effect of pH. For example, when Met121 is replaced with Leu in azurin, the redox potential increases by 100 mV. This again shows the sensitivity of E° to the axial Met ligand. The increase of E° value has been explained due to placement of a hydrophobic residue near the Cu center (Pascher et al., 1993). Another example is the pseudoazurin mutant Pro80Ala. After the replacement of Pro80 with Ala, the E° increased by 130 mV (Nishiyama et al., 1992). One noticeable structural change is that the space that used to be occupied by the Pro80 side chain is now filled by a water molecule. Normally, the neutral $(Cu^{+1})(S^{-})$ species should be favored by a more hydrophobic environment and the more charged $(Cu^{+2})(S^{-})$ species should be favored by a more polar environment (Pascher et al., 1993). However, a +139 mV increase favors the Cu(I) form over the oxidized Cu(II) form, so the observed change in the Pro80Ala mutant cannot be so readily explained.

Table 6.1 lists known E° values and the EPR spectral rhombicity of type 1 Cu proteins and mutants. As we can see, there is no correlation between E° and the rhombicity of the EPR spectrum. It seems that other factors must be controlling the E° value of type 1 Cu proteins. Study of protein redox properties is a complicated subject and the inaccuracy in the determination of E° makes it difficult to compare E° values from different studies. Nevertheless, a systematic study of E° will be important in understanding the relationship between E° and protein structure, and will eventually help to explain the electron transfer efficiency of each protein.

6.2 Absorption Spectra of Type 1 Cu Proteins

6.2.1 Assignment of the ~460 nm Band

Type 1 Cu proteins have an intense absorption at ~600 nm and another absorption band at ~460 nm. The intensity of the ~460 nm is variable depending on proteins, but the sum of ϵ_{460} and ϵ_{600} appears to be fairly constant. Our RR intensity studies of four proteins (pseudoazurin, azurin, nitrite reductase, and SOD zinc site mutant His80Cys) concluded that both the ~460- and ~600-nm bands have predominantly S(Cys) to Cu CT character (Chapter 4). However, absorption spectral studies on nitrite reductase and plastocyanin suggest that the ~460-nm band is due to a His → Cu CT transition (Lu et al., 1993, Gewirth and Solomon, 1988). A second (Cys)S → Cu CT transition is assigned at ~530 nm, which is neither resolved in the absorption spectra nor detected by RR excitation profiles (RREP) of any of the type 1 Cu proteins we studied. As shown in Figure 4.2, the resonance Raman excitation profiles for pseudoazurin does peak on the low energy side of the absorption maximum which could mean there is another transition at 530 nm. It is also possible that the ~460-nm band has both His → Cu and Cys → Cu CT transition components. Further studies are necessary to clarify the assignment of the ~460-nm absorption band.

Nitrite reductase would be a good candidate for the purpose of addressing the origin of the ~460 nm band. NiR has a refined crystal structure. Therefore, a complete absorption spectral study on a single crystal sample, as was done for plastocyanin, is possible. The other important reason for choosing NiR is that its ~460-nm band is stronger than its ~600-nm band (Figure 4.4). The RREP of NiR exhibits strong enhancement by the ~460 nm band and a fairly symmetrical band shape, indicative of a single component under the ~460 nm absorption envelope. Therefore, using NiR, we may have a better chance to unambiguously assign the ~460-nm transition.

So far, the assignment of the absorption spectra of type 1 Cu proteins is largely based on the study on Xα calculations for plastocyanin (Gewirth and Solomon, 1988; Solomon et al., 1992). One concern is whether the results fit all other type 1 Cu proteins. We have noticed that the relative intensities of ~460 and ~600 nm bands are quite different among type 1 Cu proteins. A more intense ~460 nm band seems correlated with the high rhombicity of the Cu site, as is the case for NiR (Chapter 4).

How this intensity change relates to the Cu-S(Cys) bonding properties (the π- and σ-bond interactions) deserves further investigation.

6.2.2 Type 1 vs. Type 2 Cu Proteins

According to Solomon et al. (1992), type 1 Cu has strong π and weak σ interactions in the Cu-S(Cys) bond. As a result, type 1 Cu has an intense S(Cys) → Cu CT transition at ~600 nm. In contrast, type 2 Cu complexes supposedly have a strong σ interaction of the Cu-ligand bond, and the LMCT band is usually at higher energy, near 400 nm. Our RR studies on SOD mutants indicate that the differences between type 1 and type 2 relate more to geometry than to differences in Cu-S(Cys) bond length (Andrew et al., 1993). Thus, more theoretical calculations are needed to see if such changes in geometry can account for the observed spectral changes.

6.3 Assignment of RR Spectra of Type 1 Cu Proteins

The assignment of the RR spectrum of azurin is discussed in Chapter 5. Among the 11 observed Raman modes in the 200-500 cm^{-1} region, the most intense band at 408 cm^{-1} is assigned predominantly to the Cu-S(Cys) stretch, and the band at 284 cm^{-1} is due to the Cu-N(His117) stretch. The rest of the bands are due to Cys ligand internal deformation modes. These Cys internal vibrations are coupled with the Cu-S(Cys) stretch and the coplanar conformation of the Cys side chain atoms is important for the enhancement of Cys internal modes. A more definitive assignment of these Cys internal modes requires further spectral information. Selective labeling of the Cys ligand with different isotopes could provide the needed information.

6.3.1 RR Study of ^{13}C- or D-Labeled Wild Type Azurin

So far, we have studied the isotope effect of $^{63/65}Cu$, $^{32/34}S$, $^{14/15}N$-NH_4^+, and H_2O/D_2O on wild type azurin. From Figure 5.2A, we can see that the carbon and hydrogen are the two kinds of atoms remaining to be studied. The remaining carbon atoms of the cysteine group are C_β, C_α, CO, and CO′. These carbon atoms are important members of Cys side chain and participate in the vibrations of free Cys as seen in Table 5.4. Therefore, a RR spectral study of ^{13}C-labeled azurin would be a valuable experiment. We assume that the protein can grow in the condition where high purity ^{13}C is the only carbon source and the protein structure is not affected by the heavy isotope.

This experiment seems achievable since ^{15}N-labeled azurin has been obtained successfully. With the $^{12/13}C$-isotope information, we may be able to identify whether particular Cys ligand modes involve carbon atom vibrations. Since hydrogens of the C-H group are generally not exchangeable in H_2O/D_2O experiment, study of azurin grown in D_2O seems necessary. The H/D isotope effects will help identify the torsional modes involving hydrogen in the 200- to 500-cm^{-1} region.

6.3.2 RR Study of Cys Related Mutants

Studies of isotopically labeled wild-type azurin, as mentioned above, may not lead to the final assignment. For example, it may still be difficult to distinguish $\delta(C_\alpha\text{-N-CO}')$ and $\delta(C_\beta\text{-}C_\alpha\text{-CO})$ modes shown in Table 5.4 because, in the ^{13}C-labeled experiment, all carbon atoms are labeled at the same time. Studies of specifically labeled Cys ligands seems to be the only way to assign each of the observed bands to a particular Cys vibration. In other words, we need to label one atom at a time such as $^{13}C_\beta$-Cys or $^{13}C_\alpha$-Cys. However, it may be very difficult to achieve this goal with WT azurin. Such isotopically labeled amino acids are quite expensive and they require use of an auxotrophic mutant which can no longer synthesize that particular amino acid. A preferable alternative would be to add labeled Cys to a mutant which lacks the Cys ligand.

In azurin, among the three ligands Cys112, His117, and His46, both His ligands have been mutated. Stable mutants His117Gly, His46Asp, and His46Gly have been obtained, and show type 1 Cu properties in the presence of appropriate exogenous ligands (den Blaauwen et al., 1991; Chang et al., 1991; Canters, 1993). However, mutation of the Cys112 ligand has failed to maintain the type 1 Cu site. Upon replacement of Cys112 with Asp, a type 2 Cu site has been obtained (Mizoguchi et al., 1992). Apparently, Asp binds to Cu as a bidentate ligand and the Cu site geometry changes to square planar. All other amino acid substitutions at this site, such as Cys112Ser and Cys112Gly, result in a protein that no longer binds Cu (Mizoguchi et al., 1992; Canters, 1993). These results demonstrate that the Cys ligand is absolutely essential to the type 1 Cu site. It seems highly worthwhile to attempt to regenerate a type 1 Cu site in Cys mutants by addition of copper and thiolates, as detailed below.

6.3.2.1 Cys112Gly + Labeled SR

It may be possible to find conditions to stabilize Cu binding by adding exogenous thiolate. This could result in either a type 1 or a type 2 site. Since both types of Cu-Cys sites show resonance-enhanced ligand modes, either would be of interest to study with labeled ligands. A ligand such as CH_3CH_2SH or $CH_3(CH_2)_2SH$ would actually be preferable to Cys because there would be less competition from the α-NH_2 or α-COO^- groups which can also serve as ligands.

6.3.2.2 Cys112His/Met121End + Labeled Cys

In this experiment, we first make the double mutant Cys112His/Met121End. Replacing Cys112 with His, we expect that the His could take the Cys position in the Cu site. The possibility of using three His-like ligands to generate a type 1 Cu site has been demonstrated in Kitajima's tris(pyrazolyl borate) model compounds (Kitajima et al., 1990, 1992). When exogenous thiolate is added, a type 1 Cu complex is obtained. The second mutation at Met121 position aims at the addition of isotopically labeled Cys back to the Cu site. The M121End mutant of azurin was created by inserting a stop codon in place of the Met codon at position 121 so that the protein terminates at residue 120 (Karlsson et al., 1991). The resultant mutant has type 1 Cu properties with only small changes in the absorption and EPR spectra. However, the copper/protein ratio of 0.19 in Met121End is lower than the value of 0.51 for the wild type protein. Since the Met121 site is quite flexible and can accommodate 18 different amino acid side chains (Karlsson et al., 1991), it is possible that it will be able to bind exogenous Cys. Although the properties of Met121Cys were not significantly different from WT azurin, this form still possesses the primary Cys112 ligand. In the proposed experiments, C112H/M121End would have three imidazole ligands and addition of an exogenous thiolate will be investigated. One possible ligand for such studies would be N-acetylcysteineamide where the α-amino and α-carboxyl groups have amide substituents similar to a polypeptide backbone.

6.3.3 RR Study of R_6-Insulin + Exogenous Cys

Insulin is one of the few proteins which can model a type 1 Cu protein (Brader and Dunn, 1991). The insulin monomer is a hormone. It aggregates into R_6 hexamers in the presence of phenol. Each hexamer chelates 2 metal ions such as Zn(II), Co(II),

or Cu(II). The crystal structure of $R_6Zn_6Cl_2$ shows two tetrahedral Zn sites (Fig. 6.1). The metal is bonded by three histidines (one histidine from each monomer at position 10 on an α-helix), and the tetrahedral geometry is dictated by the position of these three His ligands.

In Cu(II)-substituted insulin R_6, a type 1 Cu site was formed by incorporation of one exogenous thiolate ligand, e.g., pentafluorothiophenol (PFTP) (Brader and Dunn, 1990; Brader et al., 1992a, 1992b). The Cu(II)-R_6-PFTP complex has an absorption spectrum similar to that of the type 1 Cu protein with a strong band at 626 nm (ϵ = 2,000 M^{-1} cm^{-1}). The EPR spectrum of the complex exhibits a small hyperfine coupling constant of 80 $\times$ 10^{-4} cm^{-1}, similar to that of type 1 Cu protein. The RR spectrum of the complex shows multiple bands near 400 cm^{-1} and one isolated band at 213 cm^{-1} (Brader et al., 1992b). This RR spectrum is also similar to that of a type 1 Cu protein. All of these results suggest that Cu(II)-R_6 insulin is a good model for the study of type 1 Cu proteins.

The goal is to form a type 1 Cu site by adding Cys or modified Cys to Cu(II)-R_6 insulin. There has been no report using Cys in the Cu(II)-R_6 insulin system. The Cu(II)-R_6-Cys complex may not be as stable as that of Cu(II)-R6-PFTP. The latter complex gradually reduced to the Cu(I) form in a period of approximately 30 h. We could stabilize such a complex by freezing and collecting RR spectra at 15 K. Cu(II)-R_6 insulin is a better model system than small molecular compounds because the Cu(II) is in a protein environment and the system is much more stable. Its advantage compared to azurin mutants is that it appears to be capable of accommodating a variety of bulky thiolate ligands.

6.3.4 Normal Coordinate Analysis

After sufficient structural and spectral information is gathered, a rigorous normal coordinate analysis (NCA) will be the final task in the assignment of the RR spectrum of type 1 Cu proteins. At this moment, it is clear that the model used in NCA should include the Cys side-chain atoms extending as far as the amide nitrogen, and possibly the two carbonyl groups. Two His ligands of the Cu should also be included in the NCA. Since there is no evidence of imidazole ring modes in the RR spectrum, we can treat each His as a single entity with an effective mass of 68. It seems safe to exclude the

Met ligand, but H bonds to the S of the Cys probably should be included. Whether the model should include other atoms besides the first coordination sphere of the Cu and how far this sphere should extend are not clear at this point.

Urushiyama and Tobari (1990) performed NCA for the crystallographically defined type 1 Cu proteins azurin and plastocyanin. A model was constructed using 169 atoms around the Cu site. A mass-group approximation was employed for CH, CH_2, CH_3, NH, and NH_2 groups throughout. No isotope data were included. The NCA results showed extensive coupling of the Cu-S(Cys) stretching coordinate with bending coordinates, such as δ(C-C-C), δ(C-C-N), and δ(C-N-C) which were apparently widely distributed throughout the molecule. But their study also showed that coupling of the Cu-S(Cys) stretch with His and Cys side chain coordinates was small. This is surprising because the coupling of the Cu-S(Cys) stretch with motions of nearby atoms is expected to be strong. Also, the contribution of the hydrogen atom to the RR spectrum was ignored in this NCA due to the mass group approximation. This study did demonstrate the feasibility of performing NCA with a very large number of atoms. It also shows that NCA alone cannot tell whether one has picked the correct atoms for the calculation. The best way of deciding which interpretation is correct will be through the use of isotopically labeled Cys.

References

Adman, E. T. (1985) in Metalloproteins (Harrison, P., ed.) Part I, pp 2-42, Verlag Chemie, Weinheim, FRG.

Andrew, C. R, Han, J., Yeom, H., Loehr, T. M., Sanders-Loehr, J., and Valentine, J. S. (1993) Manuscript in preparation.

Brader, M. L., and Dunn, M. F. (1990) J. Am. Chem. Soc. 112, 4585-4587.

Brader, M. L., and Dunn, M. F. (1991) Trends Biochem. Sci. 16, 341-345.

Brader, M. L., Borchardt, D., and Dunn, M. F. (1992a) Biochemistry 31, 4691-4696.

Brader, M. L., Borchardt, D., and Dunn, M. F. (1992b) J. Am. Chem. Soc. 114, 4480-4486.

Canters, G. W. (1993), personal communication.

Chang, T. K., Iverson, S. A., Rodrigues, C. G., Kiser, C. N., Lew, A. Y. C., Germanas, J. P., and Richards, J. H. (1991) Proc. Natl. Acad. Sci. USA 88, 1325-1329.

den Blaauwen, T., van de Kamp, M., and Canters, G. W. (1991) J. Am. Chem. Soc. 113, 5050-5052.

Gewirth, A. A., and Solomon, E. I. (1988) J. Am. Chem. Soc. 110, 3811-3819.

Gray, H. B. and Malmström, B. G. (1983) Comments Inorg. Chem. 2, 203-208.

Gray, K. A., Davidson, V. L., and Knaff, D. B. (1988) J. Biol. Chem. 263, 13987-13990.

Karlsson, B. G., Nordling, M. Pascher, T., Tsai, Li-Chu., Sjölin, L., and Lundberg, L. G. (1991) Protein Eng. 4, 343-349.

Kitajima, N., Fujisawa, K., and Moro-oka, Y. (1990) J. Am. Chem. Soc. 112, 3210-3212.

Kitajima, N., Fujisawa, K., Tanaka, M., and Moro-oka, Y. (1992) J. Am. Chem. Soc. 114, 9232-9233.

Lu, Y., Lacroix, L. B., Lowery, M. D., Solomon, E. I., Bender, C. J., Peisach, J., Row, J. A., Gralla, E. G., and Valentine, J. S. (1993) manuscript submitted.

Mizoguchi, T. J., DiBilio, A. J., Gray, H. B., and Richards, J. H. (1992) J. Am. Chem. Soc. 114, 10076-10078.

Nishiyama, N., Suzuki, J., Ohnuki, T., Chang, H.-C., Horinouchi, S., Turley, S., Adman, E. T., and Beppu, T. (1992) Protein Eng. 5, 177.

Pascher, T., Karlsson, B. G., Nordling, M., Malmström, B. G., and Vänngård, T. (1993) Eur. J. Biochem. 555, 1-8.

Solomon, E. I., Baldwin, M. J., and Lowery, M. D. (1992) Chem. Rev. 92, 521-542.

Thomann, H., Bernardo, M., Baldwin, M. J., Lowery, M. D., and Solomon, E. I. (1991) J. Am. Chem. Soc. 113, 5911-5913.

Urushiyama, A., and Tobari, J. (1990) Bull. Chem. Soc. Jpn. 63, 1563-1571.

Table 6.1. Redox Potential (E°) and EPR Spectral Properties of Type 1 Cu Proteins[a]

Protein	E° (mV)	EPR
stellacyanin	184	rhombic
umecyanin	283	axial
amicyanin[b]	294	axial
mavicyanin	285	rhombic
plantacyanin	317	rhombic
azurin[c]	333	axial
Met121Leu (Az)[c]	433	rhombic
pseudoazurin[d]	139	rhombic
Pro80Ala(pseudoazurin)[d]	409	rhombic
rusticyanin	680	rhombic

[a]Data from Adman (1985). [b]Data from Gray et al. (1988). [c]Data from Pascher et al. (1993). [d]Data from Nishiyama et al. (1992).

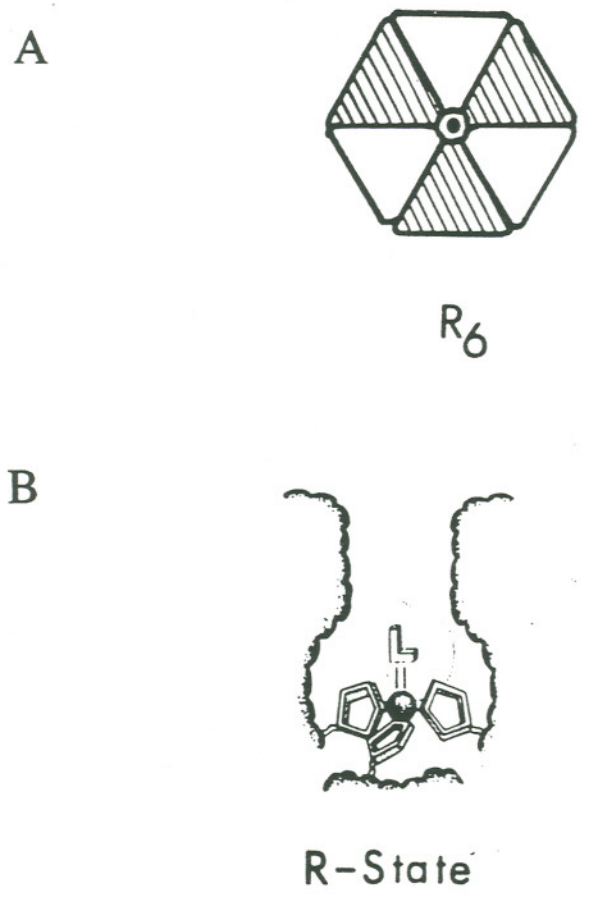

Figure 6.1. (A) Schematic representation of R_6 insulin. The shading reflects the threefold symmetry of the hexamer. (B) Metal chelate site in the R_6 insulin hexamer. The metal is coordinated by histidines from three different subunits and an exchangeable fourth ligand (denoted L) in a distorted tetrahedral geometry. Figures from Brader and Dunn (1991).

BIOGRAPHICAL NOTE

The author was born on October 26, 1959, in Wuhan, central China. She was raised in Huangshi, a city 40 miles east of Wuhan, where she received her primary and high school education. She obtained her B.S. in Physical Chemistry in 1982 from Wuhan University, and completed her M.S. in Chemistry in 1985 from Hubei Chemistry Research Institute. After she came to the United States in 1986, she became a Ph.D. student at Oregon State University in 1987, and transferred to the Oregon Graduate Institute in 1988. Since then, she has been working on the spectroscopic study of biological systems toward her Ph.D. degree.